2004

ANNUAL REPORT 2004

WORKING WITH NANOREACTORS

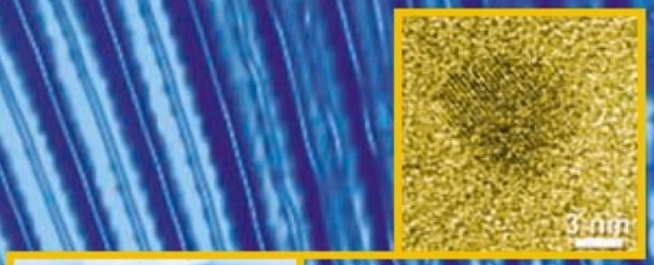

AUSTRIAN SAXS BEAMLINE AT elettra

Cover-Pictures: Taken from the user contribution Costacurta et al. *Synthesis of lead sulfide nanocrystals using mesostructured silica films as nanoreactors* (page 98)

Austrian Small Angle X-ray Scattering (SAXS) Beamline at ELETTRA

Annual Report 2004

Compiled by the SAXS-Group:

- for IBR: B. Sartori, M. Rappolt & H. Amenitsch
- for ELETTRA: S. Bernstorff

Table of Contents

› Preface *1*

› The SAXS-Group *3*

› The SAXS-Beamline in General *4*

› Application for Beamtime at ELETTRA *8*

› List of Institutes Participating in Experiments *10*

› List of Performed Experiments *18*

› User Statistics *22*

› Experimental Possibilities at the SAXS-beamline *26*

1. Accessible SAXS and WAXS ranges *26*
2. Calibration of the s-axis and flat field correction *27*
3. Elettra Virtual Collaboratory *29*
4. Site laboratories *30*
5. Available sample manipulation stages *31*

› User Contributions *38*

1. Materials Science *39*
2. Life Sciences *63*
3. Chemistry *92*

› Publications *120*

› Author Index *142*

Preface

Douptless, SAXS and its related techniques like GISAXS are playing a powerful, leading role in the concert of analytical instruments in nanosciences and technology. This is due to the fact that SAXS allows to observe the nanostructured characteristics of materials, natural or synthetic, in situ and in real time during their growth and decay and during reactions.

The present annual report gives an impression account of the developments in this field. It is evident that the nanotechnological strategy of bottom-up assembly of supramolecular structures in bulk or on solid support is now the leitmotiv of most of the described projects. This is the key market segment for the Austrian SAXS station at ELETRA.

Users should be free to concentrate on results and not have to bother about techniques and instrumentation. This is not always an easy task, since SAXS, unlike with crystallography, almost every project needs some special technique. Pressure, temperature, different sample environments, different detectors, on-site preparation etc. Our team at the SAXS station is among the world-leaders in this art of adaptation today.

Innovations at ELETTRA, such as the Virtual Collaboratory (p. 29), add to the user-friendliness and efficiency of the facility. Many others are to be expected from developments under the EC-funded collaboration with other synchrotron SAXS stations in Europe. Also the planned upgrade of ELETTRA will contribute to maintain the international competitiveness of our SAXS beamline.

Again I want to thank the SAXS team and users with their outstanding projects most cordially for making the Austrian SAXS station at ELETTRA a success story.

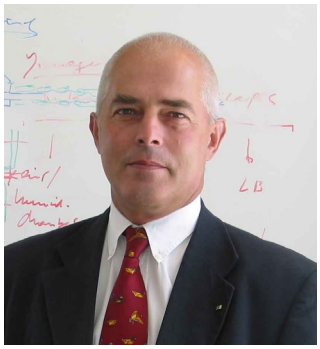

Peter Laggner
Director
Institute of Biophysics and X-Ray Structure Research
Austrian Academy of Sciences

We are pleased to welcome the publication of the 2004 Annual Report of the Austrian SAXS Beamline at ELETTRA. Many important things have changed at ELETTRA during the last year, but the SAXS beamline has remained an essential reference point for the users' community in the life sciences, materials chemistry and materials physics, providing over thirty high-quality research contributions in 2004 alone.

In October 2004 the management structure at ELETTRA was reinforced with the appointment of Massimo Altarelli as Senior Scientific Director, to provide long-term scientific advice to the Board of Sincrotrone Trieste S.C.p.A., and complement the company management provided by President Carlo Rizzuto and Chief Executive Officer Alfonso Franciosi. A new Council of Partners was established to take advantage of the advice of successful partners, such as the Austrian Academy of Sciences, in the decision-making process for important issues determining the long-term strategy of the facility.

The Council of Partners is providing recommendations from the partners to the Board of Sincrotrone Trieste on issues such as yearly and multi-year plans, new appointments of senior managers, proposed changes in the organization of the Laboratory, international activities for the expansion of the partners' and users' community, new appointments to the Committees (SAC, MAC, IAP, etc.). Peter Laggner represents the Austrian Academy of Sciences on the Council and Massimo Altarelli serves as President. Other partners currently represented on the Council include the International Center for Theoretical Physics (ICTP), the Czech Academy of Sciences, the Centre National de la Recherche Scientifique (CNRS) of France, the Universities of Trieste and Udine, the International School for Advanced Studies (SISSA) and the Consorzio Interuniversitario per la Scienza e la Tecnologia dei Materiali (INSTM).

At the very end of 2004 a decree by the Italian government re-established the yearly dowry of the ELETTRA laboratory at the € 27 million level, effectively eliminating the budget shortfall that had affected ELETTRA's development throughout 2003 and 2004. Two research agreements with the Italian Ministry for Schooling, Research and Universities (MIUR) were also signed in 2004, providing a total of € 35 millions over three years to support construction of a new booster injector. The full-energy injector will allow top-up operation of ELETTRA in two years, and free the LINAC, that will become the core of the new fourth-generation synchrotron radiation source FERMI@ELETTRA. This new free-electron-laser (FEL) source will provide femtosecond pulses of unparalleled brilliance at nanometer wavelengths. A € 60 million loan of the European Investment Bank over three years recently completed project financing for the FERMI@ELETTRA initiative.

To successfully bring about the upgrade of ELETTRA, involving a new full-energy injector, rf system and global orbit feedback, while implementing the new FEL-based source FERMI will be a major challenge for Sincrotrone Trieste in the next few years. We plan to meet this challenge with the important support of our most successful partners, such as the Austrian Academy of Sciences. We take this opportunity to warmly thank the management and staff of the SAXS beamline at ELETTRA for their enthusiasm and dedication over the years.

Alfonso Franciosi
Director, ELETTRA Laboratory
Chief Executive Officer, Sincrotrone Trieste S.C.p.A.

The SAXS-Group

HEAD OF PROJECT: Peter Laggner[1)]

e-mail: Peter.Laggner@oeaw.ac.at

SENIOR SCIENTIST: Heinz Amenitsch [1), 3)]

e-mail: Heinz.Amenitsch@elettra.trieste.it

Sigrid Bernstorff [2)]

e-mail: Sigrid.Bernstorff@elettra.trieste.it

Michael Rappolt [1), 3)]

e-mail: Michael.Rappolt@elettra.trieste.it

PHD-STUDENT: Fabian Schmid [1), 3)]

e-mail: Fabian.Schmid@elettra.trieste.it

VISITING SCHOLAR: Semra Ide (until August 2004)

e-mail: Semra.Ide@elettra.trieste.it

CHEMICAL ASSISTANT: Barbara Sartori [1, 3)]

e-mail: Barbara.Sartori@elettra.trieste.it

TECHNICIAN: Christian Morello[2)]

e-mail: Christian.Morello@elettra.trieste.it

1) Institute for Biophysics and X-ray Structure Research, Austrian Academy of Sciences, Schmiedlstraße 6, 8042 Graz, Austria.
Tel 0043-316-4120 302
Fax 0043-316-4120 390

2) Sincrotrone Trieste, Strada Statale 14, km 163.5, 34012 Basovizza (TS), Italy.
Tel 0039-040-375 81
Fax 0039-040-938 0902

3) Institute for Biophysics and X-ray Structure Research, Austrian Academy of Sciences c/o Sincrotrone Trieste

The SAXS-Beamline in General

Small Angle X-ray Scattering has become a well known standard method to study the structure of various objects in the spatial range from 1 to 1000 nm, and therefore instruments capable to perform such experiments are installed at most of the synchrotron research centers. The high-flux SAXS beamline at ELETTRA is mainly intended for time-resolved studies on fast structural transitions in the sub-millisecond time region in solutions and partly ordered systems with a SAXS-resolution of 1 to 140 nm in real-space.
The photon source is the 57-pole wiggler whose beam is shared and used simultaneously with a Macromolecular Crystallography beamline. The wiggler delivers a very intense radiation between 4 and 25 keV of which the SAXS-Beamline accepts 3 discrete energies, namely 5.4, 8 and 16 keV. The beamline optics consists of a flat double crystal monochromator and a double focusing toroidal mirror.
A versatile SAXS experimental station has been set-up, and an additional wide-angle X-ray scattering (WAXS) detector monitors simultaneously diffraction patterns in the range from 0.1 to 0.9 nm. The sample station is mounted move-able onto an optical table for optimising the sample detector distance with respect to SAXS resolution and sample size.
Besides the foreseen sample surrounding the users have the possibility to install their own specialised sample equipment. In the design phase, besides technical boundary conditions, user friendliness and reliability have been considered as important criteria.
The optimisation of the beamline with respect to high-flux and consequently high flux density, allows to perform the following experiments:

- Low Contrast Solution Scattering
- Grazing Incidence Surface Diffraction
- Micro-Spot Scanning
- X-ray Fluorescence Analysis
- Time-Resolved Studies ≥ 11 μs
- Simultaneously Performed Small- and Wide-Angle Measurements (SWAXS) on:
    - Gels
    - Liquid Crystals
    - (Bio) Polymers
    - Amorphous Materials
    - Muscles

Furthermore, using 5.4 and 16 keV energies, the beamline is widely applicable also to very thin, e.g. single muscle fibers, and optically thick (high Z) specimen, as often used in e.g., material science and solid state physics.

THE INSERTION DEVICE

The wiggler for the SAXS beamline consists of three 1.5 m long segments, each having 19 poles. The device can work with a minimum gap of 20 mm, which corresponds to K=20 at 2 GeV. The main parameters of the wiggler are:

- Critical Energy 4.1 keV
- Radiation Power 8.6 kW
- Flux 3.5×10^{14} ph/s/mrad/0.1%BW (at 400 mA)

The wiggler radiation cone has a horizontal width of 9 mrad. From this the SAXS-beamline accepts vertically 0.3 mrad, and horizontally +/-0.5 mrad at a 1.25 mrad off-axis position. The resulting source size for 8 keV photons is 3.9 x 0.26 mm^2 (horiz. x vert.).

THE OPTICS

The optics common with the diffraction beamline consists of:

- C-Filter and Beryllium window assembly to reduce the power load on the first optical elements by a factor of 2 and to separate the beamline vacuum from the storage ring.
- Beam defining slit chamber which allows to define the SAXS beam on three sides before the monochromator in order to reduce the straylight in the downstream beamline sections.

The SAXS beamline optics consists of:

- A double-crystal monochromator consisting of four individual chambers, in which three interchangeable asymmetric Si(111) crystal pairs are used to select one of three fixed energies. Each of the crystal pairs is optimised for the corresponding energy to accomplish a grazing angle of 2°. The energy resolution $\Delta E/E$ of the monochromator is in the range of 0.7 - 2.5 10^{-3}.
- A baffle chamber after the monochromator is used as an adjustable straylight fenditure.
- A segmented toroidal mirror focuses the light in horizontal and vertical direction with a 1/2.5 magnification onto the SAXS-detector.
- An aperture slit reduces the straylight after the monochromator and the toroidal mirror.
- A guard slit defines the illuminated region around the focal spot. The spot size on the detector is 1.6 mm horizontally and 0.6 mm vertically. The calculated flux at the sample is in the order of 10^{13} ph/s at 400 mA. For a maximum sample size of 5.4 x 1.8 mm^2 correspondingly a flux density of 10^{12} ph/s/mm^2 has been calculated.

SAMPLE STAGE

The multipurpose sample stage allows to perform fast time-resolved relaxation studies based on temperature- or pressure-jumps as well as stopped flow experiments. Shear jump relaxation experiments are planned. Specifically, T-jumps can be induced by an infra-red light pulse (2 ms) from an Erbium-Glass laser, raising the temperature about 20 °C in an aqueous sample volume of 10 µl. A hydrostatic pressure cell with a maximal accessible angular range of 30° for simultaneous SAXS and WAXS measurements is available. P-jumps are realised by switching fast valves between a low and a high pressure reservoir, increasing or decreasing the hydrostatic pressure in the range from 1 bar to 2.5 kbar within a few ms. A Differential Scanning Calorimeter (DSC) allows for DSC-scans simultaneously to SWAXS measurements. Also a 1.5 T magnet is available. In an overview, the following sample manipulations are possible (further details, see page 31-37):

- Temperature Manipulations: Ramps, Jumps and Gradient Scans
- Pressure Manipulation: Scan and Jumps
- Stopped Flow Experiments
- SWAXS Measurements Applying Mechanical Stress
- SWAXS Measurements Applying Magnetic Fields
- Calorimetric measurements

Scientific applications	Low Contrast Solution Scattering, Grazing Incidence Surface Diffraction, Micro-Spot Scanning, X-ray Fluorescence Analysis, Time-Resolved Studies ≥ 11 μs and Simultaneously Performed Small- and Wide-Angle Measurements (SWAXS) on: Gels Liquid Crystals (Bio) Polymers Amorphous Materials Muscles
Source characteristics	Wiggler (NdFeB Hybrid): Period: 140 mm No. full poles: 57 Gap: 20 mm B_{max}: 1.607 T Critical Energy ε_c: 4.27 keV Power (9 mrad): 8.6 kW Effective source size FWHM: 3.9 x 0.26 mm^2(HxV)
Optics	Optical elements: Double crystal monochromator: Si (111) asym. cut, water cooled. / Mirror: two–segment,toroidal, Pt coated. Distance from source: 18.4 m / 26.5 m Acceptance: 1 mrad/0.3 mrad (HxV) Energy (3 selectable): 5.4, 8, 16 keV (0.077, 0.154, 0.23 nm) Energy resolution ΔE/E: 0.7-2.5 x 10^{-3} Focal spot size FWHM: 1.2 x 0.6 mm^2 (HxV) Spot at Sample FWHM: 5.4 x 1.8 mm^2(HxV) Flux at sample: 5 x 10^{12} ph s^{-1}(2 GeV, 200 mA, 8 keV)
Experimental apparatus	Resolution in real space: 1-140 nm (small-angle), 0.1- 0.9 nm (wide-angle) Sample stage: temperature manipulations: ramps, jumps and gradient scans, pressure manipulation: scan and jumps, stop flow experiments, SWAXS measurements applying mechanical stress, SWAXS measurements applying magnetic fields. In-line calorimetric measurements simultaneously with SWAXS. Detectors: 1D gas-filled detectors for simultaneous small- and wide-angle (Gabriel type), 2D CCD-detector for small-angle.
Experiment control	Beamline control: Program-units written in LabView for Windows 1 D detector control: PC-card and software from Hecus & Braun, Graz. 2 D detector control: Software from Photonic Science, Oxford.

CURRENT STATUS

The beamline has been built by the Institute for Biophysics and X-ray structure Research (IBR), Austrian Academy of Science in collaboration with staff members from Sincrotrone Trieste, and is in user operation since September 1996. The set-up of the beamline started at the beginning of January 1995 with the installation of the support structure. Until the end of 1995, the 8 keV single energy system had been realised. The upgrade to the full three energy system was finished in spring 1998. Time resolved experiments require fast X-ray detectors and data acquisition hard- and software. Depending on the desired resolution in time and in reciprocal space, on isotropic or anisotropic scattering of the sample, one-dimensional position sensitive (delay-line type) or two-dimensional CCD detectors are employed.

In August 2002 our new chemistry and X-ray laboratory went into operation. The chemistry unit serves mainly for sample preparation and analysis for both, in house research and external user groups, whereas the X-ray laboratory allows on-site testing of samples before moving on to the SR beamline (see page 30).

In conclusion, due to wide versatility of the beamline and the highly flexible sample stage, there are nearly no limits for the realisation of an experiment, and you are welcome by our team to propose any interesting and highlighting investigation for the benefit of material and life sciences.

Application for Beamtime at ELETTRA

1. Beamtime Policy at SAXS beamline

According to the agreement from March 2001 regarding the co-operation between the Austrian Academy of Sciences and Sincrotrone Trieste, at the Austrian SAXS-beamline the available beamtime of about 5000 hours/year is distributed as follows:

- 35% for Austrian Users, type: "CRG" (Collaborating Research Group)
- 35% for Users of Sincrotrone Trieste (General Users (GU))
- 30% is reserved for beamline maintenance and in-house research

In both user beamtime contingents also any industrial, proprietary and confidential research can be performed according to the "General User Policy" of Sincrotrone Trieste.

To apply for CRG and GU user beamtime proposals must be submitted according to the rules of Sincrotrone Trieste. The international review committee at ELETTRA will rank the proposals according to their scientific merit assessment. Based on this decision beamtime will be allocated according to the specific quotes for the beamtimes (CRG/GU) either for the following semester ("normal application") or for the next two years ("long term application"). However, at the moment no more than a maximum of 10% of the beamtime will be assigned to "long term" projects.

2. How to apply for beamtime

There are two deadlines each year for proposals, namely August 31st and February 28th. Accepted proposals will receive beamtime either in the then following first or second half year period, respectively. The Application Form must be completed on-line according to the following instructions. In addition, one printed form is also required and must be send to:

ELETTRA USERS OFFICE
Strada Statale 14 - km 163.5
34012 Basovizza (Trieste), ITALY
Tel: +39 040 3758628 - fax: + 39 040 3758565
e-mail: useroffice@elettra.trieste.it

INSTRUCTIONS GIVEN BY THE USERS OFFICE
(see also: www.elettra.trieste.it/experiments/users_handbook/index.html)

1. Read carefully the following Guidelines.

2. Connect to the Virtual Users' Office: http://users.elettra.trieste.it using your favorite browser with JavaScript enabled.

3. Select the Virtual Users Office link.

4. When prompted, insert your ID and password. If you are a new user fill in the registration form with your data and choose your institution with the search button; in case your institution does not appear in the list, please contact useroffice@elettra.trieste.it giving all the details about it. When registered, you will receive an acknowledgment with your ID and password. You can change your password, if you wish. In case you forget your password, please don't register again but contact useroffice@elettra.trieste.it. At any moment you can select the help button and view more detailed instructions. By inserting your ID and password you will be able to continue.

5. Select the proposals button in the User functions group.

6. Select add and fill in on-line the proposal form. Please, type your proposal in English. Repeat this procedure for each proposal you intend to submit.

7. In case of continuation proposal: a) attach the experimental report of previous measurements; b) give your previous proposal number.

8. When finished, submit the proposal electronically, selecting the save button.

9. Print the proposal form together with each related safety form.

10. Sign the safety form(s).

11. Mail one complete printed copy to the Users Office.

NOTE

Users from developing and EU countries (with exception of Italy) can apply for financial support for their travel expenses. For further information, please have a look into the web-pages

http://www.elettra.trieste.it/experiments/users_handbook/index.html)

or contact the USERS OFFICE.

List of Institutes Participating in Experiments

Austria

Austrian Academy of Science, Institute for Biophysics and X-ray Structure Research, Graz

AMENITSCH Heinz
DANNER Sabine
DEUTSCH Günter
HICKEL Andrea
HODZIC Aden
JOCHAM Philipp
KOSCHUCH Richard
KRIECHBAUM Manfred
LAGGNER Peter
LOHNER Karl
PABST Georg
POZO-NAVAS Beatriz
RAPPOLT Michael
SARTORI Barbara
SCHMID Fabian
SEVCSIK Eva

Medical University Graz, Institute of Pathology, Graz

REGITNIG P.

Technical University, Institut of Applied Synthetic Chemistry, Division of Macromolecular Chemistry, Vienna

BINDER Wolfgang H.
FARNIK Dominique
KLUGER Christian
PETRARU Laura

University of Technology, Institute of Structural Analysis, Computational Biomechanics, Graz

SOMMER Gerhard

Universität Wien, Institut für Materialphysik, Wien
University of Vienna, Institute of Materials Physics

KERBER Michael
SCHAFLER Erhard
STEINER G.
ZEHETBAUER Michael

Vienna University of Technology, Institute of Materials Chemistry, Vienna

BRANDHUBER Doris

Vienna University of Technology, Institute of Materials Science and Technology, Vienna

FRITSCHER Christina
JAKUBIAK Patrycya
KOCH Thomas
LICHTENEGGER Helga C.
SEIDLER S.
SUPPLIT Ralf

Bulgaria

Bulgarian Academy of Sciences, Institute of Polymers, Sofia

STANEVA M.

Canada

National Research Council of Canada, Steacie Institute for Molecular Sciences, Chalk River Laboratories, Chalk River, Ontario

Katsaras J.

Croatia

"Ruder Boskovic" Institute, Zagreb

BULJAN Maya
DESNICA Uros
DESNICA-FRANKOVIC Ida-Dunja
DUBCEK Pavo
GAJOVIC A.
GRACIN, Davor
JURAIC' Krunoslav
KOVACEVIC Ivana
PIVAC Branko
RADIC Nikola

University of Zagreb, Institute for Physics, Zagreb

SALAMON Kresimir

Czech Republic

Academy of Sciences of the Czech Republic, Institute of Macro- molecular Chemistry, Prague

BALDRIAN Josef
SIKORA Antonín

University of Pardubice, Department of Physics, Pardubice, and Academy of Sciences of the Czech Republic, Institute of Macro-molecular Chemistry, Prague

STEINHART Milos

Finland

Åbo Akademi University, Dept. of Physical Chemistry, Turku

LINDÉN Mika
TEIXEIRA Cilaine Veronica

France

Université de Paris Sud, Physico-Chimie des Systemes Polyphases, Chatenay

BOURGAUX Claudic
KALNIN Daniel
KELLER Gerhard
OLLIVON Michel

PHASE, CNRS, Strasbourg

SLAOUI A.

Université Pierre et Marie Curie, Chimie de la Matière Condensée, Paris

BABONNEAU Florence
BOISSIÉRE Cédric
GROSSO David
KUEMMEL Monika
SANCHEZ Clément

University Paris-Sud, Laboratory for Solid State Physics, Orsay/Paris

ALBOUY Pierre-Antoine

Germany

Max-Planck-Institute for Colloids and Interfaces, Golm / Potsdam

BREZESINSKI Torsten
SMARSLY Bernd

Universität Bremen, Inst. für Festkoerperphysik

ALEXE Gabriela
CLAUSEN Torben
FALTA Jens
FLEGE Jan-Ingo
SCHMIDT Thomas

Universität Hamburg, Inst. für Physikalische Chemie

ALEKSANDROVIC Vesna
KORNOWSKI A.
RANDJELOVIC Igor
WELLER Horst

Universität–GH Siegen, Fachbereich Physik, Siegen
BESCH Hans-Juergen
MARTOIU Sorin
WALENTA Albert Heinrich

Universität Ulm, Inst. für Anorganische Chemie
HUESING Nicola Karola

Hungary

Eötvös Lorand University, Institute for General Physics, Budapest
NYILAS Krystian
RIBARIK Gabor
UNGÁR Tamas

Eötvös Lorand University, Institute for Physical Chemistry, Budapest
FARKAS Ödön
GYENES Tamás
SINKO Katalin

Technical University, Institute for Physical Chemistry
TORMA Viktória

India

Bhabha Atomic Research Centre, Solid State Physics Division, Trombay, Mumbai
ASWAL Vinod Kumar

Indian Institute of Science, Solid State and Structural Chemistry Unit, Bangalore
SAPRA Sameer
SARMA Dipankar Das
VISWANATHA Ranjani

UGC-DAE-CSR, BARC, Mumbai
GOYAL Prem Sagar

Ireland

University College Cork (UCC), Dept. of Chemistry, Cork City
COPLEY Mark P.
HANRAHAN John P.
HOLMES Justin D.
O'CALLAGHAN J. M.

Italy

Associazione CIVEN, Nano Fabrication Facility, Venice
FALCARO Paolo

ADRIACELL, Trieste
KÜHNE Christian

CimtecLab S.r.l., AREA Science Park, Padriciano, Trieste, Italy
BENEDETTI Elena

EniTecnologie S.p.A. – CHIF, Physical Chemistry Department, San Donato Milanese, Italy
D'ANTONA P.
Del PIERO Gastone
GHISLETTI Danila

I.N.F.M. - Laboratorio TASC, Trieste
COJOC Danut-Adrian
DI FABRIZIO Enzo
GARBIN Valeria
FERRARI Enrico

Sincrotrone Trieste, Trieste
BERNSTORFF Sigrid
IDE Semra
MENK Ralf
MORELLO Christian

Università di Bologna, Dip. di Chimica "G. Ciamician", and C.N.R., Centro di Studio per la Fisica delle Macromolecole, Bologna
FALINI Giuseppe

Università di Ferrara, Istitute for Biochemistry and Molecular Biology + ICSI, Ferrara
BERGAMINI C.M.

Università di Firenze, Dip. Scienze Fisiologiche, Firenze
BAGNI Maria Angela
CECCHI Giovanni
COLOMBINI Barbara

Università di Padova, Dip. di Biologia, Padova
VANIN Stefano

Università di Padova, Dip. di Fisica, Padova
MATTEI Giovanni
SADA C.

Università di Padova, Dep. of Mechanical Engineering, Padova
BUSO D.
COSTACURTA Stefano
GUGLIELMI Massimo
MARTUCCI A.

Università di Padova, Dep. of Organic Chemistry, Padova
MAGGINI Michele
MANEA Flavio

Università di Padova, Dip. Scienze Chimiche, Padova
MALFATTI Luca

Università di Perugia, Dipartimento di Fisica, Perugia
ONORI G.

Università del Piemonte Orientale "A.Avogadro", Dip. Scienze e Tecnologie Avanzate (DISTA), Alessandria
CROCE Gianluca
MILANESIO Marco
VITERBO Davide

Università Politecnica delle Marche, Dipartimento di Scienze Applicate ai Sistemi Complessi, sez. Scienze Fisiche, Ancona
CARACCIOLO Giacomo
FEDERICONI Francesco
MARIANI Paolo
PACCAMICCIO Lydia
ORTORE Maria Grazia
SINIBALDI Raffaele
SPINOZZI Francesco

Università Politecnica delle Marche, Dipartimento di Scienze dei Materiali e della Terra, Ancona
PISANI Michela

Università di Roma-La Sapienza, Dip. Di Chimica
CAMINITI R.
CARACCIOLO Giulio
POZZI Daniela

Università di Sassari, Dipartimento di Architettura e Pianificazione, Laboratorio di Scienza dei Materiali e Nanotecnologie, Alghero/ Sasseri
INNOCENZI Plinio

Politecnico di Torino, Dip. Scienze dei Materiali e Ingegneria Chimica, Torino
BRETCANU O.
DINUNZIO S.
ONIDA B.
VERNE' E.

University of Trieste, Dep. of Organic Chemistry, Trieste
PASQUATO Lucia

University of Trieste, Faculty of Engineering, Dep. of Electrotechnique, Electronics and Informatics
VOLTOLINA Francesco

University Ca Foscari, Dep. of Physical Chemistry, Venizia-Mestre
BUCELLA Stefania
CANTON Patrizia
RIELLO Pietro

Singapore

National University of Singapore, Dept. of Physics
CHOLEWA Marian

Slovenia

Josef Stefan Institute, Lab. for Biophysics, EPR Center, Ljubljana
STRANCAR Janez

Spain

Instituto de Investigaciones Quimicas y Ambientales de Barcelona
PEREIRA LACHATAIGNERAIS Joedmi

Sweden

Royal Institute of Technology, Department of Solid Mechanics, Stockholm, Sweden
HOLZAPFEL Gerd A.

University of Lund, Institute for Physical Chemistry 1
ALFREDSSON Viveka

Switzerland

Paul Scherrer Institute, Villigen PSI
KOHLBRECHER J.

Turkey

Middle East Technical University, Ankara
SERINCAN U.
TURAN R.

United Kingdom

University of Glasgow, Institute of Biomedical & Life Sciences, Div. of Biochemistry & Molecular Biology

LINDSAY J.G.
SMOLLE Michaela

University of Glasgow, Institute of Biomedical & Life Sciences, Division of Infection & Immunity

BYRON O.

University Laboratory of Physiology, Oxford

ASHLEY Christopher Charles
GRIFFITHS Peter John

List of Performed Experiments

2004 (first half year)

Proposal	Proposer	Institution	Country	Title	Research Area
2003470	SCHAFLER Erhard	Inst. for Materialphysics, University of Vienna	Austria	In-situ Multi-Reflection Profile Analysis (MXPA) of Ultrafine-Grained Metals; Part I: Face Centered Cubic Metals (fcc)	Materials Science
2003479	LINDEN Mika	Dep. of Physical Chemistry, Abo Akademi University, Turku	Finland	First in-situ synchrotron SAXS/XRD study on the formation of hybrid surfactant templated mesostructured organosilica with a crystalline wall structure	Chemistry
2003480	BINDER Wolfgang	Institute of Applied Synthetic Chemistry, Division of Macro-molecular Chemistry, Vienna Univesity of Technology	Austria	Investigations on Phase Segregated, Supramolecular Block Copolymers: Investigating Nanostructure Formation by SAXS	Chemistry
2003497	MARIANI Paolo	Universita' Politecnica delle Marche, Ancona	Italy	Protein structure and dynamics in not-aqueous solvents	Life Sciences
2003542	SARMA Dipankar Das	Solid State and Structural Chemistry Unit, Indian Institute of Science, Bangalore	India	Study of the growth process in technologically important semiconducting nanoparticles	Chemistry
2003549	DESNICA-FRANKOVIC Ida-Dunja	Rudjer Boskovic Institute, Zagreb	Croatia	Ion beam synthesized CdSe quantum dots	Materials Science
2003635	ASWAL Vinod Kumar	Solid State Physics Division, Bhabha Atomic Research Centre, Mumbai	India	A combined SAXS and SANS study for the determination of the structure of block copolymer micelles	Materials Science
2003649	RIELLO Pietro	Università Ca Foscari, Dip. di Fisica Chimica, Venice	Italy	Monolayer protected and functionalised gold nanoparticles.	Chemistry
2003704	LINDEN Mika	Department of Physical Chemistry, Abo Akademi University, Turku	Finland	Study of the formation process of mesoporous silica. Dependence of additives – salt and alcohols	Chemistry
2003715	COJOC Danut-Adrian	I.N.F.M. - TASC Laboratory, Trieste	Italy	Combined microSAXS-Microscopy Studies on Colloidal Dispersions	Materials Science
2003724	DESNICA Uros	Rudjer Boskovic Institute, Zagreb	Croatia	Compound semiconductor quantum dots formed by ion implantation of constituent atoms	Materials Science
2003750	LAGGNER Peter	IBR, AAS, Graz	Austria	Solid-supported lipid mesophases 1. Influence of Sodium and Calcium Chloride on the fluidity of phosphatidycholine membranes 2. Appearance of two cubic phases in POPE under excess of water conditions during cooling	Life Sciences

				3. Effect of Chain Length on the Lateral Organization of Charged Lipid Membranes	
2003021	GROSSO David	Chimie de la Matière Condensée, UMR UPMC-CNRS 7574, Paris	France	LONG TERM: Self-assembly mechanisms during aerosol generation of mesostructured macro-spheres	Chemistry
2003093	LAGGNER Peter	IBR, AAS, Graz	Austria	LONG TERM: Solid-supported lipid mesophases	Life Sciences
2003095	MARIANI Paolo	Universita' Politecnica delle Marche, Ancona	Italy	LONG TERM: Phase behaviour, molecular conformation and compressibility of lipid systems	Life Sciences
In-house	BERNSTORFF Sigrid PIVAC Branko	Sincrotrone Trieste + Rudjer Boskovic Institute, Zagreb	Croatia	GISAXS study of defects in silicon implanted with noble gas ions	Materials Science
In-house	BERNSTORFF Sigrid, RADIC Nikola	Sincrotrone Trieste + Rudjer Boskovic Institute, Zagreb	Croatia	Microstructure and phase distribution in sputter-deposited tungsten films	Materials Science
In-house	AMENITSCH Heinz KALLNIN Daniel	IBR, AAS, Graz + Physico-Chimie des Systèmes Polyphasés, UMR 8612, Univ. Paris-Sud, Chatenay	France	Crystallization properties of triacylglycerols in emulsion: Influence of processing conditions like shear and emulsifier concentration	Life Sciences
In-house	BERNSTORFF Sigrid FALTA Jens	Sincrotrone Trieste + Institut für Festkörperphysik, Universität Bremen	Germany	Ordering of CdSe quantum dots	Materials Science
In-house	BERNSTORFF Sigrid GRACIN Davor	Sincrotrone Trieste + Rudjer Boskovic Institute, Zagreb	Croatia	SAXS on amorphous silicon-carbide alloys	Materials Science
In-house	RAPPOLT Michael IDE Semra	IBR, AAS, Graz + Hacettepe University - Dept of Physics Engineering, Ankara	Turkey	SAXS Studies of Some Novel Boron- and Nitrogen-Containing Bioengineering Functional Copolymers	Life Sciences
Test	CHOLEWA Marian	National University of Singapore, Dept. of Physics, Singapore	Singapore	Observation of micelles formation, development of self-assembling of mesostructured silica films, polymer/clay nanocomposites	Material Sciences

2004 (second half year)

Proposal	Proposer	Institution	Country	Title	Research Area
2004018	GRIFFITHS Peter John	University Laboratory of Physiology, Oxford	United Kingdom	Structural changes in the myosin motor accompanying activation and work generation.	Life Sciences
2004116	HOLMES Justin	Department of Chemistry University College Cork	Ireland	Swelling of triblock copolymer templates using pressurized fluids	Chemistry
2004182	TORMA Viktoria	Technical University, Budapest	Hungary	Time resolved SAXS investigation of the formation and structure of extremely hard aluminosilicates prepared by a sol-gel route	Chemistry
2004218	FRITSCHER Christina	Institute of Materials Science and Technology, Vienna Univ. of Technology	Austria	Anisotropic, hierarchically organized nanocomposites prepared from tailored-made precursors	Chemistry
2004223	FRITSCHER Christina	Institute of Materials Science and Technology, Vienna Univ. of Technology	Austria	GI SAXS for the structural characterization of mixed metal-oxide, periodically oriented thin films from tailor-made surfactants	Chemistry
2004226	SARMA Dipankar Das	Solid State and Structural Chemistry Unit, Indian Institute of Science, Bangalore	India	Growth of ZnO nanocrystals in the sub-second time-scale and nanometric regime.	Chemistry
2004255	SMOLLE Michaela	Institute of Biomedical & Life Sciences, University of Glasgow	United Kingdom	Protein-protein interactions in the human pyruvate dehydrogenase complex	Life Sciences
2004283	VITERBO Davide	Dep. of Science and Advanced Technology Univ. del Piemonte Orientale, Alessandria	Italy	SAXS and GISAXS study of bioactive glasses before and after soaking in a Simulated Body Fluid	Life Sciences
2004413	DESNICA Uros	Rudjer Boskovic Institute, Zagreb	Croatia	Ion-beam synthesized Germanium and Diamond quantum dots	Materials Science
2004457	LAGGNER Peter	IBR, AAS, Graz	Austria	Solid-supported lipid mesophases: 4. Barotropic phase transition of binary mixtures of POPC and steroles (cholesterol and plant sterols) 5. Composition dependence of aggregation form and mixing properties in a bacterial model membrane system	Life Sciences

				6. In situ coating of phospholipid mixtures studied with surface diffraction	
2003021	GROSSO David	Chimie de la Matière Condensée, UMR UPMC-CNRS 7574, Paris	France	LONG TERM: Self-assembly mechanisms during aerosol generation of mesostructured macro-spheres	Chemistry
2003093	LAGGNER Peter	IBR, AAS, Graz	Austria	LONG TERM: Solid-supported lipid mesophases	Life Sciences
2003095	MARIANI Paolo	Universita' Politecnica delle Marche, Ancona	Italy	LONG TERM: Phase behaviour, molecular conformation and compressibility of lipid systems	Life Sciences
Property Research	ENI-TECHN.	EniTecnologie S.p.A., San Donato Milanese	Italy	Temperature-dependent phenomena in waxy oils	Materials Science / Chemistry
In-house	BERNSTORFF Sigrid FALTA Jens	Sincrotrone Trieste + Institute for Solid State Physics, Universität Bremen	Germany	Ordering of CdSe quantum dots	Materials Science
In-house	AMENITSCH Heinz INNOCENZI Plinio	IBR, AAS, Graz + Lab. Science of Materials and Nanotechnology, Uni. Sassari, Alghero	Italy	Small Angle X-Ray Scattering study of nanoparticles of palladium in mesoporous silica thin films	Chemistry
In-house	BERNSTORFF Sigrid GRACIN Davor	Sincrotrone Trieste + Rudjer Boskovic Institute, Zagreb	Croatia	SAXS on amorphous silicon-carbide alloys	Materials Science
In-house	BERNSTORFF Sigrid PIVAC Branko	Sincrotrone Trieste + Rudjer Boskovic Institute, Zagreb	Croatia	GISAXS study of Si nanoobjects formed in SiO2/SiO superstructures	Materials Science
In-house	AMENITSCH Heinz SCHMID Fabian	IBR, AAS, Graz + Univ. of Technology,Graz	Austria	Layer and Age Specific Tensile Testing of Coronary and Aorta Arteries	Life Sciences
In-house	AMENITSCH Heinz BERNSTORFF Sigrid BALDRIAN Josef	IBR, AAS, Graz + Sincrotrone Trieste + Institute of Macromolecular Chemistry, A.S. CR, Prague	Czech Republic	Influence of Symmetrical Tri-Block Copolymers to the Kinetics of Structure Development in Polymer Blends	Chemistry
In-house	AMENITSCH Heinz CARACCIOLO Giulio	IBR, AAS, Graz + Dep. of Chemistry, Univ. di Roma "La Sapienza"	Italy	Interactions of Phospholipid Vesicles with Cationic Gemini Surfactants	Life Sciences
Test	CIMTEC LAB S.r.l.	Trieste	Italy	(Property Research)	Materials Science

User Statistics

1. Number of submitted proposals and assigned shifts from 1995 until December 2005

The Austrian SAXS-beamline at ELETTRA opened to users in September 1996. Since then many experiments have been performed related to the fields of life science, materials science, physics, biophysics, chemistry, medical science, technology and instrumentation.

From September 96 on users gained access to the SAXS-beamline on the basis of the proposals received for the periods shown in Fig. 1. The assignment of beamtime at this beamline is done separately for the group of "General Users" (GU) and the "Collaborating Research Group" (CRG), i.e., the Austrian users. Beamtime was assigned to the proposals of each group in the order of the rating received by the Scientific Committee, and up to the maximum number of shifts available to each group according to the contract between "The Austrian Academy of Sciences" and the "Sincrotrone Trieste". Until December 1997 up to 30 % of the beamtime was given to CRG, up to 55 % to GU, and 15% was reserved for maintenance purposes. From January 98 to June 2001 the quota for beamtime was up to 35 % for CRG, up to 50 % for GU, and again 15% reserved for maintenance purposes. From July 2001 on the two contingents for user proposals from CRG and GU receive up to 35% of the beamtime each. The remaining 30 % of beamtime are used for inhouse research projects as well as for maintenance purposes.

Fig. 1 gives an overview of the numbers of received proposals, the numbers of requested and assigned shifts, as well as the percentage between assigned and requested shifts. Included in Fig.1 are also the same data for the period End 1995 - August 1996, during which some beamtime had been given already to users in order to perform first pilot- and test-experiments together with the beamline staff. These first experiments during the commissioning phase were not yet based on proposals, since the goal was mostly to evaluate and improve the performance of the beamline and the equipment of its experimental station. As can be seen in Fig.1, the request for beamtime at the SAXS-beamline increased continuously and strongly until the first half year of 1999 (also during the period Sept.-Dec. 1997, if one takes into account that this period was only 4 instead 6 month long, and that for this reason less proposals were submitted). Then, probably due to the high rejection rates, the number of submitted proposals decreased somewhat during 2001, which resulted in a better ratio of accepted / rejected proposals. This oscillating behaviour of beamtime request can also be seen for the period 2002 - 2005, where after higher numbers of submitted proposals slightly reduced request periods follow.

In 2004, in total 73 proposals (11 from CRG, and 62 from GU) were submitted. From these 16 proposals (1 from CRG and 15 from GU) were submitted by "new" usergroups, i.e. groups which so far had never beamtime at the SAXS beamline. From these 6 proposols (1 CRG and 5 GU) were officially accepted. In addition two groups from industry performed first measurements (one paying and one test experiment).

Figure 1 (Next page). The statistical information about the beamtime periods since end of 1995 are given for the groups "CRG", and "GU" separately, as well as for both together ("Total"). Shown are, for all beamtime periods (from top to bottom):

- Number of received proposals, ● Number of requested shifts,
- Number of assigned shifts, and ● Relation between assigned and requested shifts

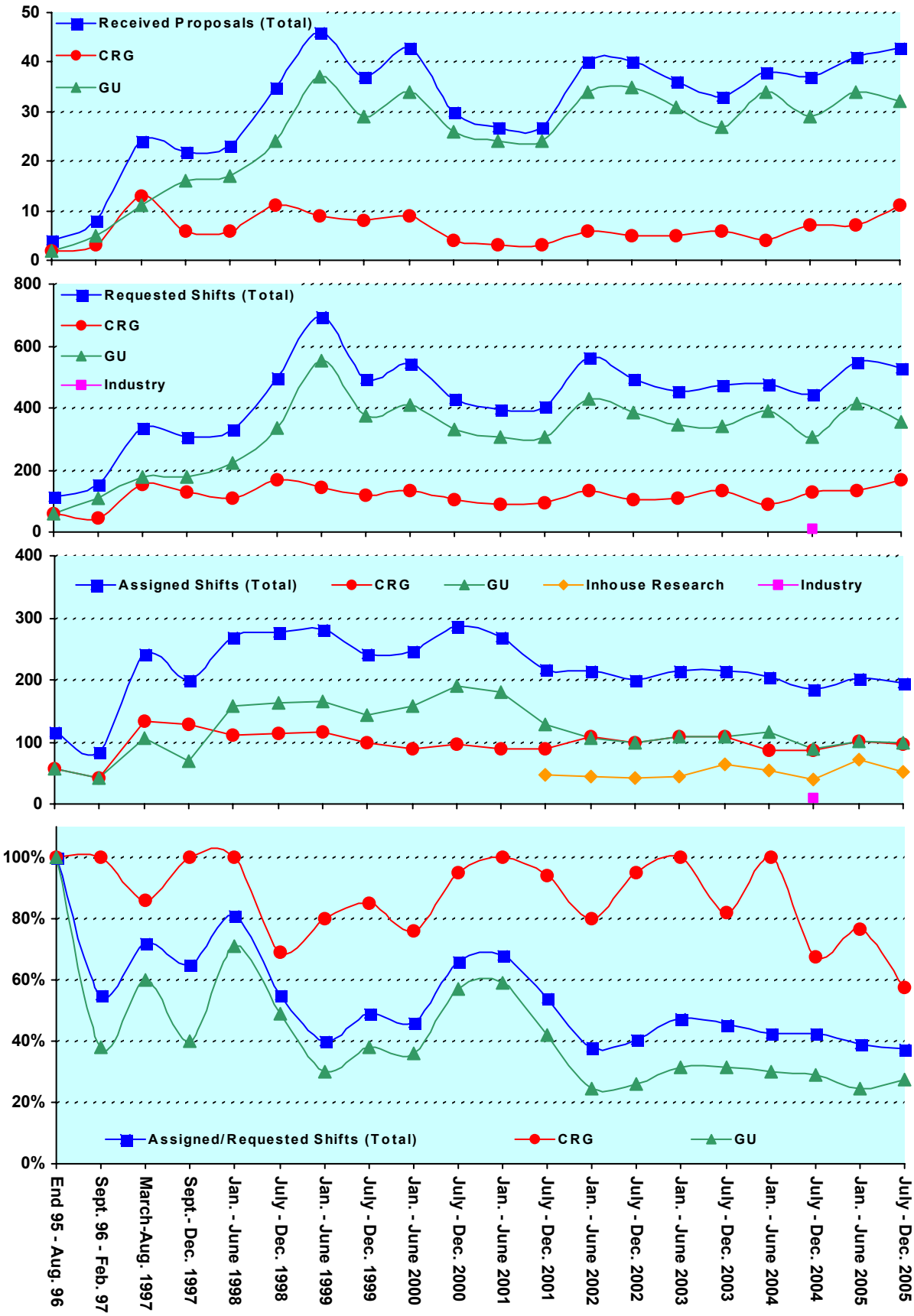
Received Proposals (Total)
CRG
GU
Requested Shifts (Total)
CRG
GU
Industry
Assigned Shifts (Total)
CRG
GU
Inhouse Research
Industry
Assigned/Requested Shifts (Total)
CRG
GU
End 95 - Aug. 96
Sept. 96 - Feb. 97
March-Aug. 1997
Sept.- Dec. 1997
Jan. - June 1998
July - Dec. 1998
Jan. - June 1999
July - Dec. 1999
Jan. - June 2000
July - Dec. 2000
Jan. - June 2001
July - Dec. 2001
Jan. - June 2002
July - Dec. 2002
Jan. - June 2003
July - Dec. 2003
Jan. - June 2004
July - Dec. 2004
Jan. - June 2005
July - Dec. 2005

2. Provenience of users

During 2004, 159 users from 64 institutes in 19 countries have performed experiments at the SAXS beamline. In Fig. 2 are shown both the provenience of these users, and of their respective institutes. Each user or institute was counted only once, even though many users performed experiments in both beamtime periods of 2004.

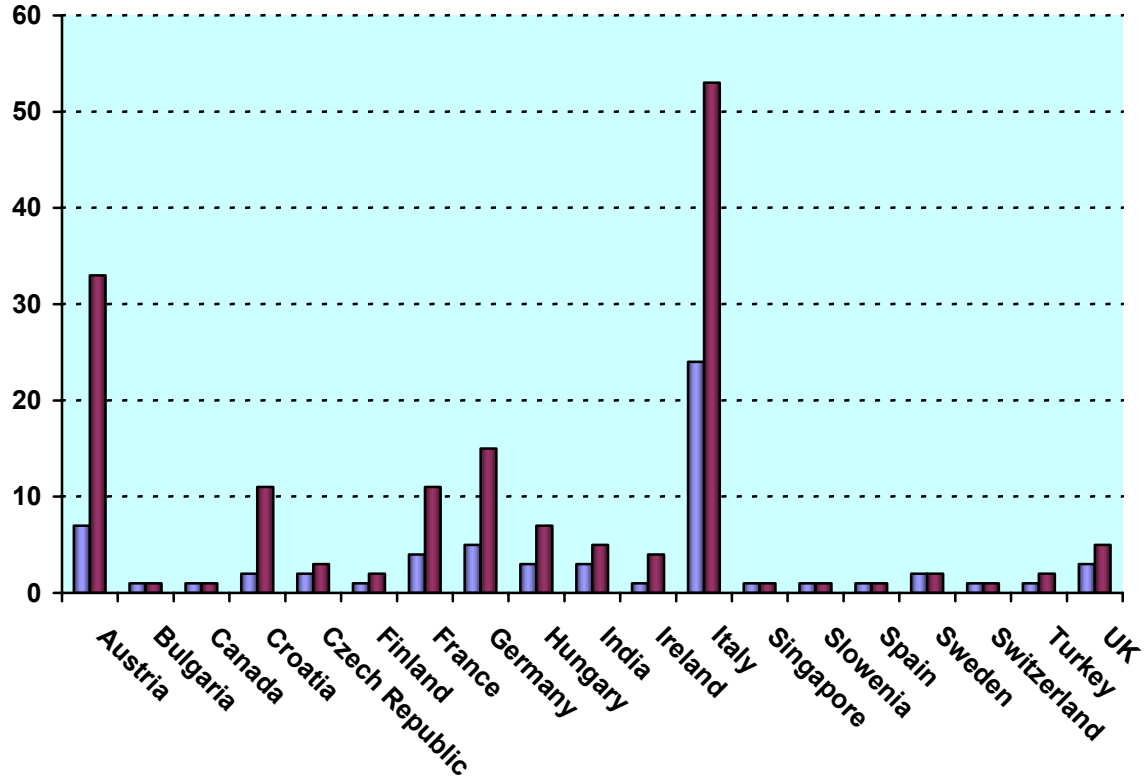

Figure 2. Provenience of users (dark grey) and of their corresponding institutes (light grey).

3. Documentation of experimental results

As could be expected, with the start of user-operation at the SAXS-beamline the number of contributions to conferences started to increase strongly. With a delay of one year - the average time needed for paper publications - also the number of publications increased accordingly, as can be seen in Fig. 3.

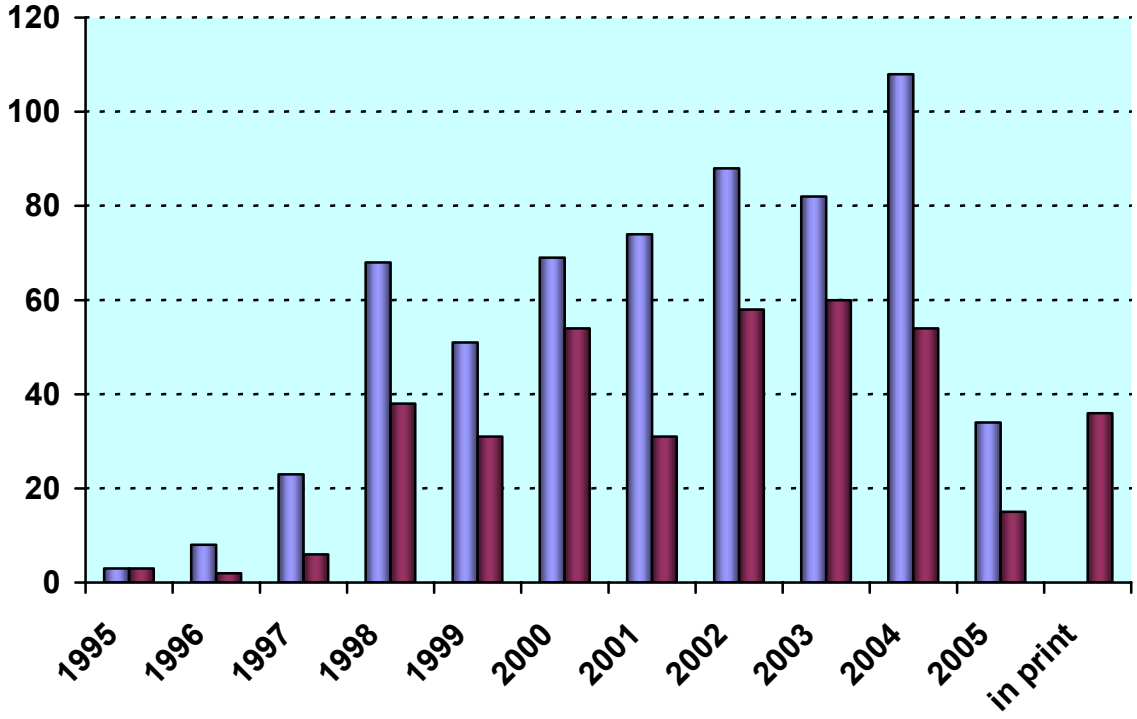

Figure 3. Number of conference contributions (light grey) and of refereed paper publications (dark grey) for the years 1995-2004. Also contributions, which have been published until July 2005 as well as those in print at that time are included.

In addition, from 1995 until July 2004, the following documentations based on instrumentation of the SAXS-beamline, or on data taken with it, have been produced.

Unrefereed publications:

Technical Reports on Instrumentation:	5
Contributions to Elettra Newsletters:	15
Contributions to Elettra Highlights:	19
Habil Thesis:	2
PhD Thesis:	42
Master Thesis :	25

Experimental Possibilities at the SAXS-beamline

1. Accessible SAXS and WAXS ranges

Simultaneous SAXS- and WAXS-measurements can be performed using a linear sensitive gas detector (Gabriel type, windows size 8 x 100 mm, active length 86.1 mm with a resolution of 0.135 mm/channel) for the WAXS-range, and either a second linear Gabriel type detector (windows size 10 x 150 mm, active length 134 mm with a resolution of 0.159 mm/channel), or the 2D CCD-system for the SAXS-range. A specially designed vacuum chamber (SWAXS-nose, see Annual Report of 1996/97, p. 32) allows to use both scattering areas below (for SAXS) and above (for WAXS) the direct beam, respectively.
Depending on the photon energy maximum SAXS resolutions of 2000 Å (5.4 keV), 1400 Å (8 keV) or 630 Å (16 keV) are available. The available possible WAXS-ranges are summarised in Table 1. The overall length of the SWAXS-nose in the horizontal direction, measured from the sample position, is 512 mm and the fixed sample to WAXS-detector distance is 324 mm. At the shortest SAXS camera-length an overlap in the d-spacings covered by the SAXS- and WAXS-detectors, respectively, is possible: then, the common regime lies around 9 Å.

Table 1. Possible d-spacing ranges in the WAXS-regime at the SAXS-beamline at ELETTRA. Since the WAXS-detector can be mounted at four different fixed positions on the SWAXS-nose (range 1-4), with the three possible energy choices (5.4, 8 and 16 keV) this results in 12 different d-spacing regimes. In italic the most common choice (8 keV, range 1) is highlighted. This range is suited for experiments, e.g., on lipid-systems and (bio)polymers.

Range	2θ [deg]	d-spacing (Å)		
		8 keV	5.4 keV	16 keV
1	9.4	*9.40*	14.03	4.27
	27.6	*3.23*	4.82	1.47
2	27.4	3.25	4.86	1.48
	45.6	1.99	2.97	0.90
3	45.4	2.00	2.98	0.91
	63.6	1.46	2.18	0.66
4	63.4	1.47	2.19	0.67
	81.6	1.18	1.76	0.54

2. Calibration of the s-axis and flat field correction

At the SAXS beamline various standards are used for the angular (s-scale) calibration of the different detectors:

- Rat tail tendon for the SAXS detector - high resolution (rtt*.dat)
- Silver behenate for the SAXS detector – medium and low resolution (agbeh*.dat)
- Para-bromo benzoic acid for the WAXS detector – WAXS range 1 and 2 (pbromo*.dat)
- Combination of Cu, Al foils and Si powder for the WAXS detector – WAXS range 2 and higher

In Fig. 1 a typical diffraction pattern of rat tail tendon is shown, depicting the diffraction orders (from the first to the 14th order) measured with a "high" resolution set-up (2.3 m) and the delay-line gas detector. The d-spacing is assumed to be 650 Å, but this value can vary depending on humidity up to 3%. Thus, the rat tail tendon is often used only to determine the position of the direct beam (zero order), while the absolute calibration is performed using the diffraction pattern of Silver behenate powder. Fig. 2 depicts a diffraction pattern of Silver behenate measured with "medium" resolution set-up (1.0 m) from the first to the 4th order (repeat spacing 58.4 Å) [1].

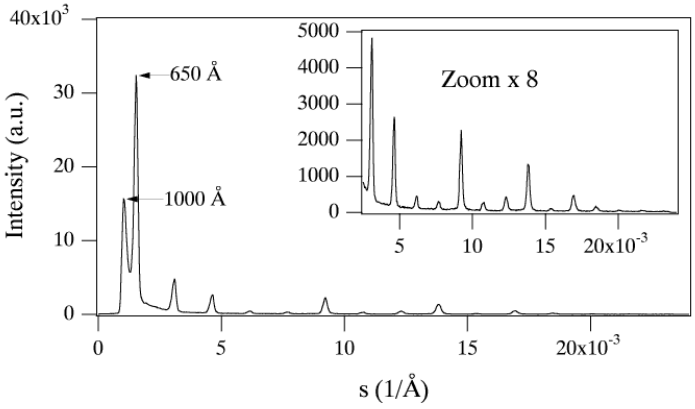

Figure 1. SAXS diffraction pattern of the collagen structure of rat tail tendon fibre at a distance of 2.3 m.

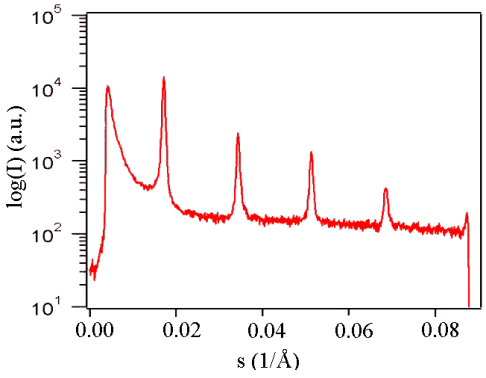

Figure 2. SAXS diffraction pattern of Ag behenate powder at a distance of 1.0 m

In Fig. 3 a typical WAXS pattern of p-bromo benzoic acid is shown. The diffraction peaks are indexed according to the values given in Table 2, taken from [2].

Table 2. d-spacings and relative intensities of p-bromo benzoic acid according to [2].

d-spacing/Å	rel. intensity	d-spacing/Å	rel. intensity
14.72	18000	4.25	490
7.36	1200	3.96	2380
6.02	330	3.84	10300
5.67	980	3.74	26530
5.21	6550	3.68	1740
4.72	26000	3.47	760

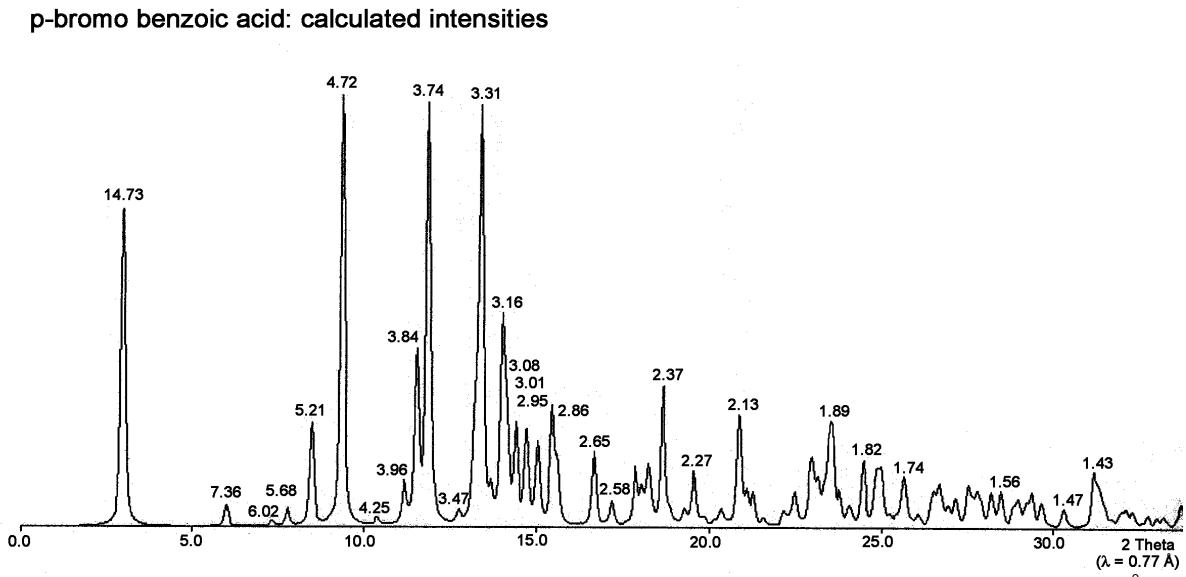

Figure 3. Calculated diffraction pattern of p-bromo benzoic acid. d-spacings are given in Å.

The s-scale for both, the SAXS and the WAXS range, can be obtained by linear regression, i.e., the linear relation between the kown s-values of the calibrant versus the measured peak positions has to be found.

A further correction is regarding the flat field response (efficiency) of the detectors. For this correction, the fluorescence light of various foils are used to illuminate the detectors rather homogeneously:

At 8 keV: iron foil (100 µm thick), fluorescence energy: 6.4 keV K_α, 7.1 keV K_β (effic*.dat)
At 16 keV: copper foil (> 100 µm thick), fluorescence energy: 8.028 keV $K_{\alpha 2}$, 8.048 keV $K_{\alpha 1}$, 8.905 keV K_β (effic*.dat)

The measured scattering pattern are corrected for the detector efficiency simply by dividing them by the fluorescence pattern. Note: The average of the detector efficiency data should be set to unity and a small threshold should be applied to avoid any division by zero.

[1] T.N. Blanton et. al., Powder Diffraction 10, (1995), 91
[2] K. Ohura, S. Kashino, M. Haisa, J. Bull. Chem. Soc. Jpn. 45, (1972), 2651

3. Elettra Virtual Collaboratory

During 2005, a new possibility for data file sharing between ELETTRA and external laboratories went into operation. The Elettra Virtual Collaboratory (EVC) is a collaborative virtual environment (i.e., a computer system that supports human to human and human to machine communication and collaboration) for X-ray experiments at the Elettra Synchrotron Light Laboratory, Trieste, Italy. The EVC allows a distributed team of researchers to share experimental data, exchange ideas, discuss problems, from data collection to results publication.

Connecting to https://evc.elettra.trieste.it/ with a web browser it is possible to enter the EVC environment. A new user can easily register from any PC workstation at ELETTRA filling in a dedicated form in the EVC web page. An already registered user then can login, open a new project folder, add new members, who will share all the information and files of the project, and operate on all projects he takes part in. However, we note these actions can only be carried out from an ELETTRA intranet workstation.

From home a registered user can download the experimental data via web browser, work on them and perform a data backup in his own PC workstation: thus a researcher can partecipate in an experimental session even if not physically present at ELETTRA. In the near future, it will also be possible to perform the data reduction online, through the web browser.

A system for data backup on DVD is also available on the EVC workstation at the SAXS beamline. For more informations, please have a look at the EVC web page, https://evc.elettra.trieste.it/

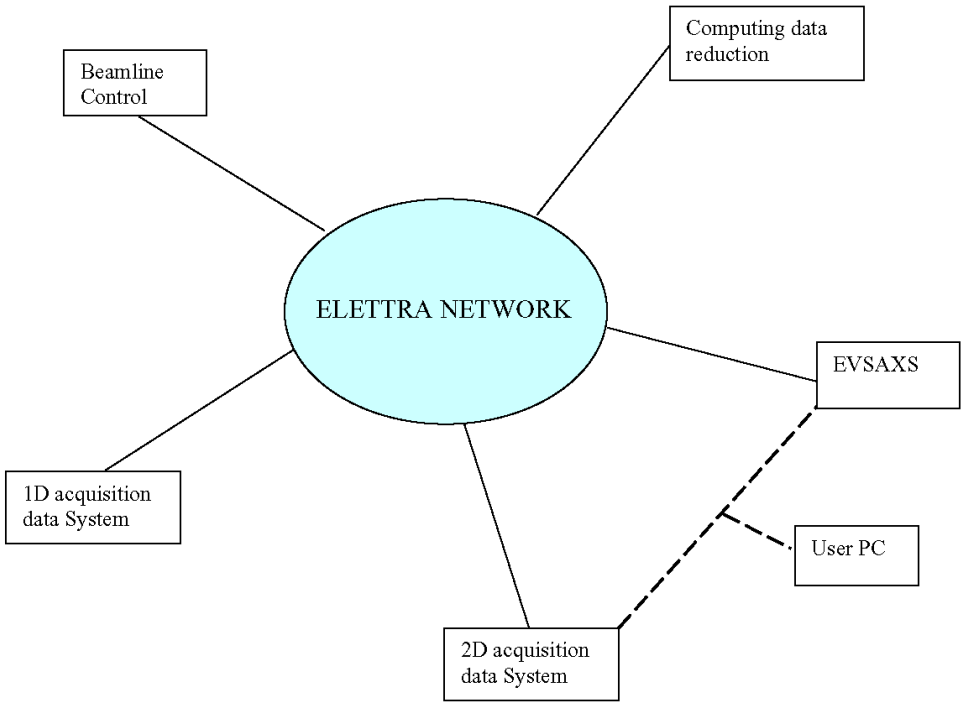

Figure 4. Overview of the local network of the SAXS beamline at ELETTRA

4. Site laboratories

In August 2002 our new chemistry and X-ray laboratory went into operation. The 70 m^2 big laboratory is divided in two parts, in which the bigger share of 43 m^2 is occupied by the chemistry lab. This unit serves mainly for sample preparation and analysis for both, in house research and external SAXS user groups. In the X-ray laboratory the set-up of a SWAX camera for simultaneous small and wide angle scattering has been completed (Hecus X-ray Systems, Graz, Austria: www.hecus.at), which allows on-site testing of samples before moving on to the SR beamline. The chemistry lab is meanwhile equipped with:

- micro centrifuge (max. 13200 rpm; model 5415D from Eppendorf , Hamburg, Germany)
- chemical fume hood (model GS8000 from Optolab, Concondordia, Italy)
- vacuum drying oven (min. pressure 1 mbar; max. T: 200 °C; Binder WTB, Tuttlingen. Germany)
- balance (min.-max.: 0.001 - 220 g; model 770 from Kern & Sohn, Balingen, Germany)
- magnetic stirrer with heating plate and a vortexer for microtubes (model MR 3001 and REAX; both from Heidolph, Schwabach, Germany)
- two water baths (the model Unistat CC is freely programmable in range from -30 to 100 °C from Huber, Offenburg, Germany; the model M3 from Lauda can only heat; Lauda-Könighofen, Germany)
- ultrasonic bath (VWR International, Milano, Italy)

Further, two working benches (one with a water sink), two fridges and a separate freezer (- 20 °C), standard glassware, syringes and needles of different sizes, µ-pipettes (10 - 50 - 200 - 1000), as well as some standard solutions (e.g., chloroform, ethanol, methanol) and de-ionized water are available.

Figure 5.
Typical lab activity: Barbara Sartori loads the centrifuge (September 2003).

5. Available sample manipulations stages

1. General

Usually the sample is mounted onto the sample alignment stage which allows the user to place the sample into the beam with a precision of 5 µm (resolution: 1 µm). In Fig. 4 the ranges for vertical and horizontal alignment as well as the maximum dimensions of the sample holders are given. The maximum weight on the sample stage is limited to 10 kg. In case the envelope dimensions of a sophisticated sample station provided by the users are slightly larger than those given in Fig. 4, the user can ask the beamline responsible for a check up of his space requirements. If it does not fit at all to these specifications, user equipment can also be mounted directly onto the optical table, which allows much larger spatial dimensions.

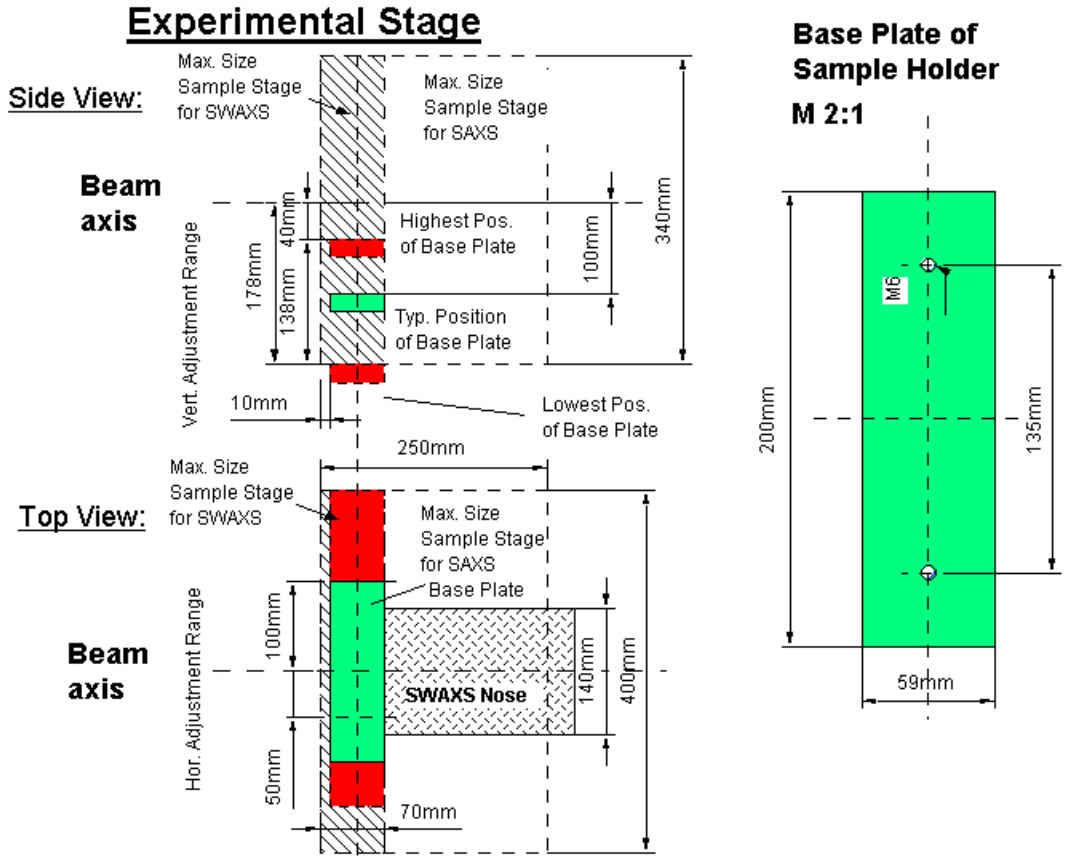

Figure 6. Maximum dimensions and alignment range of the sample holder to be mounted via a base-plate onto the standard alignment stage (left), and dimensions of the base-plate (right).

2. Sample holders

As standard equipment for liquid samples Paar capillaries (diameter: 1 and 2 mm) are used thermostated with the KHR (electrical heating) or KPR (Peltier heating/cooling) sample holders (Anton Paar, Graz, Austria). For use in these sample holders flow through capillaries and Gel holders are standard equipment. Temperature scans can be performed with KHR and/or KPR in the range from 0 to 150 °C, typically the precision and the stability of this systems is < 0.1 °C. Additionally thermostats for temperature control or cooling proposes can

be used at the beamline (0-95 °C, at present). Helium and Nitrogen gas bottles are available at the beamline, for other gases please contact the beamline responsible.
Multiple-sample holders can be mounted onto the standard sample manipulator. At present holders are available for measuring in automatic mode up to 30 solid samples at ambient temperature or up to 4 liquid or gel samples in the temperature range 0 – 95 °C.

3. Online exhaust system

At the experimental station is available a custom-built fume cover and chemical exhaust system for toxic gases. Thus it is possible to e.g. study in-situ chemical reactions, during which toxic gases might develop.

4. Magnet System

For studying magnetic effects in samples, capillaries or sample holders with suitable dimensions can be mounted inside an electromagnet. Up to now a sample holder for standard Paar capillaries (Anton Paar, Graz, Austria) is available for ambient temperature only. The alignment of the magnetic field is horizontal or vertical (transversal to the photon beam). For short times the maximum magnetic field can be up to 1.5 T, and 1.0 T for continues operation, respectively, assuming a pole gab of 10 mm for both.

5. Stopped Flow Apparatus

A commercial stopped flow apparatus (manufactured by Bio-Logic, Paris, France), especially designed for Synchrotron Radiation SAXS investigations of conformation changes of proteins, nucleic acids and macromolecules, is available. The instrument consists of a 4 syringe cell with 3 mixer modules manufactured by Bio-Logic. Each syringe is driven independently from the others by an individual stepping-motor, which allows a high versatility of the mixing sequence (flow-rate, flow duration, sequential mixing). For example, injection sequences using one or up to 4 syringes, unequal filling of syringes, variable mixing ratio, reaction intermediate ageing in three- or four-syringe mode etc.. The solution flow can be entirely software-controlled via stepping motors, and can stop in a fraction of a millisecond.

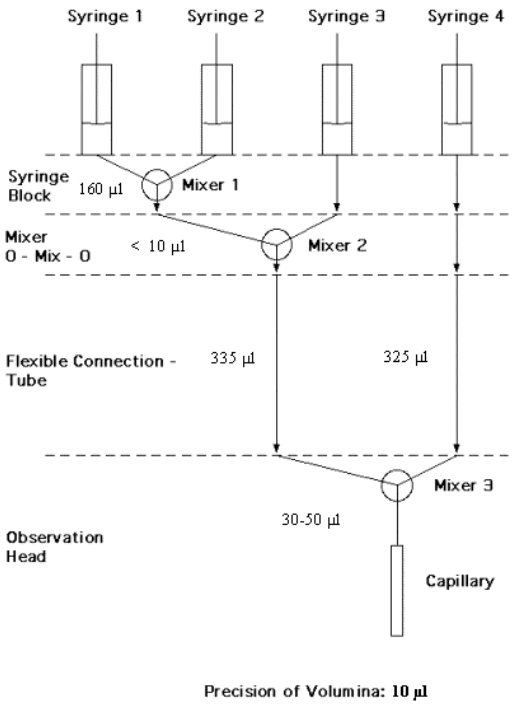

The software allows the set-up of the shot volumes of each of the 4 syringes in a certain time interval. Up to 20 mixing protocols can be programmed. Additionally macros for the repeated execution of individual frames can be defined. Furthermore, the input and output trigger accessible for user operation can be programmed. In the usual operation modus the start of rapid mixing sequence is triggered from our X-ray data-acquisition system (input trigger).

After the liquids have been rapidly mixed, they are filled within few ms into a 1 mm quartz capillary - situated in the X-ray beam- , which is thermostated with a water bath. Depending on the diffraction power of the sample time resolutions of up to 10 ms can be obtained.

Figure 7. Sketch of the stop flow system.

The main parameter of the system are:

- Thermostated quartz capillary (1 mm)
- Temperature stability 0.1 °C
- Total sample used per mixing cycle (shot volume): 100 µl
- Maximum 2θ angle of 45°
- Total Volume 8 ml
- Dead volume 550 µl
- Speed: 0.045 – 6 ml/s
- Duration of flow 1 ms to 9999 ms/Phase
- Dead time: 1 ms
- Reservoir volume: 10 ml each

Further information can be found in the homepage: http://www.bio-logic.fr/

6. Grazing Incidence Small Angle X-ray Scattering

Grazing incidence studies on solid samples, thin film samples or Langmuir-Blodget-films can be performed using a specially designed sample holder, which can be rotated around 2 axes transversal to the beam. Furthermore the sample can be aligned by translating it in both directions transversal to the beam. The precisions are 0.001 deg for the rotations and 5 µm for the translations. Usually the system is set to reflect the beam in the vertical direction. According to the required protocol and the actual assembly of the rotation stages ω, θ, 2θ and φ scans can be performed.

7. Temperature Gradient Cell

A temperature gradient cell for X-ray scattering investigations on the thermal behaviour of soft matter manybody-systems, such as in gels, dispersions and solutions, has been developed. Depending on the adjustment of the temperature gradient in the sample, on the focus size of the X-ray beam and on the translational scanning precision an averaged thermal resolution of a few thousands of a degree can be achieved.

8. IR-Laser T-Jump System for Time-Resolved X-ray Scattering on Aqueous Solutions and Dispersions

The Erbium-Glass Laser available at the SAXS-beamline (Dr. Rapp Optoelektronik, Hamburg, Germany) delivers a maximum of 4 J per 2ms pulse with a wavelength of 1.54 µm onto the sample. The laser-beam is guided by one prism onto the sample, which is filled in a glass capillary (1 or 2 mm in diameter) and Peltier or electronically thermostated in a metal sample holder (A. Paar, Graz, Austria). With a laser spotsize of maximal 7 mm in diameter a sample-volume of maximal 5.5 µl or 22 µl, respectively, is exposed to the laser-radiation. In a water-solutions/dispersions with an absorption coefficient of A = 6.5 cm^{-1} T-jumps up to 20 °C are possible.

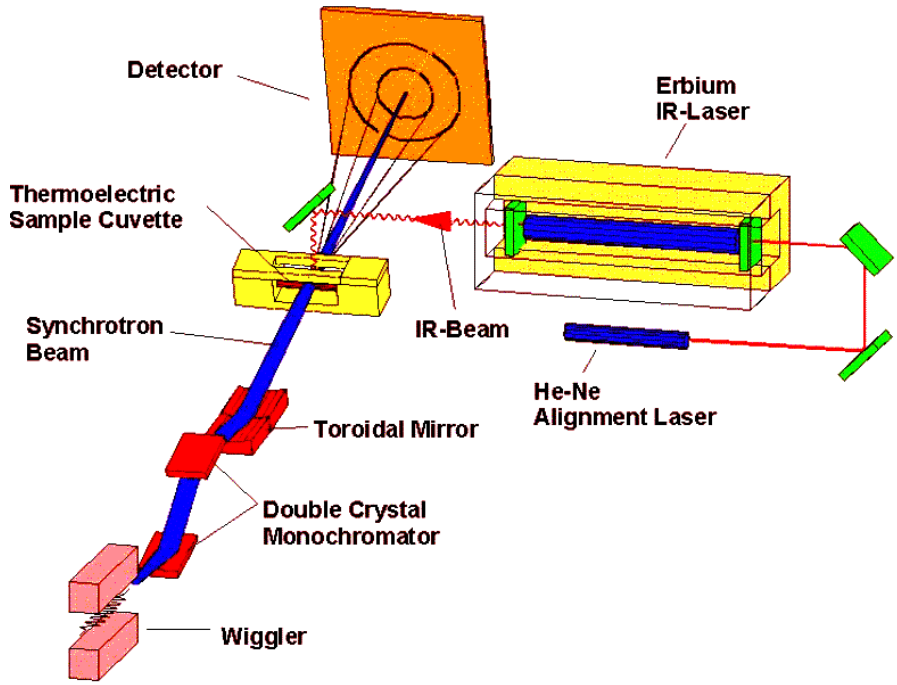

Figure 8. Sketch of the T-jump set-up.

9. High Pressure Cell System

SWAXS measurements of samples under pressure can be performed from 1 to 2500 bar, from 0 to 80 °C in the scattering angle region up to 30 degrees, both in the static or time-resolved mode, e.g. p-jump or p-scan, with a time-resolution down to the ms range. Precise pressure scans of any speed within a broad range (e.g. ca. 1.0 bar/s - 50 bar/s in the case of water as pressurising medium, and a typical sample volume) can be performed. Alternatively, dynamic processes can be studied in pressure-jump relaxation experiments with jump amplitudes up to 2.5 kbar/10ms in both directions (pressurising and depressurising jumps).

In most applications diamond windows of 0.75 mm thickness (each) are used. The transmission of one pair (entrance and exit window) is 0.1 at 8 keV, i.e. lower than 0.3, the value for the originally used 1.5 mm thick Be-windows. However the loss in intensity is more than compensated for by the considerably lower background scattering of diamond thus leading to higher q-resolution in the experiments.
The sample thickness can be 0.6-4.0 mm, with a volume of approximately 0.5-3 mm^3 completely irradiated by pin-hole collimated (< 1.0 mm diameter) X-rays.
The pressure cell system is flexible and can be built according to the needs of the particular experiment. Normally, a liquid (water, ethanol or octanol) is used as pressurising medium. But in principle, also gaseous media can be employed as well. N_2 has been successfully tested, and measurements in supercritical CO_2 became frequent.
Beside bulk measurements on samples in transmission set-up, also grazing incidence experiments using silicon wafer with highly aligned samples on its surface inserted in the high-pressure cell have been carried out successfully.

10. Oxford Cryostream Cooler

The Cryostream cooler creates a cold environment only a few millimeters from the nozzle position. The temperature and the flow of the nitrogen gas stream is controlled and regulated by a Programmable Temperatur Controller based on an 'in stream' heater and a thermo-sensor before it passes out over the sample.

The system has been especially developed for X-ray crystallography to perform diffraction experiments on e.g. shock frozen bio-crystals. However, the programmable temperature controller allows further implication for SAXS-experiments, e.g., rapid temperature drops in solvents. The design of the Cryostream Cooler facilitates:

- Nitrogen stream temperatures from -190 to 100 °C
- Stability of 0.1 °C,
- Refill without any disturbance of the temperature at the sample
- Temperature ramps can easily be carried out remotely controlled with scan rates up 6 °C/min
- Individual temperature protocols can be cycled
- T-jumps in both directions can be performed by rapid transfer of the sample in a pre-cooled or -heated capillary using an fast syringe driver reaching a minimum temperature of -80 °C. Here, typical scan rates are about 15 °C/sec with a total process time in the order of 10 sec.

11. In-line Differential Scanning Calorimeter (DSC)

The in-line micro-calorimeter built by the group of Michel Ollivon (CNRS, Paris, France) allows to take simultaneously time-resolved synchrotron X-ray Diffraction as a function of the Temperature (XRDT) and high sensitivity DSC from the same same sample.
The microcalorimetry and XRDT scans can be performed at any heating rate comprised between 0.1 and 10 °C/min with a 0.01 °C temperature resolution in the range -30/+130 °C. However, maximum cooling rates are T dependent and 10°C/min rates cannot be sustained below 30°C since cooling efficiency is a temperature dependent process. Microcalorimetry scans can be recorded independently, and also simultaniously, of X-ray patterns. The

microcalorimeter head can also be used as a temperature controlled sample-holder for X-ray measurements while not recording a microcalorimetry signal. Isothermal microcalorimetry is also possible when a time dependent thermal event such as meta-stable state relaxation or self-evolving reaction, is expected. The sample capillaries have a diameter of 1.5 mm and are filled over a length of 10 mm.

12. The 2D CCD-camera system

The CCD has a 115 mm diameter input phosphor screen made of a gadolinium oxysulphide polycrystalline layer. The screen is coupled by means of a fiber optic to the image intensifier. The image intensifier is coupled again with an additional taper to the CCD itself. The achieved spatial resolution of a pixel is 79 μm for the whole set-up.
The number of pixels is 1024 x 1024 and they can be pinned down to 2 x 2 and 4 x 4. The dynamic range of the CCD is 12 bit. The dark current of the CCD is in the order of 100 ADU (off-set) and the readout noise (read out speed: 10 MHz) is in the order of 6 ADU. (The CCD is cooled by multistage Peltier element for reducing the dark noise.) The intensifier gain is adjustable between 200 and 20000 photons full dynamic range. Typical readout times and exposure times are 150 ms and 100 ms, respectively. The readout times can be reduced down to 100 ms by using the pinning mode of the CCD. Between the frames additional wait times can be programmed e.g. for reducing the radiation damage in the sample or to extend the time for measuring long time processes.
For the external control a TTL trigger signal is provided (active low, when the CCD is accumulating an image), which is used to control the electromagnetic fast shutter of the beamline on one hand. On the other hand this signal can be used also to trigger processes as requested by the user.
The CCD is controlled by Image Pro+, which also includes non too sophisticated data treatment capabilities. The program is featuring a comprehensive set of functions, including:

- flat fielding/background corrections
- enhanced filters and FFT
- calibration utilities (spatial and intensity)
- segmentation and thresholding
- arithmetic logic operations
- various measurements, like surface, intensity, counts, profiles
- advanced macro management

The data are stored in 12 bit – TIFF format. At the present state up to 300 full images (1024 x 1024) can be recorded by the system, but a strict conservation of the timing sequence is maintained only for the first 15 - 17 frames until the RAM memory is full. Afterwards the images are stored in the virtual memory on the hard disk. At present a software development for the CCD readout system is under way to improve the stability of the readout cycles.
For the complete treatment of the 2D data Fit2D available from the ESRF is used, which is able to perform both interactive and "batch" data processing (homepage: http://www.esrf.fr/computing/expg/subgroups/data_analysis/FIT2D/index.html, programmed by Dr. Andy Hammersley), which supports a complete spatial correction, flat field correction and background correction. Furthermore more elevated data-treatment can be performed within this software package, like circular integration, segment integration and similar.

13. Tension cell

Together with the external user group Schulze-Bauer/Holzapfel the research team constructed a general-purpose tension cell. This particular cell was designed for *in-situ* tensile testing with the particular feature that the sample could be completely immersed in a solvent (e.g. physiological solution), which is of particular interest for the blood vessel or collagen fiber testing. The sample container can be attached to a thermal bath to control the temperature in the range from 5 to 95 ºC. A screw with an appropriate opening for the passage of the X-ray beam can adjust the optical thickness of the sample container continuously and optimize the set-up for different sample geometries.
The fully remote controlled system allows to control not only the fiber extension from 0 to 50 mm, but also it records simultaneously the force signal in the range from 0 to 25 N and as an option the optically determined Video extensometer signal to measure the transversal contraction of the sample.

User Contributions

1. Materials Science

USE OF COMBINED SAXS AND SANS TO THE STUDY OF SELF-ASSOCIATION OF BLOCK COPOLYMERS IN AQUEOUS SOLUTION

V.K. Aswal,[1] P.S. Goyal,[2] S. Bernstorff[3] and J. Kohlbrecher[4]

1.) Solid State Physics Division, Bhabha Atomic Research Centre, Mumbai 400 085, India
2.) UGC-DAE-CSR, Mumbai Centre, Bhabha Atomic Research Centre, Mumbai 400 085, India
3.) Sincrotrone Trieste, SS 14 km 163.5, 34012 Basovizza, Italy
4.) Paul Scherrer Institute, CH 5232 PSI Villigen, Switzerland

There is a lot of current interest in polyethylene oxide – polypropylene oxide – polyethylene oxide (PEO-PPO-PEO) tri-block copolymers as they are widely used for various applications in the nanotechnology, pharmaceutical, textile and detergent industries. Tri-block copolymers self-associate to form micelles in aqueous solution composed of a core of PPO blocks and an outer shell consisting of PEO end blocks and water. These micelles can be formed by either increasing temperature and/or copolymer concentration at a specific concentration (critical micelle concentration) or temperature (critical micellization temperature) [1].

The dehydration of water from PPO blocks with the increase in temperature results in transformation of unimers to the micelles. This makes temperature an important parameter to control the properties of micellar solutions of block copolymers. We show the effect of addition of selective additives (e.g. salt) is similar to that of increasing temperature in the self-association of tri-block copolymers. The results are of great interest for practical applications as it may not always be possible to vary the temperature to get the required properties of these systems [2]. Use of combined SAXS and SANS is useful to the study of features of self-association of block copolymers as in SANS the scattering mostly occurs from the contrast of both the hydrophobic PPO and hydrophilic PEO parts [3], however, for x-rays the contrast is from the hydrophilic PEO part [4] and also it will be sensitive to the presence of salt [5].

SAXS experiments were carried out from the aqueous solutions of two tri-block copolymers P85 $[(EO)_{26}(PO)_{39}(EO)_{26}]$ and F88 $[(EO)_{103}(PO)_{39}(EO)_{103}]$. The amount of hydrophilic volume in F88 is much larger than in P85. The measurements were made for copolymer concentration of 5 wt % and at different temperatures in the range 20 – 60 ^{o}C. To compare the effect of different salts, the measurements were made for different salts KCl, KBr, KI, NaBr and CsBr, with the varying concentration in the range 0 – 1000 mM and at a constant temperature 20 ^{o}C.

Figure 1 shows the SAXS data on 5 wt% P85 block copolymer solution at varying temperatures. The inset shows the corresponding SANS data. The low scattering in both SAXS and SANS data at 20 ^{o}C is an indication that the block copolymers at this temperature are dissolved as unimers. As the temperature is increased, the self-association of block copolymers to micelles gives rise to increase in the scattering intensity. It is interesting to note that the scattering features of SAXS and SANS data are markedly different. In particular, the peak at the larger Q values is only seen in the SAXS data. This suggests while neutrons see the whole micelle, the x-rays only see a shell. This can be explained in terms of quite different interactions of neutrons and x-rays with matter. The neutrons interact with the nuclei, whereas x-rays with the electrons. For neutrons the scattering length of hydrogen and deuterium is quite different and the contrast is obtained by preparing the samples in D_2O. It turns out that the polymer has a scattering length density close to zero whereas D_2O has a large scattering length density. For x-rays the contrast is due to electron density. Usually, organic polymers have electron densities, which are quite close to the electron density of water. Therefore, the contrasts are very sensitive to the actual value of the specific volume of the polymer. Accurate density measurements suggest that in PEO-PPO-PEO copolymers, the main contrast is from the PEO blocks. This confirms that it is PEO, which is observed in SAXS. The effect of

temperature on F88 block copolymer solution (Figure 2) also shows the similar features (Figure 1) but less pronounced as compared to P85 because of the higher hydrophilicity of the block copolymer.

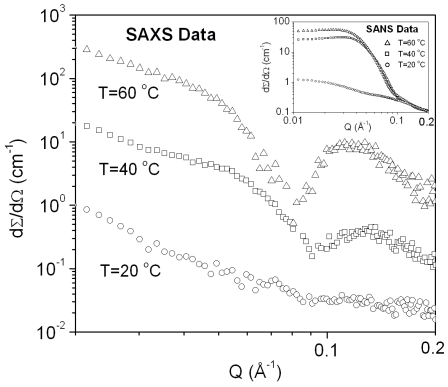

Figure 1. Small-angle scattering data from 5 wt% P85 at varying temperatures

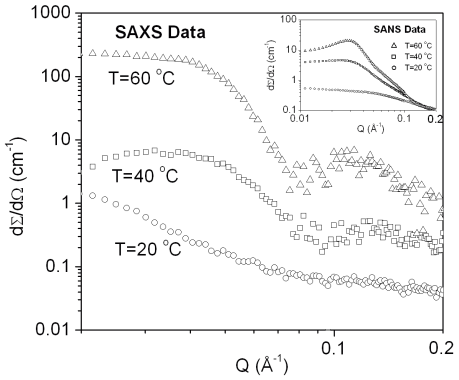

Figure 2. Small-angle scattering data from 5 wt% F88 at varying temperatures

Figures 3 and 4, respectively, show the small-angle scattering data from 5 wt% P85 and F88 block copolymer solutions in presence of varying concentration of salt KCl. The measurements were performed at low temperature 20 ^{o}C, so that the effect of temperature on the self-association of block copolymer is minimized. It is observed that the presence of salt is similar to that of increasing the temperature of the solution. The scattering intensity increases significantly with the presence of salt as with the increase in temperature. At low temperature and without presence of any salt, the block copolymers are dissolved as unimers and thus the scattering from the solution is quite low. The scattering intensity increases since the unimers self-associate to form large micelles. The addition of salt plays important role as entropically it favors the dehydration of water attached to the block copolymer similar to that of increasing the temperature.

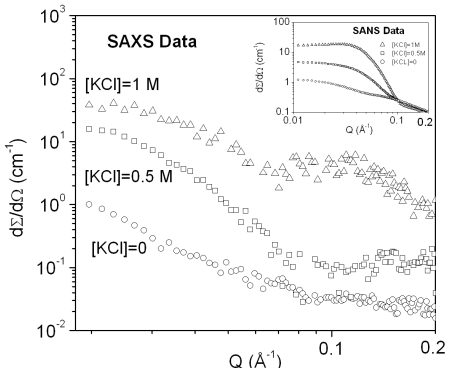

Figure 3. Small-angle scattering data from 5 wt% P85 in presence of varying KCl

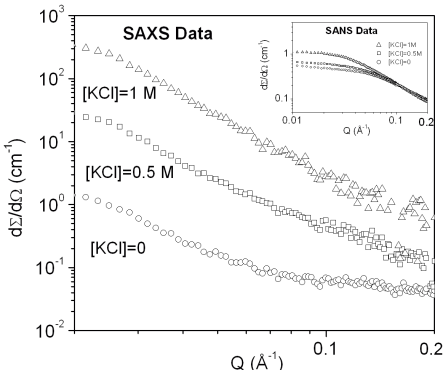

Figure 4. Small-angle scattering data from 5 wt% f88 in presence of varying KCl

References:

[1] K. Mortensen, Polym. Adv. Technol. 12, 2 (2001)
[2] V.K. Aswal, P.S. Goyal, J. Kohlbrecher, P. Bahadur, Chem. Phys. Lett. **349**, 458 (2001)
[3] N. Jain, V.K. Aswal, P.S. Goyal, P. Bahadur, J. Phys. Chem. B **102**, 8452 (1998)
[4] O. Glatter, G. Scherf, K. Schillen, W. Brown, Macromolecules **27**, 6046 (1994)
[5] V.K. Aswal et al., Chem. Phys. Lett. **329**, 118 (2000)

ION-BEAM SYNTHESIZED GERMANIUM QUANTUM DOTS

U.V. Desnica[1], P. Dubcek[1], K. Salamon[2], I.D. Desnica-Frankovic[1], M. Buljan[1], S. Bernstorff[3], U. Serincan[4] and R. Turan[4]

1.) R. Boskovic Institute, Bijenicka 54, 10000 Zagreb, Croatia
2.) Institute of Physics, 10000 Zagreb, Croatia
3.) Sincrotrone Trieste, SS 14 km163,5, 34012 Basovizza, Italy
4.) Middle East Technical University, Ankara, Turkey

There is an intense research activity going on to develop technology for an efficient and controllable synthesis of nanocrystals or quantum dots (QDs). This, because their particular properties can be tailored through the control of the size of the QDs due to quantum confinement effects [1-3]. Specifically, physical properties of Ge nanocrystals (Ge QDs), like tunable absorption, intense photo- and electroluminescence and third-order optical nonlinearities, are particularly strongly dependent on QDs size [4], which enables tunability of the nano-Ge band-gap over a considerable part of the visible light wavelength-range. This makes Ge QDs suitable for electronic, optoelectronic and photonic applications, like in sensor technology, for integrated opto-couplers in microsystems in biotechnology, for electronic nonvolatile memories, graded solar cells, etc [1].

We present results obtained by the Grazing Incidence Small Angle X-ray Scattering (GISAXS) technique which was used to study the synthesis and properties of Ge nanoparticles obtained by implantation of high doses (up to $1x10^{17}/cm^2$) of Ge atoms into SiO_2 substrate [1]. Ge QDs are formed when, by subsequent thermal annealing, Ge atoms become de-mixed and aggregated into Ge nanoparticles. Well defined GISAXS Ge QDs-related signals were obtained, examples of which are shown in Fig. 1, left. The shape, size, inter-particle distance, spatial correlation (Fig. 1, Table) and depth profiling (not shown) of such QDs were determined. From Fig. 1 we infer that 3D arrays of Ge QDs were formed; these QDs are spherical, and are distributed isotropically in the subsurface layer of SiO_2 (up to T_a= 800° C). After T_a = 1000° C, fast diffusion processes lead to the spatial de-correlation of QDs and to the formation of large QDs (larger than 10 nm) intermixed with small QDs (in the sub- 2 nm size range).

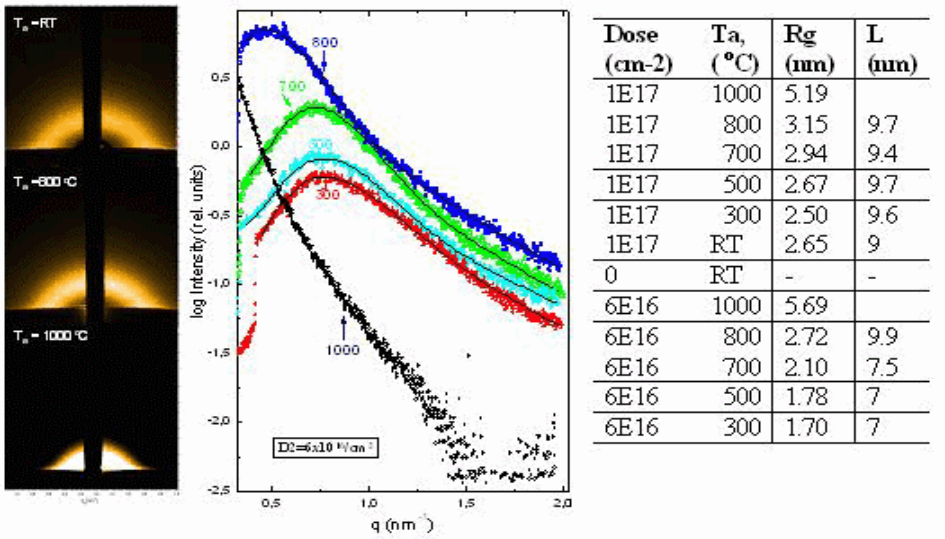

Dose (cm-2)	Ta, (°C)	Rg (nm)	L (nm)
1E17	1000	5.19	
1E17	800	3.15	9.7
1E17	700	2.94	9.4
1E17	500	2.67	9.7
1E17	300	2.50	9.6
1E17	RT	2.65	9
0	RT	-	-
6E16	1000	5.69	
6E16	800	2.72	9.9
6E16	700	2.10	7.5
6E16	500	1.78	7
6E16	300	1.70	7

Figure 1. GISAXS results: left: 2D spectra for three selected annealing temperatures T_a; right: Vertical cross-sections of 2D spectra for Ge ion dose D2=6× 10^{16} /cm^2, and annealed at various T_a; for 1h in N_2**.** The fits depict LMA results, using a log-normal size distribution, and a single width distribution s = 0.9 in all fits. Table: Rg denotes the Guinier radius of Ge QDs and L the inter-particle distance.

Complementary information on the examined QDs were obtained using additional methods, see Fig. 2. The successful introduction of Ge atoms into SiO_2 substrate was determined by Rutherford back-scattering (RBS), which also confirmed that there was no considerable diffusion or loss of Ge atoms due to post-implantation annealing. The formation of the second phase as QDs in the SiO_2 substrate was determined by low-frequency Raman (LFR) and Transmission Electron Microscopy (TEM). The chemical nature of QDs as Ge phase was identified by the appearance of Ge-related signals at characteristic angles in grazing incidence X-Ray Diffraction (XRD) and from the characteristic a-Ge vibrational band or TO crystalline Ge vibrational mode in Raman spectroscopy. In as implanted SiO_2 the Ge QDs were amorphous, but they crystallize after annealing in the T_a = 500-800 ^oC range.

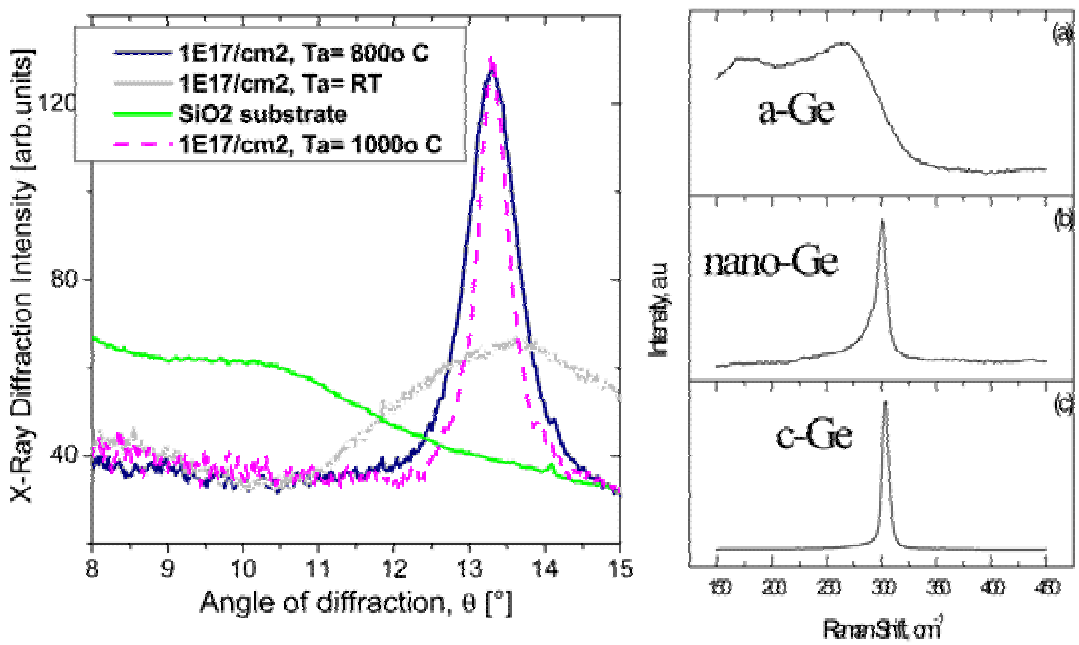

Figure 2a. Left: XRD for Ge ion dose D1= $10^{17}/cm^2$: after T_a =1000 ^oC, the sharp peak at θ = 13.6^o is related to the <111> Ge reflection, and suggests large QDs. In the as-implanted sample, the peak is drastically broadened, indicating that Ge QDs are synthesized but that they are highly disordered, probably amorphous. Right: Raman for Ge ion dose D1=$10^{17}/cm^2$: before annealing: a-Ge related signal, after annealing (at 800 ^oC) – TO mode of Ge QDs, bulk Ge: -TO mode of Ge.

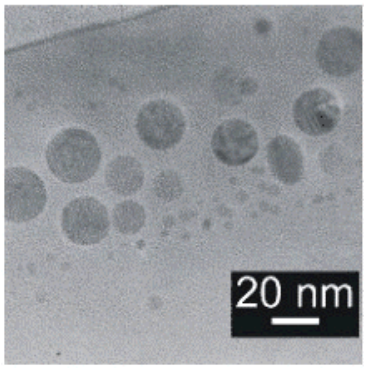

Figure 2b. TEM image of a SiO_2 film implanted with a $1x10^{17}$ cm^{-2} dose of Ge ions after annealing for 1h at 900 °C under N_2.

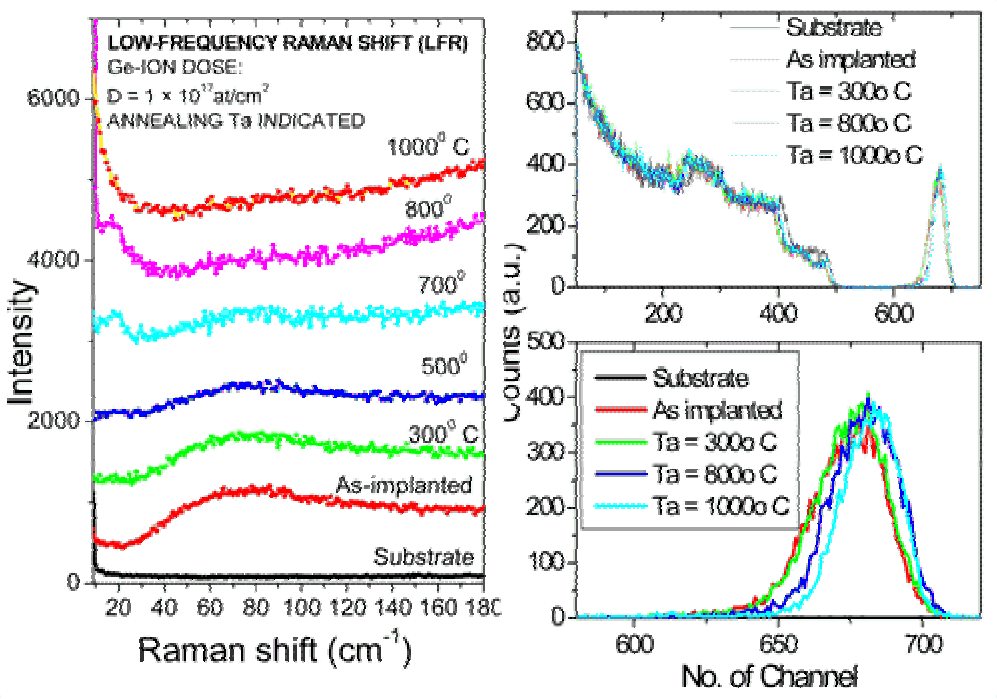

Figure 2c. Left: The LFR broad band indicates the formation of QDs in SiO_2. Right: RBS - Ge atoms are clearly seen in SiO_2, minimal change with annealing

This work was a successful continuation of previous work performed at the SAXS beamline in Elettra (presented in the ELETTRA Highlights 2000-2001, p.33, and in the SAXS Annual Report 2000-2003), in which 3D arrays of various semiconductor QDs (primarily binary semiconductors, like CdS, CdTe, ZnTe, CdSe or PbTe) formed by implantation of constituent atoms into the subsurface layer of light matrices (amorphous SiO_2, hexagonal Al_2O_3 or cubic, monocrystalline silicon) were studied with GISAXS and complementary methods [6-7]. A full characterization of these QDs, their morphology, average size, and size distribution, and their self-organization into 3D ensemble in the shallow implanted substrate layer was obtained, as a function of implantation and post-implantation treatment parameters. Those are very important pieces of information since through the control over the size of QDs many other properties of these "new materials" can be controlled.

References:

[1] W. Scorupa, L. Rebohle, T. Gebel, Appl. Phys. A 76, 1049-1058, (2003)
[2] A. Meldrum, R.F. Haglund, Jr., L.A. Boatner, C.W. White, *Advanced Materials* 13, 1431 (2001)
[3] J.D. Budai, C.W. White, S.P. Wiothrow, M.F. Chisholm, J. Zhu, R.A. Zuhr, *Nature* 390, 384-85 (1997)
[4] C. Boested, T.van Buuren, T.M. Willey, N. Franco, L.J. Terminello, C.Heske, T.Moeller, *Apl. Phys. Lett.*, 84, 4056-58 (2004)
[5] U V. Desnica, P. Dubcek, K. Salamon, I.D. Desnica-Frankovic, M. Buljan, S. Bernstorff, U. Serincan, R. Turan, *Nucl. Instr. Methods Phys. Res. B*, in press. (2005)
[6] U. V. Desnica, M. Buljan, I.D. Desnica-Frankovic, P. Dubcek, S. Bernstorff, M. Ivanda, H. Zorc, *Nucl. Instr. Methods Phys. Res. B*, 216, 407-413 (2004)
[7] U. V. Desnica, P. Dubcek, I.D. Desnica-Frankovic, M. Buljan, S. Bernstorff and S.W. White, *J. Appl. Cryst.*, 36, 443-446 (2003), and other references therein

GISAXS INVESTIGATION OF COLLOIDAL $CoPt_3$ NANOPARTICLE FILMS

J. I. Flege[1], Th. Schmidt[1], I. Randjelovic[2], V. Aleksandrovic[2], G. Alexe[1], T. Clausen[1], S. Bernstorff[3], A. Kornowski[2], H. Weller[2] and J. Falta[1]

1.) Institute of Solid State Physics, University of Bremen, Otto-Hahn-Allee 1, 28359 Bremen, Germany
2.) Institute of Physical Chemistry, University of Hamburg, Grindelallee 117, 20146 Hamburg, Germany
3.) Sincrotrone Trieste, Strada Statale 14, km 163.5, 34012 Basovizza/Trieste, Italy

The preparation of ordered arrays of nanoparticles has attracted a tremendously increasing interest in the last years due to their wide range of potential applications e. g. in opto-electronics, ultra-dense magnetic storage devices and catalysis [1]. In this respect, the "bottom-up" concept of two-dimensional self-assembly of ex-situ prepared quantum dots from colloidal solutions with well-defined electronic properties is very promising for industrial use. In comparison to the alternative "top-down" approach which comprises a lithographic patterning process in which the required lateral resolution has to be enhanced to the near-atomic scale, using self-organization would allow the manufacturing of highly-integrated devices at reasonable costs. However, for an efficient and optimized fabrication of dense nanoparticle films a thorough structural characterization of the prepared overlayers as function of the parameters governing the preparation process is necessary. Grazing-incidence small-angle x-ray scattering (GISAXS) represents an ideal tool for the characterization of the ordering properties with both high spatial resolution and statistics.

The samples were prepared as follows: $CoPt_3$ nanoparticles of well-defined size and shape were synthesized via the simultaneous reduction of $Pt(acac)_2$ and thermal decomposition of $Co_2(CO)_8$ in a high-boiling coordinating solvent mixture of hexadecylamine-diphenyl ether, as described elsewhere [2]. For a given set of preparational parameters, this procedure results in the formation of monodisperse (standard deviation of size distribution functionbetween 5% to 10%) spherical $CoPt_3$ nanoparticles with adamantane carboxylic acid (ACA) and hexadecylamine as ligands of which the ACA molecules were exchanged to sorbic acid (SA) [3]. In the case presented here, particles with a size of 5.2 nm were grown as determined by x-ray powder diffraction [2]. After the redissolution of the nanocrystal precipitate in a non-polar solvent the colloids were deposited on commercial Si(001) wafers covered by native SiO_2 using a commercial Langmuir-Blodgett trough by retracting the substrate from the compressed monolayer. In the course of the present study, the retraction speed was varied in order to deduce its influence on the structural properties of the overlayer. These results were compared to real-space images obtained employing a commercial high-resolution scanning electron microscope (SEM).

The GISAXS experiments were performed at the SAXS beamline using 8 keV photons irradiated on the sample at a grazing angle of 0.6°. The 2D scattering pattern was recorded using a CCD camera (1024×1024 pixels). A semi-transparent aluminum absorber foil was incorporated in order to attenuate the diffuse scattering intensity and the strong specular reflectivity at $q_{\parallel} = 0$. Figure 1a shows a GISAXS pattern for a sample prepared with a retraction speed of 1 mm/min. The bright satellite spots at $q_{\parallel} = 0.76\ nm^{-1}$ are a direct evidence for a lateral correlation of the $CoPt_3$ nanoparticles adsorbed on the SiO_2 surface. Moreover, the shape of the scattering features under consideration is rod-like with decreasing intensity in the $+q_{\perp}$ direction which is compatible with the model of a monolayer of nanoparticles. From inspection of the data displayed in Table 1, it is evident that the average inter-particle distance and the correlation length of the close-packed particle arrangement do not depend on the retraction speed. This suggests that these values are entirely determined by the specific type of ligands surrounding the nanoparticles and the solvent used during Langmuir-Blodgett

coating. However, the intensity drops rapidly with increasing retraction speed. Since the ordering properties of the film do not change, this can be attributed to a decrease in the total nanoparticle coverage. These findings are in accordance with information extracted from large-scale SEM images [4]. Because no fully-closed nanoparticle film was observed with SEM even for the slowest retraction speed of 1mm/min, these results indicate that higher coverages may be achieved with an even slower retraction speed.

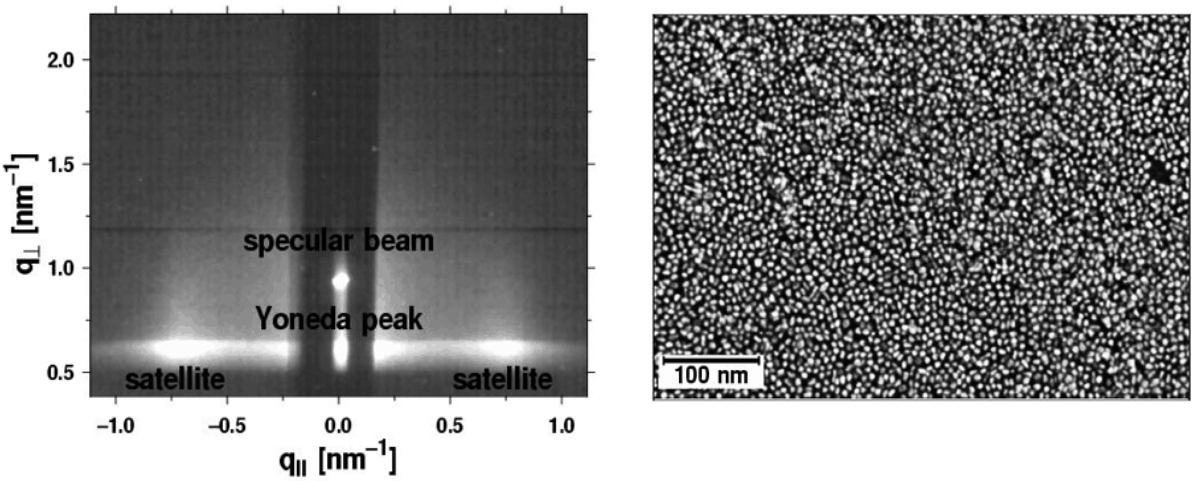

Figure 1. (a) GISAXS image of $CoPt_3$ nanoparticles adsorbed on SiO_2/Si(001) by Langmuir-Blodgett coating taken at an incident angle of approx. 0.6° using 8 keV photons. The vertical black stripe indicates the position of the semi-transparent Al absorber. **(b)** High-resolution SEM image for the same sample as investigated in (a). Nanoparticles appear bright in contrast.

Table 1. Structural parameters derived from GISAXS data as functions of the retraction speed for $CoPt_3$ nanoparticles adsorbed on SiO_2 by Langmuir-Blodgett coating.

Retraction Speed (mm/min)	Particle Distance (nm)	Correlation Length (nm)	Intensity (a. u.)
1	8.23±0.06	22.3±1.2	1.00
5	8.21±0.08	22.5±2.1	0.33
10	8.23±0.15	23.7±4.9	0.13

References:

[1] G. Schmidt, *Nanoparticles: From Theory to Application*, Wiley-VCH, Weinheim (2004)

[2] E. V. Shevchenko, D. V. Talapin, H. Schnablegger, A. Kornowski, Ö. Festin, P. Svedlindh, M. Haase, and H. Weller, Study of Nucleation and Growth in the Organometallic Synthesis of Magnetic Alloy Nanocrystals: The Role of Nucleation Rate in Size Control of $CoPt_3$ Nanocrystals, J. Am. Chem. Soc. 125, 9090-9101 (2003)

[3] V. Aleksandrovic et al., in preparation

[4] J. I. Flege, Th. Schmidt, G. Alexe, T. Clausen, S. Bernstorff, I. Randjelovic, V. Aleksandrovic, A. Kornowski, H. Weller, and J. Falta, $CoPt_3$ nanoparticles adsorbed on SiO_2: a GISAXS and SEM study, Mater. Res. Soc. Proc. 840, Q6.10.1 (2005)

TEMPERATURE-DEPENDENT PHENOMENA IN WAXY OILS

D.Ghisletti, G. Del Piero and P. D'Antona

EniTecnologie S.p.A., Via Maritano 26, 20097 San Donato Milanese, Italy

Flow Assurance is a very important issue for all the activities and business involving oil and gas transportation in pipeline. The continuous flow of hydrocarbons is an important condition for both safe and economic management of oil/gas production and delivery plants. This is true, in particular, for oil pipelines or sealines located in low temperature environments. In this case, in fact, the low temperatures present in the pipelines can lead to the separation of higher molecular-weight paraffins, mostly in the range from C_{18} to C_{65}, and create deposits which can lead to complete pipeline obstructions.

The phase stability of the wax component of crude oils (or distillates such as diesel) is defined by the Wax Appearance Temperature (WAT), i.e. the temperature at which the first wax crystals appear during cooling. Below the WAT, at a characteristic temperature called Pour Point (PP), crude oils undergo a gel transition at which the fluid displays the rheological properties of a viscoelastic solid. When the environmental temperature of the pipeline is lower than the PP, a condition frequently encountered subsea or in cold climates, a flow interruption may lead to cooling and to complete oil gelation. In this case, the successful production restart depends on the ability to pressurize the pipeline sufficiently to cause gel breakdown and flow.

In a study program about these phenomena, SAXS and WAXS experiments were performed at temperatures ranging from 50°C to 5°C on two real crude oils (later called BOURI and KITINA) and a model mixture of n-paraffins (called MIX) prepared to have a rheological behavior similar the crude oils.

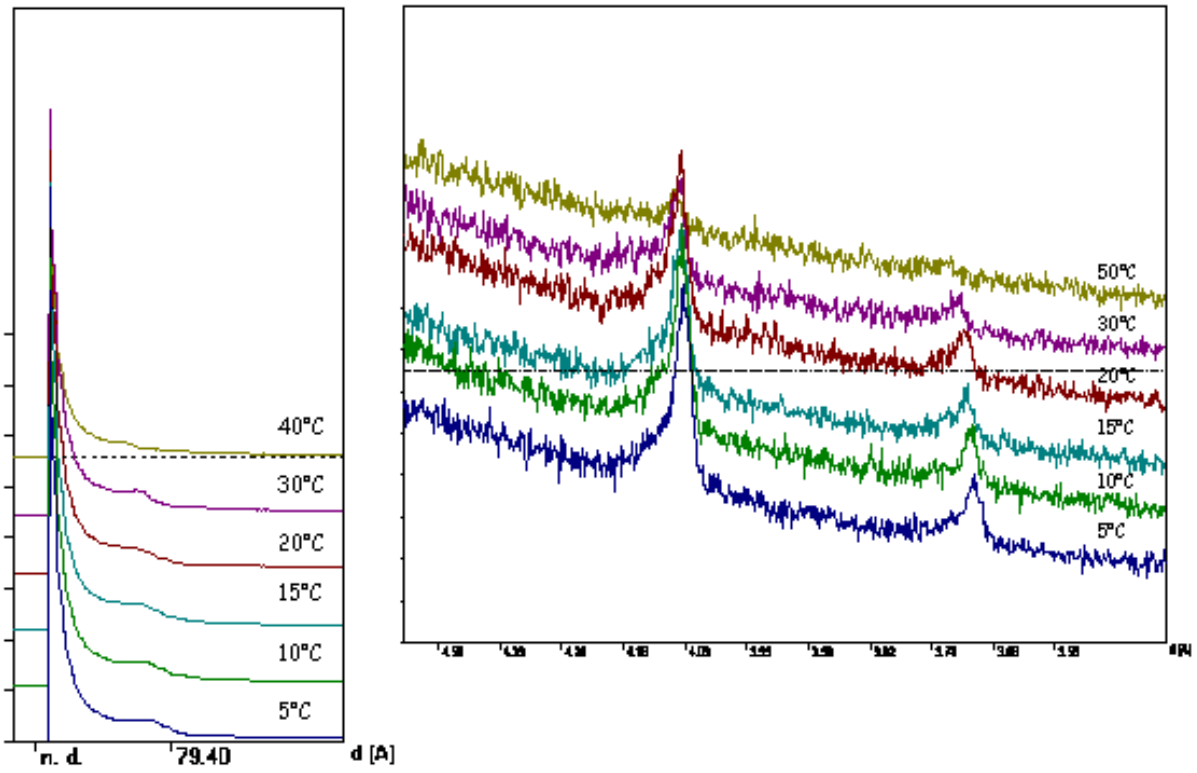

Figure 1. SAXS (left, ELETTRA) and WAXS (right, EniTecnologie) spectra for the model system MIX at different temperatures (abscissae in Å)

The objective of the study was to discriminate between the formation of isolated wax crystals and their organization into more extended structures, also comparing the behavior of the crude oils (BOURI, KITINA) and the model system (MIX).
To perform the measurements, the samples were loaded in thin capillary (ϕ = 1.5 mm) and put in a sample holder inside the heating/cooling device inserted in the ELETTRA SAXS line. The SAXS camera length was chosen at 1750 mm and the photon energy was 8 KeV.
In Fig.1 a comparisons of the SAXS and WAXS spectra acquired for M at different temperature are reported. At 40°C a small angle component already exists that can be attributed to wax crystals-ordered aggregation rather than to electronically-homogeneous wax-domains into the oil. This component increases in intensity, while shifting toward smaller spacing values (more compact structure) on decreasing temperature (Fig.2).
Even though no small angle component was observed in the SAXS spectrum at 50°C, still the paraffins begin to crystallize, as can be seen from the WAXS data (Fig.1, right). The WAXS reflections increase in intensity on cooling, since more paraffin chains get ordered.

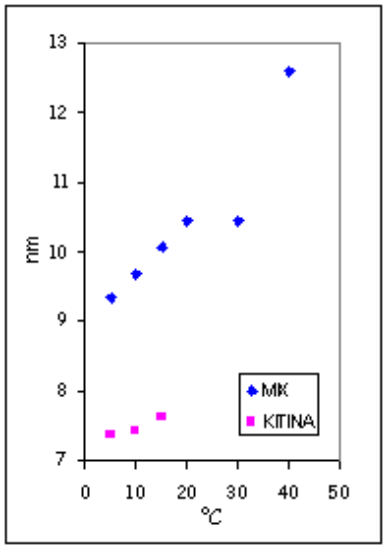

Figure2. Spacing measured from MIX's and KITINA's small angle component, at different temperatures.

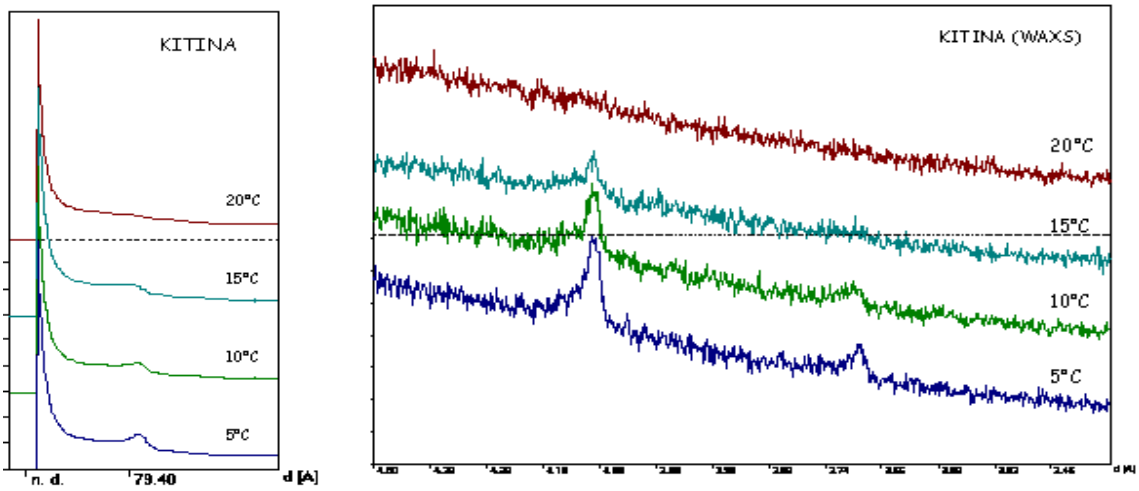

Figure 3. SAXS (left, ELETTRA) and WAXS (right, EniTecnologie) spectra for the crude oil KITINA at different temperature (abscissae in Å)

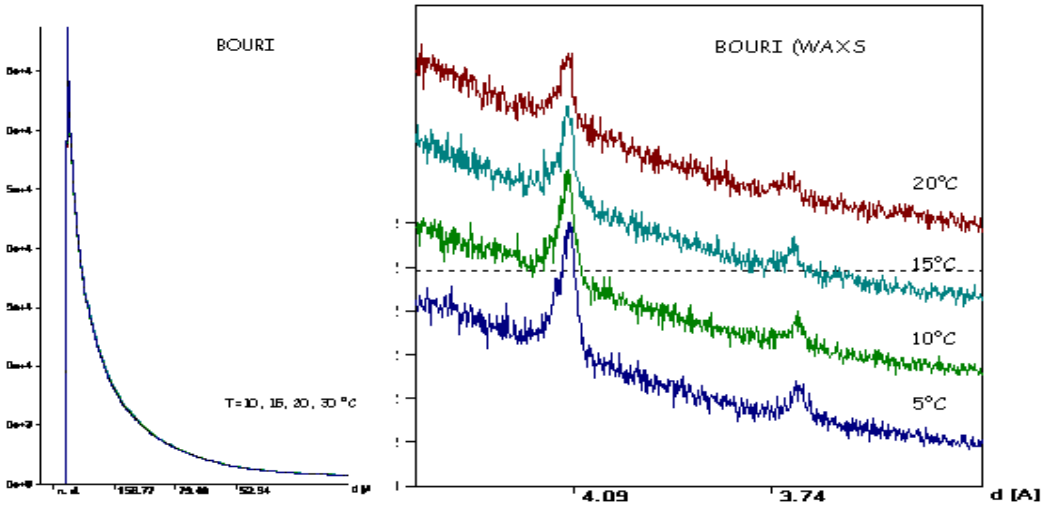

Figure 4. SAXS (left, ELETTRA) and WAXS (right, EniTecnologie) spectra for the crude oil BOURI at different temperatures. No ordering of wax crystals was observed. (abscissae in Å)

In Fig.3 and Fig.4 the analogous comparisons of SAXS and WAXS spectra respectively for the crudes BOURI and KITINA are reported.

As far as the KITINA crude is concerned, the ordering of wax crystals takes place below 20°C, right simultaneously with the beginning of crystallization, giving rise to more compact aggregation respect to what observed for MIX (Fig.2). On the contrary, no small angle components were observed for the crude B, which starts to crystallize at 20°C but without giving rise to any ordering of wax crystals.

In conclusion, the joint application of SAXS and WAXS techniques could differentiate between different crystallization and aggregation mechanisms present in the examined crude oils and may allow, in the future, the formulation of more accurate model systems.

ANALYSIS OF THE NANO-STRUCTURAL PROPERTIES OF THIN FILM SILICON-CARBON ALLOYS

D.Gracin[1], K.Juraic[1], P.Dubcek[1], A.Gajovic[1] and S. Bernstorff[2]

1.) Rudjer Boskovic Institute, 10000 Zagreb, Croatia
2.) Sincrotrone Trieste, SS 14 km 163.5, 34012 Basovizza (TS), Italy

By reducing the crystal dimensions down to nm – scale it is possible to change the optical, electrical and other properties of a material. This fact can be used in many practical applications, as solar cells, fleet screens etc. For any practical use, it is important to establish a plausible characterization procedure that enables to make the correlation between the film properties and dimension of nano-objects on one hand side, and the nano-structure and growing condition on the other hand side. In the case of thin film silicon alloys, SAXS has been successfully applied for the confirmation of the crucial role of nano-structure in opto-electrical properties, in light induced degradation, in hydrogen diffusion, phase segregation etc [1-7].

For estimating the structural properties on the nano-scale, SAXS has advantages over microscopy because it gives a certain average over the material. However, since with SAXS only objects can be detected whose electron density differs from the average electron density of the material ("particles" in / on a substrate), for a complete analysis this technique has to be combined with other methods.

In our work we studied the nano-structural properties of two series of non-stechiometric silicon carbide in a wide structural and compositional range. The first series was completely amorphous while the second was partially crystallized by thermal annealing.

For the GISAXS measurements we used a X-ray beam energy of 8 keV (λ = 0.154 nm). The samples were mounted on a stepping-motor-controlled tilting stage with a step resolution of 10^{-3} deg. The grazing angle of incidence was selected in the range $0.4° < \alpha < 1.4°$. X-ray scattering intensity spectra were acquired with a 2D position sensitive CCD detector at a detector to sample distance L = 2000 mm. The typical distribution of the 2D signal from amorphous $Si1_{-x}C_x$: H is plotted in Fig. 1, and a corresponding 1D angle distribution for a set of these $Si_{1-x}C_x$: H samples is shown in Fig 2.

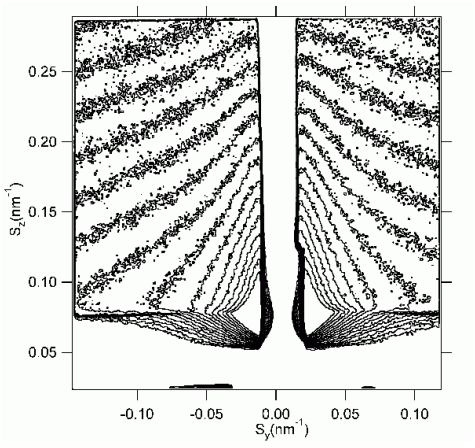

Figure 1. The typical distribution of the 2D signal from amorphous $Si1_{-x}C_x$: H

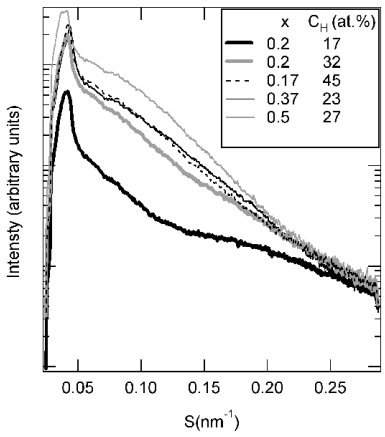

Figure 2. 1D-spectra measured on $Si_{1-x}C_x$: H with different compositions (assigned on the graph)

Both sets of specimens show a strong signal from “particles” with dimensions between 1 and 6 nm, depending on growing conditions and composition. For completely amorphous samples, the “particles” are identified as voids agglomerates consisting of a large number of smaller voids with dimensions of a few tenths of nm [8]. In favour of this assumption is the comparison between voids size and gyro radius, shown in Fig3.

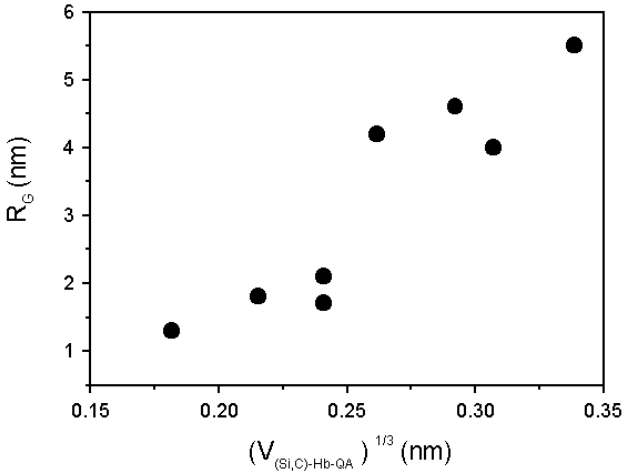

Figure 3. The radius of gyration, R_G, plotted versus cube root of the average volume of void per Si,C-H bond, $V_{(Si,C)\text{-}Hb\text{-}QA}$.

For the second set of samples, the structure is expected to be a combination of amorphous material with nano-crystalline immersions. Vibrational spectroscopy combined with Auger spectroscopy show the presence of nano-crystalline carbon particles, most probably on the surface. The analysis of the SAXS signal originating from the surface confirms the presence of objects with nanometer size but these could be also ascribed to the surface roughness. The infa-red spectroscopy shows the presence of small crystals in the bulk of the sample while Raman spectroscopy confirms the amorphous structure of the silicon tissue. That is why the nano-particles in the bulk, identified by SAXS, were ascribed to the cubic nano-crystals of SiC, embedded in amorphous silicon matrix. This assumption is further supported by comparison between “particle sizes”, R_G, and the shape of the absorption peak in the infrared corresponding to SiC crystallites as plotted in Fig 4. It shows that larger R_G correspond to smaller frequency and narrower distribution; that in turn assumes the larger size of the crystallites. However, the direct correlation between the crystallite size and the frequency of Si-C stretching vibrations is hard to do since "particles" observed by SAXS does not mean single crystals of that size [9].

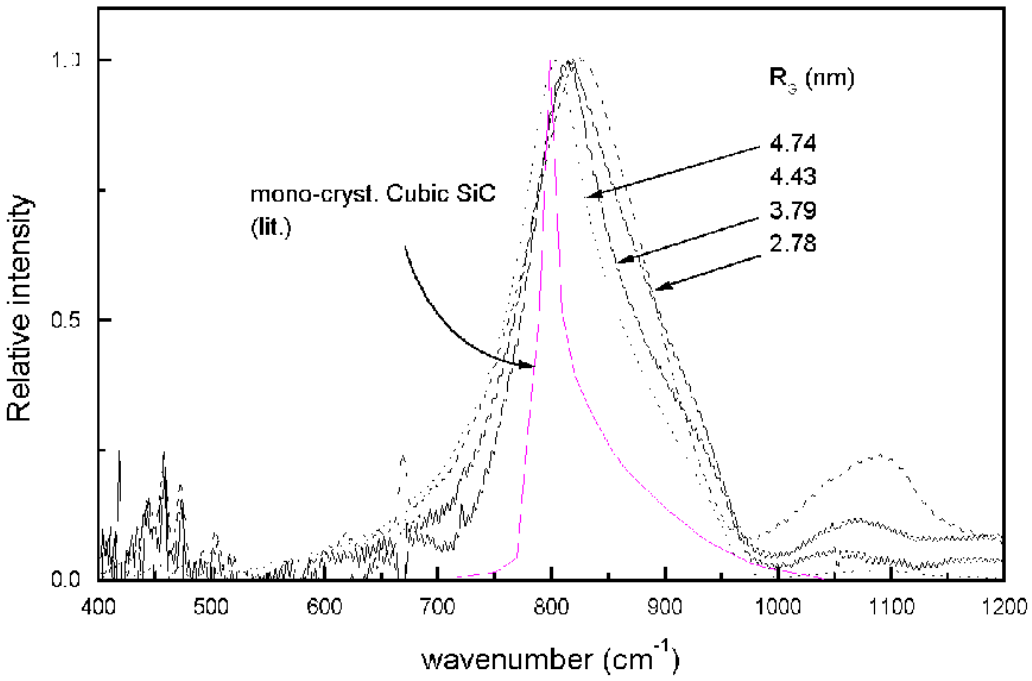

Figure 4. The infrared absorption peak corresponding to crystalline SiC vibrations for a series of $Si_{1-x}C_x$ samples after annealing at 1050^0C. The corresponding gyro radius, R_G, is denoted on each graph

References:

[1] R.J. Prado, D.R.S. Bittencourt, M.H. Tabacniks, M.C.A. Fantini, M.N.P. Carreno and I. Pereyra., J.Appl. Cryst. 30 (1997) 659

[2] D.L.Williamson, Mater.Res.Soc.Symp.Proc. 377 (1995) 251

[3] U.K. Das, J.K. Rath, D.L. Williamson and P. Chaudhuri, Jap.J.Appl.Phys. 39 (2000) 2530

[4] U.K. Das, A.R. Middya, J.K. Rath, C. Longeaud, D.L. Williamson and P. Chaudhuri J. Non-Cryst. Solids. 276 (2001) 46

[5] J. Shinar J, R. Shinar, D.L. Williamson, S. Mitra, H. Kavak and V.L. Dalal, Phys.Rev.B 60 (1999) 15875

[6] A.H.Mahan, Y. Xu, D.L. Williamson, W. Beyer, J.D. Perkins, M. Vanecek, L.M. Gedvilas and B.P.Nelson, J. Appl.Phys. 90 (2001) 5038

[7] S.J. Gurman, B.T. Williams and J.C. Amiss, Journal of Physics-Condensed Matter. 12 (2000) 5981

[8] D.Gracin, P.Dubcek, M.Jaksic, S.Bernstorff, Thin Solid Films 433 (2003) 88

[9] D.Gracin, K.Juraic, P.Dubcek, A.Gajovic, S.Bernstorff, Vacuum (accepted, to appear in 2005)

SELF-ORGANIZED GROWTH OF Ge ISLANDS ON Si(100) SUBSTRATES

B. Pivac[1], I. Kovačević[1], P. Dubček[1], N. Radić[1] andS. Bernstorff[2]

1.) R. Bošković Institute, P.O. Box 180, Zagreb, Croatia
2.) Sincrotrone Trieste, SS 14, km 163.5, Basovizza (TS), Italy

Ge islands form spontaneously on silicon substrate due to the 4.17 % lattice mismatch. This lattice mismatch causes a Ge film to undergo a layer-to-island transition, when the Ge coverage exceeds three monolayers. The three dimensional Ge (band gap 0.6 eV) islands embedded in a Si (gap 1.12 eV) matrix with a larger band gap may act as confining centers both for electrons and holes. Following island formation, the islands evolve further, undergoing a rich sequence of shape changes, till they seek the shape and composition which minimizes their free energy [1]. Following the first experimental detection of Ge so-called hut clusters on Si(100) made by Mo et al.[2], several types of islands have been observed in different systems. For better device performance, it is important to obtain islands of the same size and shape, and to find a mechanism for self-organized ordering. Despite the intensive research in the last few years, careful cataloging of the shape and size evolution of the islands as a function of growth conditions has not yet been performed.

GISAXS experiments were carried out using synchrotron radiation with wavelength λ=0.154 nm. The grazing angle of incidence was selected in the range $0.4° < \alpha_i < 1.4°$, i.e. α_i was larger than the critical angle for total external reflection of the silicon substrate $\alpha_{crit}(Si) = 0.23°$. AFM images were recorded with a Nanoscope IIIa microscope (Digital Instruments Inc., Santa Barbara, CA). All samples were imaged in tapping mode with a silicon cantilever that had a resonance frequency of 250-300kHz.

Figure 1a shows the 2D GISAXS pattern of a Ge layer evaporated on Si and annealed at 700 °C in vacuum. Figure 1b depicts a 1D vertical cut (perpendicular to the surface) of the 2D GISAXS pattern from (a). After high-temperature annealing at 700 °C the total scattering intensity increases and localizes, while the Yoneda peak decreases. The steeper decay of the intensity parallel to the sample surface compared to the perpendicular direction means that the scattering particles are flat, i.e. the lateral sizes are larger than the height. Since the signal is not distributed symmetrically around the direction of the incoming beam it is originating from particles that are distributed on the sample surface, and are not present deeper in the substrate. Furthermore, the intensity maximum has moved toward larger q. The absence of an intensity maximum other than one at q_y=0 means that there is a broad distribution in island sizes and/or that the inter particle distances are large enough that the particle-particle correlation does not pay a significant contribution to the scattering, i.e. the scattering is dominated by the form of the islands.

Qualitatively, the 2D GISAXS pattern present two large scattering lobes visible along the parallel direction (parallel with q_z) separated by the specular plane. The extent of the intensity parallel (perpendicular) to the surface is inversely proportional to the average lateral size (height) of the island. In principle, the average distance between islands can be determined from the intensity maximum, $D=2\pi/q_m$, but in case of a broad size distribution combined with a wide range of interparticle distances, there is no significant particle to particle correlation and the interference peak is missing from the spectra. To get some quantitative information about formed Ge islands we have used the Guinier's approximation. The radius of gyration

R_g has been calculated from the slope of the linear region of the I(q) versus q^2. The estimated values are R_{GL}=6.2 nm laterally and R_{GV}=2.2 nm vertically.

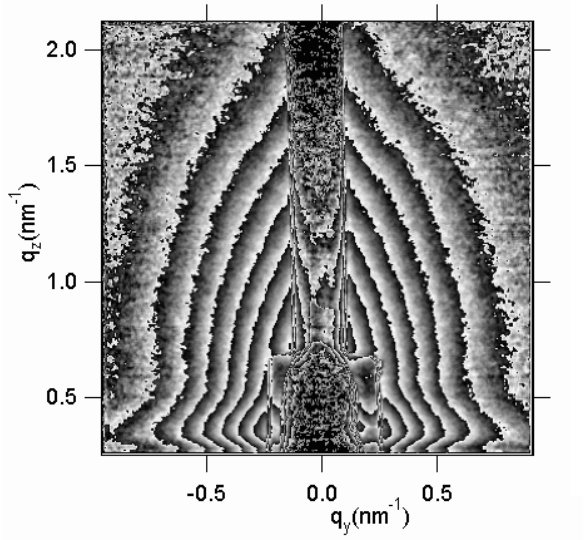

Figure 1a.. 2D GISAXS pattern of the thin Ge layer evaporated on the Si (100) substrate after annealing at 700°C for 1 h in vacuum.

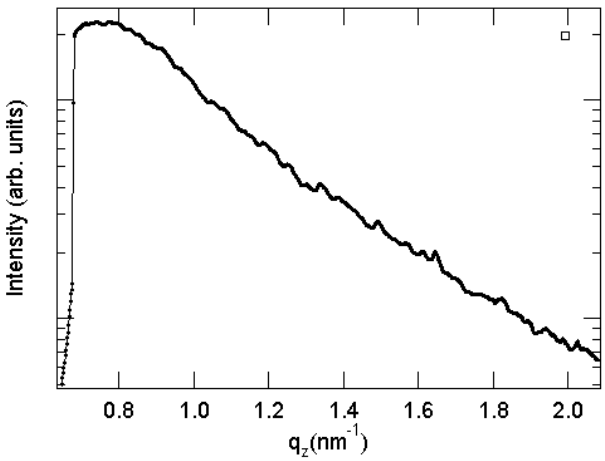

Figure 1b.. 1D vertical cut (perpendicular to the surface) of the 2D GISAXS pattern shown in Fig. 1a.

From the 2D GISAXS pattern we can make some conclusions about the morphology of the Ge islands. When all the islands have a similar shape and size, it results in a characteristic scattering pattern. The typical GISAXS pattern for spherical-shaped particles is represented by a spherical half-ring, while for pyramid-shape particles it is represented by inclined streaks. In our case, neither of those features is present. Using the information about the average size and inter-island distance as initial parameters, we have used the Fortran program IsGISAXS [3] for simulations. The best similarity to the experimental data was obtained for cylindrically shaped islands [4].

It is well known that structures like islands formed on a surface are easily accessible to different techniques that are commonly used to explore the morphology, like atomic force microscopy (AFM). Therefore, we used AFM to check our analysis with GISAXS. Figure 2 shows a typical AFM picture of a 10 nm Ge layer evaporated on a Si (100) substrate heated at 200 °C, and then annealed at 700 °C in vacuum. The process of formation of germanium islands on silicon substrate has finished. They vary considerably in size, as predicted by the GISAXS investigation, but their shape is very similar, a sharp cone rather than a pyramid. The typical height is about 5 nm which corresponds well to the vertical Guinier radius R_{GV}=2.2nm determined by GISAXS. However, the lateral size (diameter) is about 20 nm which is about twice what would be expected from the R_{GL}= 6.2nm lateral value. This could be ascribed partly to the information covered by the central beamstop in Fig. 2 (the larger particle scattering is concentrated at smaller angles) especially when the rather broad size distribution is taken into account.

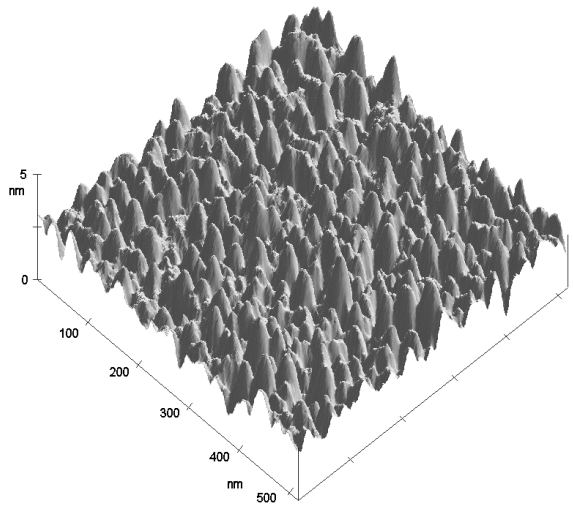

Figure 2. A typical AFM image of the 10 nm Ge layer evaporated on a Si (100) substrate heated at 200°C and then annealed at 650°C for 1 h in vacuum.

References:

[1] S.A.Chaparro, Y.Zhang, J.Drucker, D.Chandrasekhar, D.J.Smith, J.Appl.Phys. 87 (2000) 2245
[2] Y.–W. Mo, D. E. Savage, B. S. Swartzentruber, M. G. Lagally, Phys. Rev. Lett. 65 (1990) 1020
[3] R.Lazzari, J.Appl.Cryst. 35 (2002) 406
[4] I. Kovačević, P. Dubček, H. Zorc, N. Radić, B. Pivac, S. Bernstorff, Vacuum (in press)

GISAXS STUDY OF SiO/SiO_2 SUPERLATTICE

B. Pivac[1], I. Kovačević[1], P. Dubček[1], N. Radić[1], S. Bernstorff[2] and A. Slaoui[3]

1.) R. Bošković Institute, P.O. Box 180, Zagreb, Croatia
2.) Sincrotrone Trieste, SS 14, km 163.5, Basovizza (TS), Italy
3.) PHASE, CNRS, 23 rue du Loess,B.P. 20, Strasbourg, France

The correlation between the structural and optoelectronic properties of Si nanocrystals prepared by a variety of methods is still an unresolved problem. For better understanding of that correlation, it is necessary to learn more about the structural properties of Si nanocrystals. That includes nanocrystal size, spatial position, density and volume fraction. The most widely used technique for the structural investigation of Si nanocrystals has been transmission electron microscopy (TEM). Because of the insufficient contrast between Si and SiO_2 Si nanocrystals show only a weak amplitude and phase contrast when imaged with TEM.

To avoid possible errors and/or limitations of TEM we have applied grazing incidence small angle x-ray scattering (GISAXS) for the study of structural properties of SiO/SiO_2 superlattices and Si nanocrystals observed in superlattices after thermal annealing.

Amorphous SiO/SiO_2 superlattices were prepared by high vacuum evaporation of alternating films of SiO and SiO_2 on Si (100) substrate. After evaporation, the samples were annealed at 1050 °C and 1100 °C for 1h in vacuum. The GISAXS experiments were carried out using synchrotron radiation with wavelength λ=0.154 nm. The grazing angle of incidence was selected in the range $0.4° < \alpha_i < 1.4°$. A two-dimensional CCD detector with 1024 × 1024 pixels, positioned perpendicular to the incident beam was used to record the SAXS intensity. The spectra were corrected for background intensity and detector response.

In Fig. 1 a 1D vertical cut (i.e. perpendicular to the surface, along q_z, shown in full circles) of a 2D GISAXS pattern from a not annealed sample is shown. As expected, oscillations of the intensity are present in the spectra because the correlation between film and substrate surface is good. A monotonously decaying amplitude of the oscillations signifies that the interference comes from a single layer film structure, in this case the whole evaporated structure, and the rate of decay is due to the film to substrate surface correlation range. The total thickness of the film structure is estimated to be around 55 nm, which was also expected from the evaporation parameters. On the other hand, due to the weak electron density contrast between SiO and SiO_2 the single film layers could not be resolved well. The scattered intensity only has a broad and weak shoulder centered at about q=1.0nm^{-1} which is where the first maximum

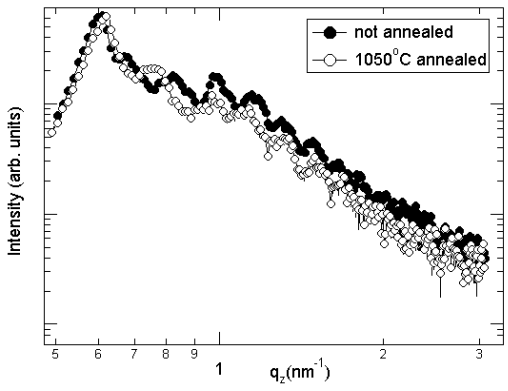

Figure 1. Vertical cuts from a not annealed sample (full circles) and from a sample annealed at 1050 °C (open circles)

from the bilayer thickness of 6nm is expected to be. A corresponding 1D vertical cut taken from the 2D pattern of a sample annealed at 1050°C is also shown (open circles). The oscillating intensity in the specular plane is still present. But it is not so well defined anymore, which means that the film-like structure is partly destroyed by temperature treatment at 1050 °C, indicating the beginning of the crystal nucleation leading to the nanoparticle formation.

Fig. 2 shows: (a) a 2D GISAXS pattern of the SiO/SiO_2 superlattice annealed at 1100 °C for 1h in vacuum; (b) a 1D vertical cut of the 2D GISAXS pattern from (a). The absence of fringes in the SAXS pattern shown in Fig. 2a demonstrates that the film-like structure is no more present in the sample. The single maximum in intensity at $q_z=0.45nm^{-1}$, parallel to the Yoneda peak at $q_z=0.40nm^{-1}$ is the only leftover from the fringes, since the film to substrate surface correlation is reduced greatly, due to the particle formation. This measurement can still be used to estimate the thickness of the overall film structure. It was found to be about 55 nm, when refraction was taken into consideration. The scattering intensity spread from the specular plane indicates that particles are formed in our samples.

Qualitatively, the 2D GISAXS pattern present two large scattering lobes visible along the parallel direction (parallel with q_z) separated by the specular plane. The extent of the intensity parallel and perpendicular to the surface is inversely proportional to the average lateral size and height of the particles, respectively.

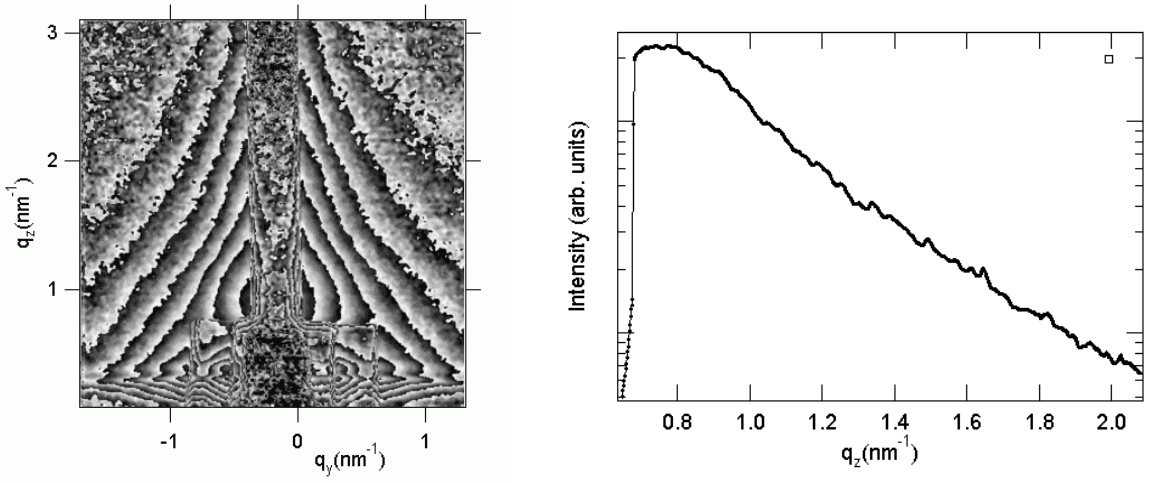

Figure 2.
(a) GISAXS pattern from a sample annealed at 1100ºC for 1hour

(b) Vertical cut from a)

When Guinier's approximation is applied to the experimental results shown at Fig. 2b, the radius of gyration for silicon nanocrystals is estimated to be around 1.5 nm. It should be noted that the thickeness of the SiO films in as prepared SiO/SiO_2 superlattices was 3 nm. Our results are consistent with the theory that nanocrystals sizes are well controlled by the SiO layer thickness.

Furthermore, a well defined maximum in intensity can be seen in the specular plane ($q_y=0$) at $q_z=1.0nm^{-1}$. Since nanocrystalline Si is located only where the SiO layer used to be, the overall bilayer repetitive structure is formally preserved: silicon nanocrystals' positions are well correlated in the direction perpendicular to the substrate surface. On the other hand, there is no particle to particle correlation within a single layer, as is evident from the lateral position

of the intensity maximum, which is placed in the specular plane. Fig. 3 shows the comparison of the cuts parallel to the q_y and q_z direction. A great similarity between the two curves for small q values indicates that the radius of the objects is the same in direction parallel and perpendicular to the surface, indicating hence, that we are having spherical particles contrary to the findings of Zacharias et al. [1,2].

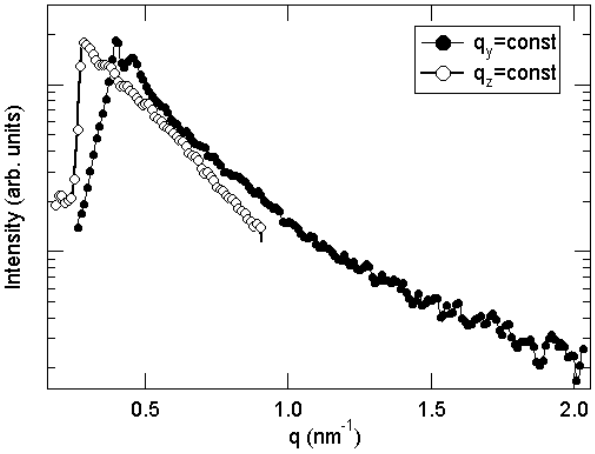

Figure 3. Comparison of the scattered intensities in vertical and horizontal direction

References:

[1] M.Zacharias**,** J. Heitmann, R. Scholz, U. Kahler, M. Schmidt, and J. Bläsing, Appl. Phys. Lett. 80 (2002) 661
[2] M.Zacharis and P. Streitenberger, Phys.Rev.B 62 (2000) 8391

TUNGSTEN MULTILAYERS

N. Radic[1], P Dubcek[1], S. Bernstorff[2] and K. Salamon[3]

1.) Rudjer Bošković Institute, Bijenička 54, HR-10000 Zagreb, Croatia,
2.) Sincrotrone Trieste, SS 14 km 163,5, I-34012 Basovizza (TS), Italy
3.) Institute of Physics, Bijenička 46, HR-10000 Zagreb, Croatia

The superior properties of tungsten make it suitable for gate contacts and interconnects in ULSI/ VLSI devices, diffusion barriers in Al-W based technology, absorption layer for masks in x-ray lithography, and alternating layers in X-ray mirrors.

Different phases of tungsten are produced by magnetron sputtering under different preparation conditions: stable alpha-W phase (b.c.c. structure) is obtained at low working gas pressure, metastable beta-W phase (A15 structure) is obtained at increased working gas pressure, and amorphous-like tungsten (a-W) is obtained at even higher pressure. The occurence of various phases is related to the oxygen content and built-in stresses in the prepared thin films. We employed these facts to produce tungsten films composed of stacked layers of different tungsten phases.

The prepared films generally contain stable alpha-W phase layers prepared at low argon pressure, alternating with the layers of metastable beta-W phase or amorphous-like tungsten prepared at 3.5 Pa argon pressure. From the results on single-phased films it is expected that the stress of the layers prepared at 0,7 Pa is strongly compressive, while the alternating layer is in tensile stress.

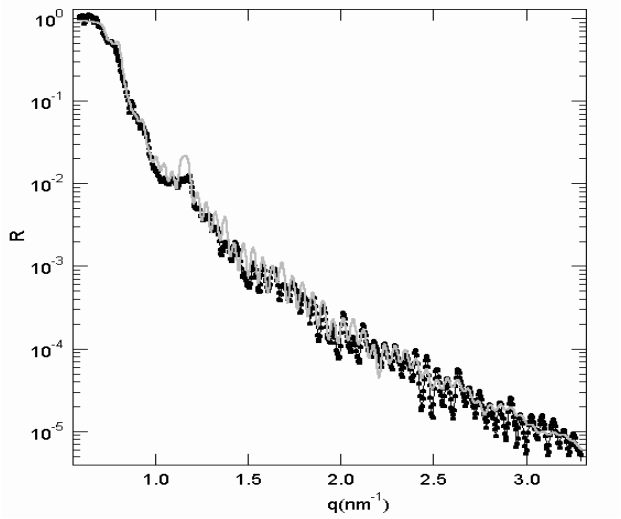

Figure 1. X-ray reflectivity of a stack of 10 bilayers of of α–W and β–W, about 2.5nm thick each (black) together with the best fit (gray)

The overall stress in prepared tungsten films results from the opposite stresses of individual layers. However, the effective stress cannot be simply derived from data for single-phase films, probably due to the variation of stress with the layer thickness and the contribution of the interfaces.

X-ray reflectivity of the multilayer is shown in Fig. 1. It reveals only a weak first order Bragg peak whose position corresponds to the bilayer thickness. It is otherwise dominated by oscillations whose amplitude vary quite irregularly and are due to the whole tungstan film thickness. When fitted to a model of ten bilayers, it shows that the thickness of a α–W layer is 5% smaller than that of a β–W layer. Due to the internal stress, already the first layer has a

not so good defined thickness. The fit reveals its surface roughness to be 0.4 nm. That is increased to 1.1 nm surface roughness on top of the film.

The topology of the film surface is shown in Fig. 2. It contains structures that are up to 15 nm tall, peak to peak. Keeping in mind that the single layer thickness is only 3-5 times larger than the layer interface roughness, we can conclude that the internal stress is a limiting factor in producing this multi-layered structure.

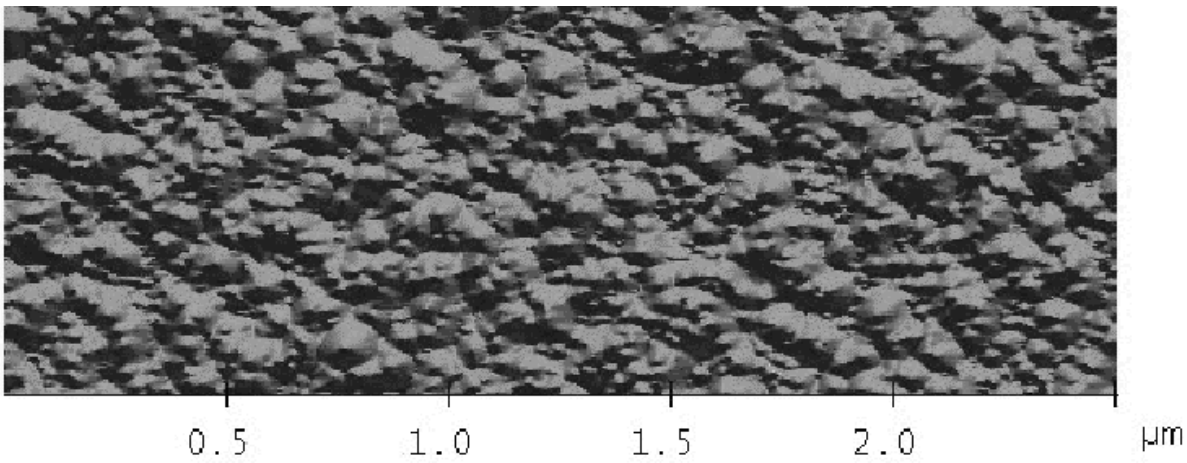

Figure 2. Atomic force microscope image of the film surface.

COMBINATION OF MULTIREFLECTION X-RAY LINE PROFILE ANALYSIS, CALORIMETRY AND ELECTRICAL RESISTOMETRY TO DETERMINE VACANCY CONCENTRATION IN ECAP-CU

E. Schafler[1], M. Kerber[1], G. Steiner[1], T. Ungàr[2], S. Bernstorff[3] and M. J. Zehetbauer[1]

1.) Institute of Materials Physics, University of Vienna, A-1090 Wien, Austria
2.) Department of General Physics, Eötvös University Budapest, H-1518 Budapest, Hungary
3.) Sincrotrone Trieste, 34012 Basovizza, Italy

The mechanisms of plastic deformation and large-strain hardening under enhanced hydrostatic pressure, called "severe plastic deformation (SPD)", revealed to be relevant for the realisation of the nanocrystalline state. The specific evolution of different lattice defects and their densities, their interaction mechanisms and arrangements control the hardening behaviour, but also seem to be responsible for the enhanced ductility which has been repeatedly observed as an additional feature of materials produced by SPD.
With measurements of residual electrical resistivity (RER), the number of all deformation induced lattice defects i.e. dislocations and vacancies [1] can be determined, i.e. from the resistivity difference between deformed and undeformed material [2]. Similarly, the method of differential calorimetry (DSC) reveals the energy stored in dislocations and vacancies during plastic deformation [3]. Since the X-ray Bragg Profile Analysis (XPA) is able to quantify the density of dislocations solely (i.e., lattice distortions caused by defects not being smaller than 5 nm [4]), the concentration of deformation induced vacancies can be determined by a quantitative comparison of results from XPA with those from either DSC and/or RER.
The investigation was done on Cu samples which have been subject to SPD by Equal Channel Angular Pressing (ECAP) up to shear strains $\gamma \sim 5$. The residual electrical resistivity of the deformed samples was measured at liquid helium temperature with the conventional four-wire method. The DSC measurements were performed by a Perkin Elmer DSC-7 calorimeter using linear heating from 40°C to 600°C. For the first time ever multi-reflection XPA (MXPA) was done using a synchrotron source at the SAXS Beamline at Sinchrotrone ELETTRA, Trieste, Italy by recording the first 6 reflections simultaneously, using four position sensitive detectors. The wavelength used was $\lambda = 0.154$ nm, the spot size on the sample was about 100 x 500 μm^2. This spot size guarantees little geometrical broadening of the peaks, which is necessary for MXPA. Scans were performed over the samples and the results of each measurement were averaged for statistical reasons. The experimental data has been evaluated using a whole profile fitting procedure [5].
The MXPA method yielded the evolution of the dislocation density with increasing deformation; these reach values up to 2 x 10^{15} m^{-2} at $\gamma \sim 4.5$ (Fig. 1). The magnitude of these values is about the same as of conventional deformation with comparable degree of deformation. Using these dislocation density values, the concentrations of deformation-induced vacancies (and/or -agglomerates) have been determined by differential scanning calorimetry and residual electrical resistometry in independent ways (Fig. 2). The correspondence of the results from both is excellent [6].
The vacancy concentrations shown in Fig. 2 are of the order of 10^{-4}, a high value for deformation-induced vacancies even for cold work conditions. The evaluation of the difference of the dislocation density measured by RER and XPA in [7] by the same method used here, a markedly lower vacancy concentration is obtained for conventionally deformed Cu (dashed-dotted line in Fig. 2). Thus after ECAP, irrespective of the deformation path, the concentration of vacancies is about three times higher than after cold rolling, while the dislocation densities are in the same range. This may be due to the fact that the vacancy concentration is more sensitive to the extent of hydrostatic pressure than the dislocation

density [3]. Generally a steady increase of vacancy concentration has been observed with proceeding deformation, which is not necessarily correlated with the dislocation densities of the different routes, which partially tend to saturate [8].

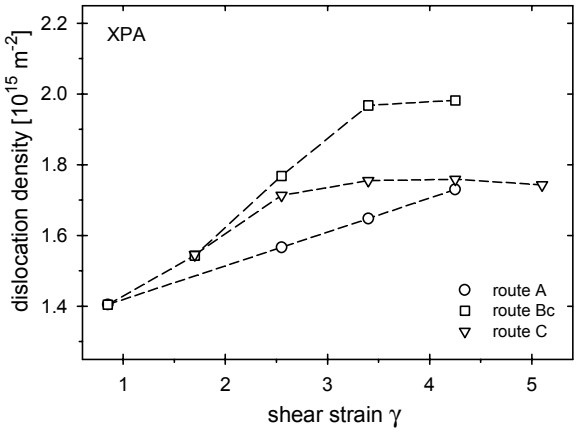

Figure 1. The dislocation density determined from X-ray line profile analysis (XPA) as a function of shear strain, for deformation routes A, B_C and C. The measuring error is smaller than the symbol size.

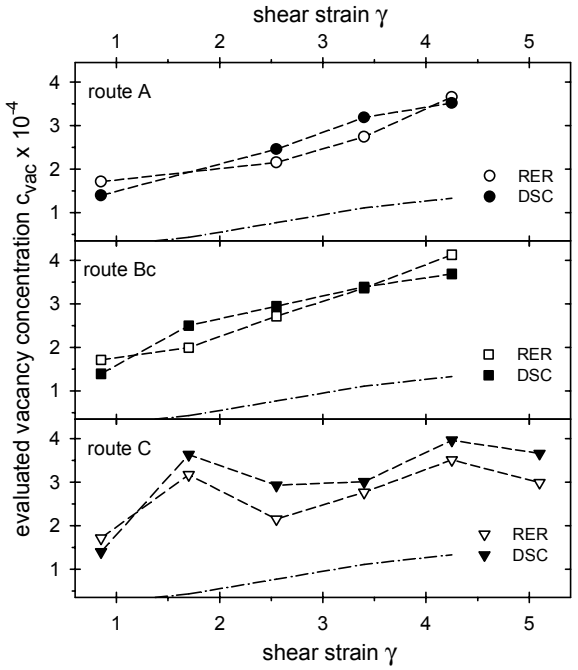

Figure 2. The evaluated vacancy concentrations determined from the results of differential scanning calorimetry (DSC) as well as residual electrical resistometry (RER), as functions of shear strain, for deformation routes A, B_C and C. The dashed dotted line indicates the evolution of vacancy concentration after conventional cold working. Measuring errors are about the symbol size for DSC measurements, and much smaller than symbol size for RER measurements.

References:

[1] M. Zehetbauer, Key Eng. Mater. 97-98, 287-305 (1994)

[2] M. Kocer, F. Sachslehner, M. Müller, E. Schafler, M. Zehetbauer, M., Mater. Sci. Forum 210–213, 133-140 (1996).

[3] M.B. Beaver, D.L. Holt, A.L. Titchener, Prog. Mater. Sci. 17, 5-177 (1973)

[4] Ungár, T., Mughrabi, H., Rönnpagel, D., Wilkens, M., Acta metall. 32, 333-342 (1984)

[5] G. Ribarik, T. Ungar, J. Gubicza, J. Appl. Cryst. 34, 669-676 (2001)

[6] E. Schafler, G. Steiner, E. Korznikova, M. Kerber, M. J. Zehetbauer, Mater. Sci. Eng. A, accepted for publ.

[7] M. Müller, M. Zehetbauer, A. Borbely, T. Ungar, Proc. 4th Europ. Conf. Adv. Mat. and Processes, EUROMAT `95, Padua/Venice, Italy, 305-308 (1995)

[8] M. Zehetbauer, E. Schafler, T. Ungar, Z. Metalk., submitted

2. Life Science

REDUCED FORCE PRODUCTION BY THE MYOSIN MOTOR AFFECTS X-RAY SIGNALS FROM SKELETAL MUSCLE FIBRES

H. Amenitsch[1], C.C. Ashley[2], M.A. Bagni[3], S. Bernstorff[4], G. Cecchi[3], B. Colombini[3] and P.J. Griffiths[2]

1.) Institute of Biophysics and X-ray Structure Research, Austrian Academy of Sciences, Schmiedlstraβe 6, A-8042 Graz, Austria
2.) University Laboratory of Physiology, Parks Road, Oxford, OX1 3PT, U.K
3.) Dipartimento di Scienze, Università degli Studi di Firenze, Viale G.B. Morgagni 63, Firenze, I-50134, Italy
4.) Sincrotrone Trieste, Area Science Park, Basovizza/TS, I-34012, Italy

Linear molecular motors (i.e. dynein, kinesin and myosin) are involved in myriad essential cell functions, including cell division, directional transport of intracellular organelles, exo-, endo- and pinocytosis, sound transduction into electrical signals in the ear, and the contraction of all forms of muscle tissue. Myosin II is the motor protein in contractile systems, powering voluntary movement, cardiovascular circulation, peristalsis and respiration. It is unique amongst the myosins in that it aggregates into highly ordered filaments. In skeletal muscle, these filaments overlap actin filaments in a hexagonal lattice, giving a quasi-crystalline structure and enabling simultaneous collection of X-ray diffraction and mechanical data from a working population of myosin motors. The subfragment 1 (S1) moiety of myosin is the protein 'engine', composed of a ‘motor domain’ (bearing the actin and ATP binding sites) and a 9nm long ‘lever arm’. ATP hydrolysis at the catalytic site while bound to actin results in structural rearrangement of the amino acid chains composing the motor domain, causing a change in angle of tilt of the lever (the motor power stroke [1]). If free to move, this tilting produces a translational movement of the lever tip of 4-10nm or, if movement is prevented, 2-4pN of force.

The X-ray pattern of striated muscle is divisible into 3 components; equatorial, meridional and off-meridional reflections. These components provide information about the radial, axial and helical mass distribution, respectively, within the filament lattice. The meridional M3 reflection, the strongest reflection on the meridian, has a spacing equal to the axial period of S1 projections from the surface of the myosin filaments, and its intensity (I_{M3}) originates principally from scattering by these S1 moieties. I_{M3} detects changes in S1 structure during the power stroke, and its behaviour during the synchronized power stroke, which accompanies a step change in actin-myosin overlap, is consistent with a change in lever arm tilt. The 10 and 11 equatorial reflections are the strongest reflections in the pattern. Upon binding of S1 to actin, these reflections undergo an intensity reversal, 10 becoming weaker and 11 becoming more intense. This behaviour can be simulated by a radial mass transfer from the myosin to the actin filament, and these reflections are therefore used as a probe of the degree of actin-myosin interaction.

Previous studies by our group have shown that the I_{M3} response to a sinusoidal length change imposed on the muscle cell is a distorted sinusoid. We showed that the extent of distortion becomes greater when the average force generated per actin-bound S1 increases, using the temperature sensitivity of the power stroke to vary S1 force [2]. The muscle relaxant, 2,3-butanedione monoxime (BDM), is thought to act by blocking the power stroke, trapping S1 in a low force state. One would therefore predict that BDM would reduce I_{M3} distortion during sinusoidal oscillations. We studied the two dimensional X-ray pattern of small bundles of tibialis anterior fibres from *Rana temporaria* in the relaxed state and during isometric tetanic contractions in BDM. Patterns were collected on a 2D CCD detector during a 300ms X-ray

exposure, and were corrected for background scattering and spatial aberrations in the detector response. Reflection intensities were measured by projection onto the meridian or the equatorial, then by fitting with gaussian intensity distributions superimposed on a polynomial background. Dynamic data was captured using a delay line one dimensional detector. Fibre bundles were subjected to length oscillations (amplitude 0.5% of bundle rest length) at 1kHz. Experiments were performed at a sarcomere length of 2.2μm (full filament overlap) and sarcomere length was measured continuously throughout the experiment using a laser diffractometer.

We find that, contrary to expectations, I_{M3} distortion was increased by BDM in the range 1-8mM, and effect previously observed only under conditions where S1 force generation has been increased. In this concentration range, BDM has no effect on the electrical properties of the cell and produces no change in activating Ca^{2+} release nor in Ca^{2+}-binding to the regulatory proteins. The increased distortion must therefore be due to a BDM-induced alteration in the S1 structural changes accompanying length oscillations. Simulation of the changes in lever tilting during sinusoidal oscillations by a molecular model of actin-bound S1 is now being used to examine the change in I_{M3} in the presence of BDM and to determine the molecular basis of this anomalous effect of BDM.

References:

[1] Rayment, I., H.M. Holden, M. Whittaker, C.B.Yohn, M. Lorenz, K.C. Holmes and R.A. Milligan. 1993. Structure of the actin-myosin complex and its implications for muscle contraction. *Science*. 261: 58-65

[2] Griffiths, P.J., Bagni, M.A., Colombini, B., Amenitsch, H., Bernstorff, S., Ashley, C.C. and Cecchi, G. 2002. Changes in myosin S1 orientation and force induced by a temperature increase. *Proc. Nat. Acad. Sci. U.S.A.,* 99: 5384-5389

IN SITU COATING OF PHOSPHOLIPID MIXTURES STUDIED WITH SURFACE DIFFRACTION.

H. Amenitsch, B. Sartori, M. Rappolt, G. Pabst, and P. Laggner

Institute of Biophysics and X-ray Structure Research, Austrian Academy of Sciences, Schmiedlstr. 6, A-8043 Graz, Austria

The cell membrane is the interface between the single cell and its environment. Its function is given by the structure and interaction of the constituting molecules, mainly various phospholipids and their embedded proteins. For the development of biomimetic coatings or biosensors it is of importance to produce complex coatings, which are on the one hand easy to manufacture and on the other hand homogeneous. In particular surface deposited lamellar structures are widely studied as biomimetic coatings (see [1] and therein). There exit various deposition methods such as (i) spin-coating, (ii) spray-coating, (iii) the well established spreading technique or (iv) the dip-coating [2,3]. However, only the last allows to produce easily homogenous films with a small mosaic spread over a relatively broad range of thickness (0.1 to 2 μm). This, because the dip-coating techniques takes advantage of the evaporation induced self-assembly process [4]. We have applied this method for a phospholipid oleyl alcohol mixture in order to compare the film quality achieved with a former study, in which the films were deposited by spin coating [1].

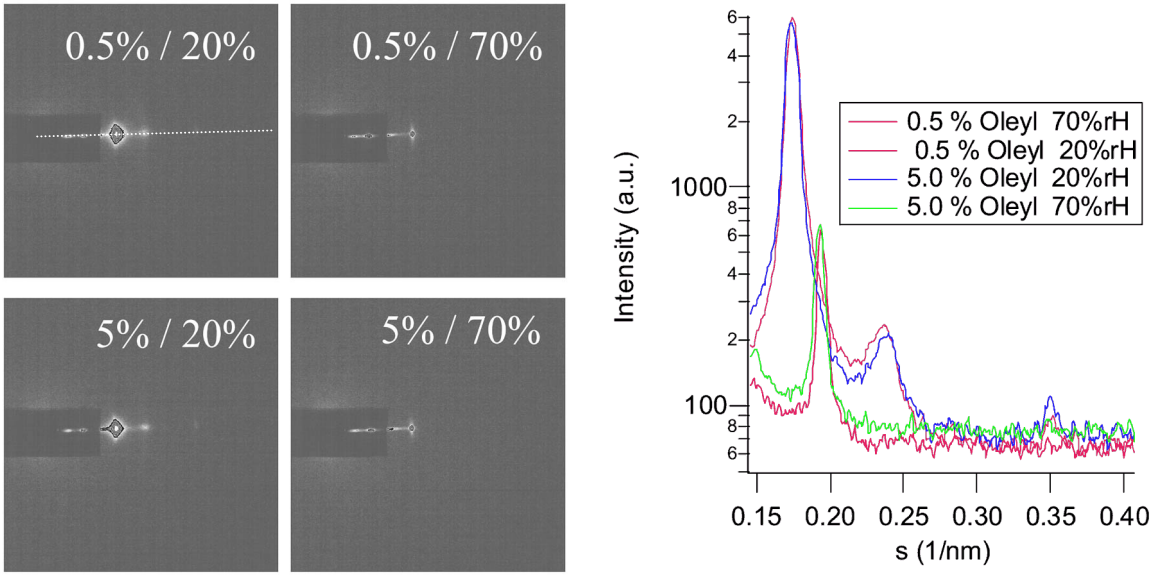

Figure 1. (Left) Surface diffraction pattern of POPC/oleyl alcohol mixtures (0.5 and 5 wt% oleyl alcohol content) at 20 and 70 % relative humidity (RH), respectively. Films were produced with the dip-coating technique. (Right) Scattered intensity recorded along the diffraction plane (compare dotted line in the 2D-image).

Figure 1 shows the surface diffraction pattern of multilamellar films of palmitoyl-oleoyl-phosphatdylcholine (POPC), which were mixed with 0.5 and 5 wt% oleyl alcohol (OA), respectively. Former investigations have shown [1] that this additive has two effects, first it anneals defects in the supported lipid bilayer stacks and second, it seems to induce a higher flexibility of the lipid membrane. However, the spin-coated films were not perfectly homogeneous: while the major part of the films were enriched with OA, a minor fraction showed almost pure POPC stacks. This was approved from the different d-spacings [1]. In

fact also for the dip-coated films two different spacing appear at 20 % RH. The less intense first order Bragg peak at around 4.2 nm (Fig. 1) compares well to the value found in pure POPC-films at this dry condition [2]. Thus, the strong reflection with a corresponding d-spacing of 5.6 nm is interpreted to arise from OA-rich domains in the sample. Finally, at 70 % RH perfectly homogenous films with a low mosaic spread have been produced. Only one sharp and intense first order reflection at s ~ 0.2 nm^{-1} is visible (Fig. 1). This demonstrates nicely the benefits of the dip-coating technique, but also the necessity to control the environmental condition such as temperature and relative humidity [3] for the production of homogenous high quality coatings.

References:

[1] Amenitsch, H., M. Rappolt, C.V. Teixeira, M. Majerowicz, and P. Laggner. 2004. In situ sensing of salinity in oriented lipid multilayers by surface X-ray scattering. *Langmuir* **20**, 4621-4628.

[2] Rappolt, M., H. Amenitsch, J. Strancar, C.V. Teixeira,, M. Kriechbaum, G. Pabst, M. Majerowicz, and P. Laggner, P. 2004.Phospholipid mesophases at solid interfaces: in-situ X-ray diffraction and spin label studies. *Advances in Colloid Interface Sciences* **111**, 63-77.

[3] Cagnol, F., D. Grosso, G.J.D.A. Soler-Illia, E.L. Crepaldi, F. Babonneau, H. Amenitsch, and C. Sanchez. 2003. Humidity-controlled mesostructuration in CTAB-templated silica thin film processing. The existence of a modulable steady state. *Journal of Materials Chemistry* **13**, 61-66.

[4] Lu, Y.F., H.Y.Fan, A. Stump, T.L. Ward, T. Rieker, and C.J. Brinker. 1999. Aerosol-assisted self-assembly of mesostructured spherical nanoparticles. *Nature* **398**, 223-226.

EFFECTS OF LIGANDS ON THE STABILITY OF TISSUE TRANSGLUTAMINASE

C. M. Bergamini[1], F. Spinozzi[2], H. Amenitsch[3], S. Bernstorff[4] and P. Mariani[2]

1.) Department of Biochemistry and Molecular Biology and Intedisciplinary Centre for the Study of Inflammation (ICSI), University of Ferrara (Italy)
2.) Department of Science Applied to Complex Systems, Physical Sciences Section, Marche Polytechnique University, Ancona (Italy).
3.) Institute of Biophysics and X-ray Structure Research, Austrian Academy of Sciences, Schmiedlstrasse 6, A-8042 Graz, Austria
4.) Sincrotrone Trieste, Area Science Park, 34012 Trieste, Italy

In this report we address effects of ligands on thermodynamic stability of tissue transglutaminase (Tgase) [1,2], taking into account different conformers stabilized by binding of the regulatory ligands calcium (an essential activator) and GTP (an inhibitor), employing heat as an external probe. This "cryptic" enzyme catalyzes in a strictly calcium-dependent way acyl-transfer reactions from peptidyl glutamine residues to accepting primary amines, yielding, as products, proteins modified either by covalent incorporation of amines or by crosslinkage through proteinase-resistant isopeptide bonds [1]. However, several studies indicate that tissue transglutaminase is a bifunctional enzyme displaying activities of GTP hydrolysis and of protein transamidation in an alternative switching-on pattern [3] related to the well defined conformational changes [2]. Under basic conditions the transamidation reaction is inactive because activation requires near-millimolar concentrations of calcium ions and breakdown of cell GTP, which is an inhibitor. Actually the physiologic function of tissue transglutaminase is a still unresolved issue and it has been proposed that the enzyme is involved in different cell reactions as programmed cell death death [4] and stimulation to proliferation [5]. To contribute to understand degradative events in the biology of transglutaminase we studied the effects of regulatory ligands on the in vitro thermodynamic stability of tissue transglutaminase. This issue has been marginally dealt with previously, mostly in relation to exposition to shifts in pH [1,6] but not in relation to effects of the physiologically relevant regulatory ligands.

Previous data (C.M. Bergamini, to be published) indicate that heating has different effects on protein stability depending on the absence/presence of ligands, the temperature of treatment and the parameter investigated. At relatively low temperatures (in the range 38 to 45 °C), the enzyme undergoes time-dependent thermal inactivation with first order kinetics. Regulatory ligands influence deeply the pattern of inactivation, with protection and accelerated inactivation in the presence of GTP and of calcium, respectively. These processes occur without major disruption of the protein structure, monitored by spectroscopic approaches, indicating that local perturbations at the active site region, likely due to rearrangement of ordered structures without modification of tertiary conformation, are instrumental in the ligand-controlled thermal inactivation. At higher temperatures (52-56 °C), the enzyme undergoes progressive unfolding, with alterations in interdomain interactions, depending on the presence of the ligands. The tight interactions occurring between the N-terminal and C-terminal domain pairs are the targets of thermal effects under these conditions. DSC experiments clearly indicate that this interaction is reinforced in the presence of the inhibitor GTP and weakened in the presence of calcium ions (allowing access of substrate proteins to the active site). Furthermore fluorescence spectroscopy data indicate appreciable alterations in the microenvironment of tryptophan containing regions only in the high temperature range, in concomitance with the domain unfolding. It is thus clear that regulatory actions of ligands are quite complex, involving localized and multidistance effects.

In solution SAXS experiments were performed at the ELETTRA synchrotron (Trieste, Italy), essentially as previously described [2]. The X-ray wavelength was 0.154 nm and the sample-to-detector distance was 2.5 m, so that the scattering vector Q range was 0.1-2.5 nm-1. Protein solutions were inserted into a sealed 1 mm glass capillary enclosed within a thermostated compartment connected to an external circulation bath and a thermic probe for temperature control. Heating cycles were performed stepwise with a 2-3 °C increase in the temperature range from 25 up to 70 °C, the highest temperature allowed on the instrument. Experimental intensities were corrected for background, buffer contributions, detector inhomogeneities and sample transmission. A few SAXS curves are reported in Figure 1.

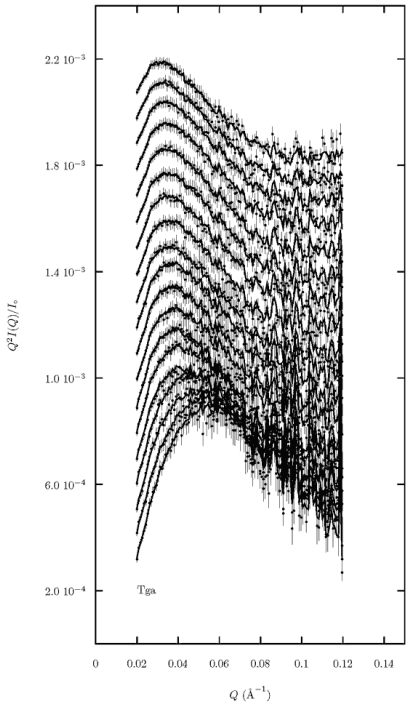

Figure 1. Small angle X-ray scattering profiles, in the form of Kratky plots, obtained by native Tgase at different temperatures. Temperature increases from the bottom to the top.

Data analysis was performed in the frame of the so-called two-phase model, as previously described [2]. Particle gyration radii (Rg) and scattering intensities at zero angle (Io) were derived as a function of the sample temperature, in the absence of ligands and in the presence of 4 mM calcium or of 0.5 mM GTP. Moreover, all the scattering curves were analyzed applying the Singular Value Decomposition (SVD) procedure to derive the number and the kind of particles present in the different experimental conditions.

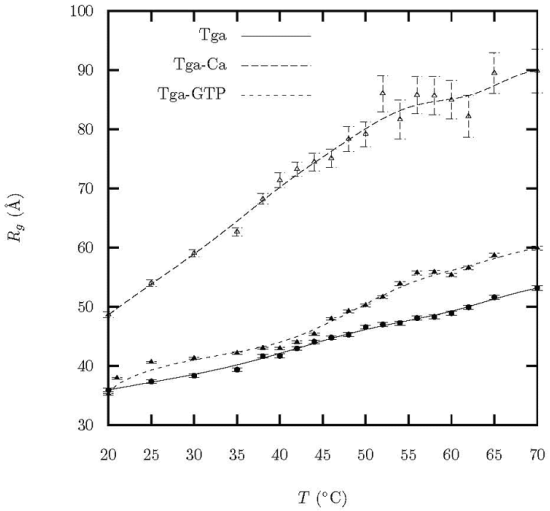

Figure 2. Temperature dependence of the gyration radii measured in the three different Tgase forms

Results provide evidences of different effects of heating in the absence /presence of ligands, since during heat treatment the Guinier radius, Rg, increases in a biphasic fashion, through

well populated intermediates, to approximate limit values of 52 and 60 Å, in the absence of ligands and in the presence of GTP, while a higher Rg value of about 90 Å is attained in the presence of calcium, with a monotonic increase. Therefore, the protein appears progressively unfolded during heating (with an increase in Rg), in a fashion facilitated by calcium, which breaks-down domain-domain interactions, but hampered by GTP which reinforces them. These differences in the thermal unfolding pathways are explained by SVD results which evidence the existence of a stable tightly packed intermediate, probably formed by interaction of the N- and the C-terminal domains with each other. Its stability at moderate temperatures represents the limiting step in the unfolding pathway in the absence of ligands and in the presence of GTP. Conversely, its disappearance in the presence of calcium ions promotes a rather ”monotonic” unfolding (i.e. without energy barriers) with a uniform increase in Rg at increasing temperature, with attainment of a maximal Rg value of 5.6 nm.

References:

[1] Casadio, R., E. Polverini, P. Mariani, F. Spinozzi, F. Carsughi, A. Fontana, P. Polverino de Laureto, G. Matteucci and C. M. Bergamini. 1999. The structural basis for the regulation of tissue transglutaminase by calcium ions. Eur. J. Biochem. 262, 672-679.

[2] Mariani, P., F. Carsughi, F. Spinozzi, S. Romanzetti, G. Meier, R. Casadio and C. M. Bergamini. 2000. Ligand-induced conformational changes in tissue transglutaminase: Monte Carlo analysis of small-angle scattering data. Biophys. J. 78, 3240-3251.

[3] Griffin, M., R. Casadio, R. and C. M. Bergamini. 2002. Transglutaminases: nature's biological glues. Biochem. J. 368, 377-396.

[4] Fesus, L., A. Madi, Z. Balajthy, Z. Nemes and Z. Szondy. 1996. Transglutaminase induction by various cell death and apoptosis pathways. Experientia 52, 942-949.

[5] Mian, S., S. el Alaoui, J. Lawry, V. Gentile, P. J. Davies and M. Griffin. 1995. The importance of the GTP-binding protein tissue transglutaminase in the regulation of cell cycle progression. FEBS Lett. 370, 27-31.

[6] Bergamini C. M., M. Dean, G. Matteucci, S. Hanau, F. Tanfani, C. Ferrari, M. Boggian and A. Scatturin. 1999. Conformational stability of human erythrocyte transglutaminase. Patterns of thermal unfolding at acid and alkaline pH. Eur. J. Biochem. 266, 575-582.

IN-SITU FORMATION OF SOLID-SUPPORTED LIPID/DNA COMPLEXES

G. Caracciolo[1], H. Amenitsch[2], D. Pozzi[1] and R. Caminiti[1]

1.) Dipartimento di Chimica,Università degli Studi di Roma "La Sapienza",P.le A. Moro 5, 00185 Roma, Italia
2.) Institute of Biophysics and X-ray Structure Research, Austrian Academy of Sciences

When mixing aqueous solutions of DNA with a suspension of cationic liposomes, highly condensed self-assembled cationic lipid/DNA complexes, named lipoplexes, are formed with the negative charge carried by the phosphate groups of the DNA neutralized by the cationic lipids [1]. The present knowledge about the structural properties of lipoplexes has been recently reviewed [1] and it is now well established that the lipoplex often consists of a multilamellar structure comprising a periodic one dimensional lattice of parallel DNA strands confined between two dimensional (2D) lipid bilayers.

For gene delivery purposes, multi-lamellar vesicles (MLV) are widely utilized consisting of independent scattering domains each of which is a stack of parallel bilayers with the normals to the bilayers in independent stacks isotropically distributed in space. Such powder-like samples weakly diffract and the intensity rapidly falls off with increasing transfer momentum q. Conversely, solid-supported highly aligned lipid multilayers safeguard spatial information and give more intensity for higher orders of diffraction allowing for more accurate diffraction analyses.

Here we extended this approach to the *in situ* formation of solid-supported lipoplexes by using highly-aligned stacks of membranes as a template. To our knowledge, no previous experimental study has concerned the *in situ* formation of solid-supported lipoplexes. Kinetic experiments performed both by time-resolved Energy Dispersive X-ray Diffraction (EDXD) and synchrotron Small Angle X-ray Scattering (SAXS) allowed us to resolve the lipid/DNA complex formation *in situ*.

Furthermore we retrieved detailed information about the structure, the degree of order and the orientation of the emerging solid-supported lipoplexes, both dehydrated and fully hydrated from a vapour saturated atmosphere. By orientation, important new insight may be obtained into the structural organization of lipoplexes. For example, the line-shape analysis of high-resolution diffraction peaks from oriented samples is expected to clarify the short-ranged positional cross correlations between the DNA of adjacent layers whereas effects of powder-averaging can cause this cross correlations to vanish and not to be observed in unoriented samples. Thus, the use of oriented samples, could shed more light into the existence of the theoretically predicted 'new sliding columnar phase' of matter which has been supposed to exist in layered systems composed of weakly-coupled 2D smectic lattices. Such biomolecular templatings could also be relevant on the future development of practical device engineering of industrial interest.

A drop of 40 μl of a DNA solution 5.6 mg/ml was then carefully spread onto the solid/air interface of the lipid film at a lipid/DNA weight ratio $\rho = 4.1$, covered the overall surface of the lipid film and the solvent was let evaporate.

After complete drying, the final EDXD pattern displayed in Figure 1 (panel A) shows a sharp peak at $q = 0.113$ Å^{-1} corresponding to the (*001*) reflection of an ordered multilamellar structure with a periodicity $d \sim 55.7$ Å. Our experimental findings are clearly interpretable in

terms of DNA condensation between lipid bilayers and are in excellent agreement with structural information previously obtained on unoriented dehydrated lipid/DNA complexes [1]. This result has confirmed the general expectation that the physical mechanisms underlying the lipoplex formation are the same even in the case of solid-supported samples, enforcing the idea of using them as model systems for the study of the structural properties of lipoplexes. [2]

Before attempting to claim that the proposed experimental procedure effectively resulted in the formation of oriented lipoplexes, the degree of orientation in the samples was promptly investigated. To this end, rocking scans were taken at both the first-order BP of the complex and the lipid and are simultaneously displayed in the inset of Figure 1 (panel A). The rocking scan proves the good alignment of the lipid/DNA complex with a mosaicity (FWHM =0.1°) lower but comparable with that of the pure lipid system (FWHM =0.06°). The increase of diffuse scattering illustrates the simultaneous presence of liposome-like structures probably induced by hydrophobic interactions at the early stage of the complex formation.

In order to shed more light on the degree of orientation of the emerging lipid/DNA complexes synchrotron SAXS measurements were also performed and a representative 2D X-ray pattern is displayed in Figure 1, panel B. Two evident Bragg reflections (d= 57.1 and 48.5 Å respectively) closely resemble those previously detected by EDXD experiments (Figure 3, panel A). In addition, 2D X-ray pattern gives unambiguous information about the orientation of the lipoplexes formed *in situ*. While traces of the first-order BP of the pure lipid (BPL) remain, the SAXS pattern demonstrates that, upon spreading the DNA solution at the lipid/air interface, the DNA fragments penetrate into the major part of the aligned multilamellar DOTAP stacks. Even more remarkably, the pattern indicates that the arising multilamellar structure is preferentially oriented along the z-direction. However, subtle Debye-Scherrer rings due to traces of nonoriented liposomal scattering contributions (LS) are also detected. EDXD and SAXS combined results suggest that the overall process can be simply schematized as displayed in Figure 2. The excellent agreement between EDXD and SAXS results confirms that the proposed experimental procedure effectively resulted in the formation of solid-supported DOTAP/DNA complexes preferentially oriented along the normal to the support. [2]

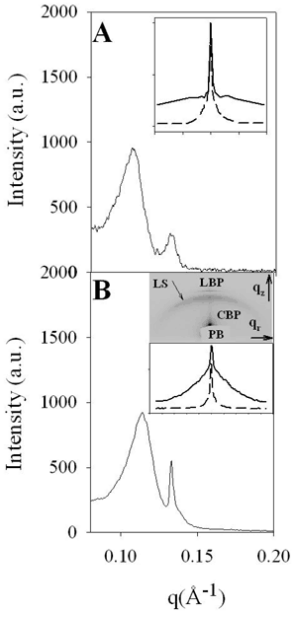

Figure 1. EDXD pattern of dehydrated DOTAP-DNA complex plus DOTAP membranes (panel A). In the inset of a direct comparison between the rocking scans measured at the first-order Bragg peak of the complex (solid line) and the pure lipid (dashed line) is reported. In the panel B, a synchrotron SAXS pattern is shown. In the inset of panel B, a 2D X-ray pattern (top) elucidates the orientation and of both the complex and the lipid. The first-order Bragg peak of the oriented complex (BPC) and that of the pure lipid (BPL) are evident even if unambiguous traces of liposomes-like structures (LS) are also present. The primary beam (PB) is also indicated. The curves (bottom) obtained by azimuthal integration (complex: solid line; pure lipid: dashed line) confirm the EDXD results.

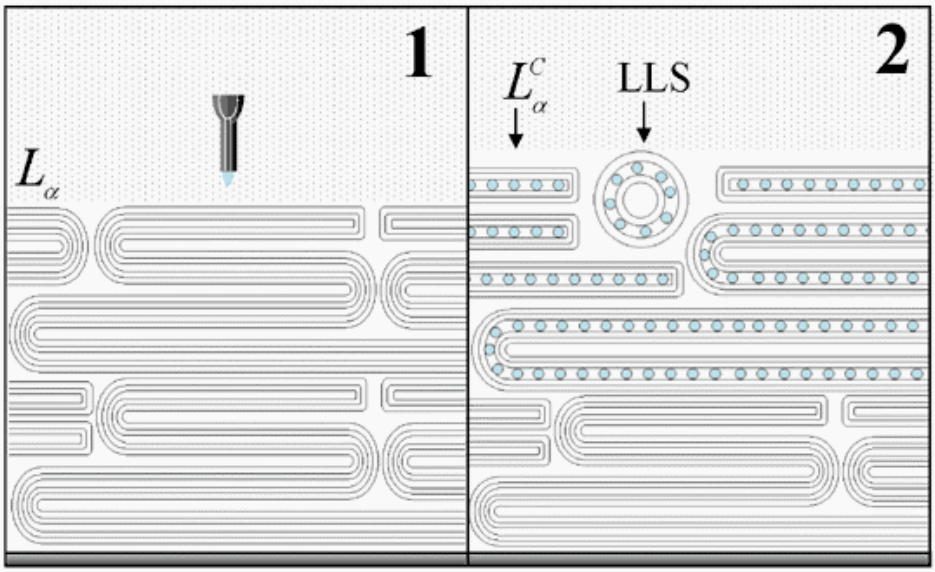

Figure 2. Solid-supported aligned DOTAP multibilayers system in the liquid crystalline phase (1). A drop of a DNA solution was spread at the lipid/air interface. This resulted in the spontaneous DNA condensation between opposing bilayers. After excess solvent evaporation, the emerging DOTAP/DNA complex was found to coexist with liposome-likes structures (LLS). The DNA double helices are schematically represented by rods.

References:

[1] C. R. Safinya; Structures of lipid-DNA complexes: supramolecular assembly and gene delivery; Curr. Opin. Struct. Biol. 11 440(2001)

[2] G. Caracciolo, H. Amenitsch, C. Sadun and Ruggero Caminiti; In situ formation of solid-supported lipid/DNA complexes; Chem. Phys. Lett. 405 252-257 (2005)

SAXS, GISAXS AND GIWAXS INVESTIGATIONS OF BIOACTIVE GLASSES

G. Croce[1], M. Milanesio[1], D. Viterbo[1], E. Verné[2], B. Onida[2], O. Bretcanu[2], S. Dinunzio[2] and H. Amenitsch[3]

1.) Dipartimento di Scienze e Tecnologie Avanzate, Università del Piemonte Orientale, Via Bellini 25/G, I-15100 Alessandria, Italy
2.) Dipartimento di Scienza dei Materiali e Ingegneria Chimica, Politecnico di Torino, Corso Duca degli Abruzzi 24, I-10129 Torino, Italy
3.) IBR, Austrian Academy of Sciences, Schmiedlstr. 6, A-4082 Graz, Austria

Several bioactive materials have been studied in the last decades for many applications in medicine. The term "bioactive" refers to their ability to bond to the living tissue and so most of them have been studied as materials for small bone substitutes, coatings for orthopedic prostheses, maxillofacial surgery [1,2]. Up today, the bioactive behavior can be induced on a variety of materials, belonging to different classes: glasses, glass-ceramics, ceramics and in some cases also metals (after proper surface modifications)[3]. Our attention will be focused on bioactive glasses, which represent the first class of inorganic materials that showed the peculiar surface property of bonding to living bone. When a bioactive glass is soaked in a simulated body fluid, called SBF, mimicking the inorganic composition of human plasma, several surface reactions can occur, leading, by a complex mechanism including ion leaching, silica gel formation, Ca^{++} and PO_4^{3-} diffusion, to the precipitation of hydroxy-carbonate apatite (HCA) with composition and structure close to the mineral phase of bone. The precipitation of these calcium phosphates on the surface of bioactive glasses has been extensively investigated[4,5,6], but information on the structural features of the HCA film, especially in the early stages of the deposition, is rather scant. Bioactive glasses can be massive or porous to host drugs to be delivered after prosthesis insertion. We present here the characterization of different kinds of bioactive glasses and glass-ceramics (both massive and porous) for applications in orthopedic and dental devices, to shed some light on the mechanism of growth of: *i)* mesoporous SBA phase in macroporous SCK bioactive glass scaffold and *ii)* HCA on massive SCK bioactive glass slices.

SCK is a glass with a molar composition of 50% SiO_2, 44% CaO, 6% K_2O. Two kinds of samples, that will be named from now on *SCK(scaffold)* and *SCK massive samples*, were studied. The porous glass-ceramic *SCK(scaffold)* was obtained by mixing SCK powders with polyethylene particles and by uniaxially pressing the powders to obtain a compact of powders (named *green*). The *green* was then thermally treated to remove the organic phase and to sinter the inorganic one. The macroporous SCK(scaffold) (pores in the 100-500μm range) was then used as a substrate for the growth of a crystalline mesoporous SBA phase (pores of about 5 nm) [7]. Two samples, with different SBA growing time, were prepared: 1) 24 h at room temperature and 48 h at 60°C (sample **a**); 2) 72 h at 60 °C (sample **b**). The SBA phase grown inside the macroporous scaffold was studied by transmission SAXS on the whole scaffold. The *SCK massive samples* are bioactive glasses obtained in form of slices, by melting the reagent grade precursors in a platinum crucible at 1500°C for 1 hour. Slices of SCK were soaked in SBF for different periods of time (1 hour, 6 hours, 1 day, 3 days and 7 days) in order to study *ex situ* the different steps of formation of HCA on their surfaces, by GISAXS/GIWAXS measurements.

The SAXS patterns of the *SCK(scaffold)* composite materials **a** and **b** are shown in Figure 1. They indicate the presence of three peaks for both samples, corresponding to d-spacings consistent with the presence of an hexagonal phase. We thus obtained a clear indication that

indeed an ordered mesoporous SBA phase is deposited on the surface of the SCK macropores.

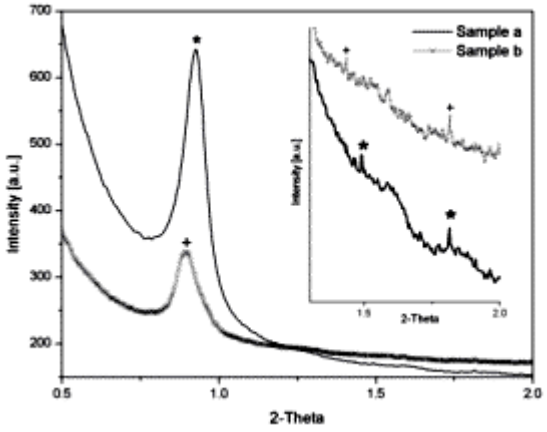

Figure 1. SAXS patterns of the *SCK(scaffold)*-SBA composite materials

A complete GISAXS analysis and interpretation of *SCK massive samples* is still in progress, but preliminary results clearly show that the width of the curve profiles increases proportionally to the soaking time of the samples and this trend is observed at all different ω angles. The comparison of the profiles obtained at all different ω angles on the same 7-day sample shows that the curves decrease in height and width while increasing the grazing angle (figure 2). Finally the GIWAXS analysis, used to monitor the HCA presence, shows the presence of an amorphous phase, due to the studied bioactive glasses, and the presence of a crystalline phase is only evident for the 7-day sample (data not shown).

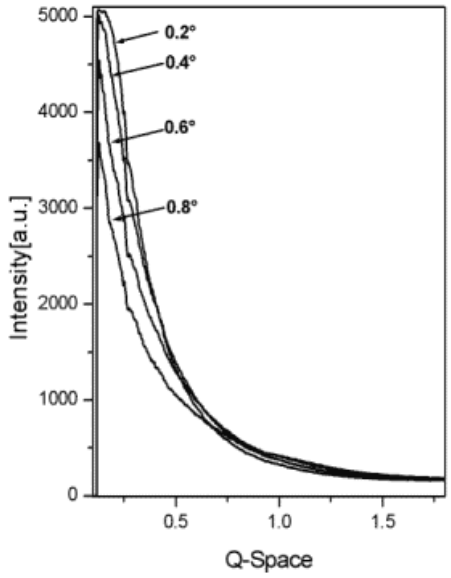

Figure 2. GISAXS patterns of the 7-day *SCK massive sample* at all different ω angles

References:

[1] L.L. Hench, *Am. Ceram. Soc. Bull.* 77, VII (1998) 67
[2] L. L. Hench, *J.Am.Ceram.Soc.*74(7), 1487 (1991)
[3] B.C.Yang, J.Weng, X.D.Li, X.D.Zhang, *J.Biomed.Mat.Res.* 47, 213 (1999)
[4] L.L. Hench., *J. Am. Ceram. Soc.* 81(7), 1705 (1993)
[5] W.Cao, L.L Hench, *Ceram. Int.* 22, 493 (1996)
[6] T. Kokubo, H. Kushitai, C. Ohtsuki, S. Sakka, T. Yamamuro, *J.Mater.Sci.:Mat.Med*. 3, 79 (1992)
[7] H.Yang, Q.Shi, B. Tian, S. Xie, F. Zhang, Y. Yan, B. Tu, D.Zhao , *Chem. Mater. 15*(2), 536 (2003)

APPEARANCE OF TWO CUBIC PHASES IN POPE UNDER EXCESS OF WATER CONDITIONS DURING COOLING

A. Hickel, M. Rappolt, K. Lohner, H. Amenitsch and G. Pabst

Institute for Biophysics and X-ray Structure Research, Schmiedlstr. 6, 8042 Graz, Austria

It is well known that in pure PE lipid systems, such as palmitoyl-oleoyl-phosphatidyl-ethanolamine (POPE), cubic phases do not form instantaneously, but instead, it can take days of equilibration until the evolution of a bicontinuous cubic lattice is fully accomplished. Alternatively, cubic phases can be induced by temperature cycling of several hundred or thousand times through the lamellar/inverse hexagonal phase transition [1]. In this report we show that already during the first cooling ramp two cubic phases occur after passage through the hexagonal/lamellar phase transition. Although the diffraction peaks of the cubic phase are quite weak, the indexing of two different cubic lattices is assured (Fig. 1). In Figure 2 the progression of their unit parameters is displayed. These results will serve on-going investigations on the role of antimicrobial peptides to strongly destabilize the lamellar phase of PEs in the lamellar/inverse hexagonal coexistence region.

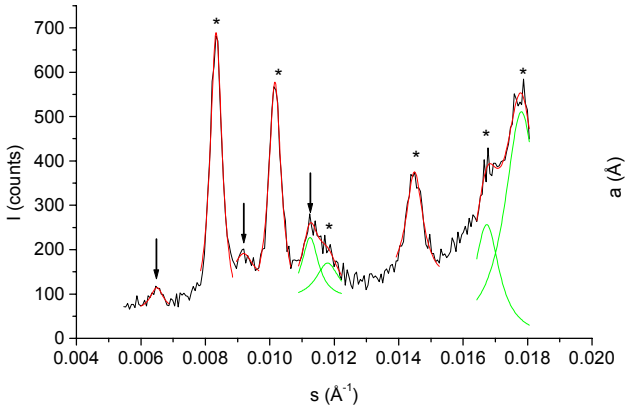

Figure 1. Diffraction pattern of the P_{n3m}-phase (*) plus traces of I_{m3m} (arrows) @ 35.5 °C. The peak positions were determined by fitting the reflections with Lorentzian distributions.

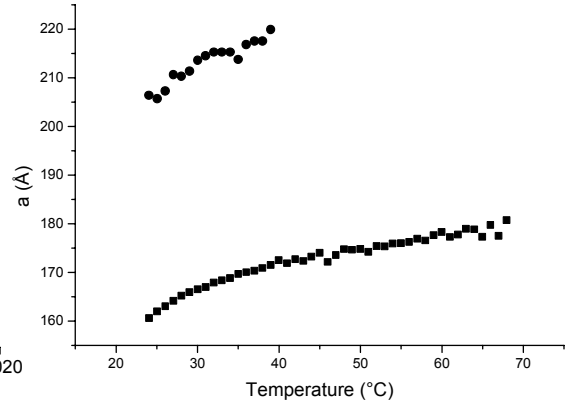

Figure 2. Evolution of the unit cell parameters during a cooling ramp of 1°C/min (P_{n3m} (squares) and I_{m3m} (circles)).

References:

[1] J. Erbes, J., C. Czeslik, W. Hahn, R. Winter, M. Rappolt, and G. Rapp. On the existence of bicontinuous cubic phases in dioleoylphosphatidy-lethanolamine.Ber. Bunsenges. Phys. Chem. 98, 8776–8779 (1994)

INFLUENCE OF SODIUM AND CALCIUM CHLORIDE ON THE FLUIDITY OF PHOSPHATIDYLCHOLINE MEMBRANES

A. Hodzic[1], M. Rappolt[1], J. Štrancar[2], P. Laggner[1] and G. Pabst[1]

1.) Institute of Biophysics and X-Ray Structure Research, Schmiedlst. 6, Graz, Austria
2.) Laboratory for Biophysics - EPR Center, Jožef Stefan Institute, Ljubljana, Slovenia

Alkali chlorides play an important role in several biological processes. The specific binding of cations with biological membranes influences not only their fluidity and structure, but consequently also processes like endo- and exocytosis or membrane fusion. Especially calcium ions play a decisive role in neural signal transduction and are believed to be an important driving force of fast transmitter release in the central synapse. In this work we report about the effect of sodium and calcium chloride (0 - 330 mM) on the stability, structure and dynamics of palmitoyloleoylphosphatidylcholine (POPC) bilayers. Combining the techniques of small angle X-ray scattering and spin-label electron paramagnetic resonance spectroscopy, both the global and local parameters of the chosen model membrane systems are characterized. Both salts perturb the positional order within the multibilayer systems considerably. In the case of NaCl we find no significant changes to the overall bilayer structure at all concentrations (see bilayer thickness d_B in Table 1), but simply a screening of the van der Waals interactions between adjacent bilayers. In contrast, $CaCl_2$ leads at low concentrations to a strong bilayer repulsion (see water layer thickness d_W in Table 1), which is completely screened at higher concentrations. In the latter concentration regime we also find a strong increase of the lipid acyl chain order and henceforth an increase of membrane thickness. Our results are confronted with recent molecular dynamics simulation studies, which were carried out on the same model system (see [1] and references therein).

Table 1: POPC multibilayer parameters.

Parameter	0 NaCl	50 mM NaCl	220 mM NaCl	330 mM NaCl	220 mM $CaCl_2$	330 mM $CaCl_2$
χ^2	6.0	4.1	3.5	8.38	7.768	8.619
d (Å)	63.0 ± 0.1	63.2 ± 0.1	64.3 ± 0.1	64.88 ± 0.01	69.30 ± 0.01	63.44 ± 0.01
d_{HH} (Å)	36.4 ± 0.1	36.2 ± 0.1	36.4 ± 0.1	36.18 ± 0.1	36.02 ± 0.1	18.55 ± 0.1
d_B (Å)	48.4 ± 0.2	48.2 ± 0.2	48.4 ± 0.2	48.18 ± 0.2	48.02 ± 0.2	49.1 ± 0.2
d_W (Å)	14.6 ± 0.2	15.0 ± 0.2	15.9 ± 0.2	16.7 ± 0.2	21.28 ± 0.2	14.34 ± 0.2
d_C (Å)	14.2 ± 0.2	14.1 ± 0.2	14.2± 0.2	14.09 ± 0.2	14.01 ± 0.2	14.55 ± 0.2
A ($Å^2$)	65.5 ± 1	66.0 ± 1	65.5 ± 1	66.00 ± 1	66.38 ± 1	63.92 ± 1
n_W	29.0 ± 1	29.7 ± 1	30.5 ± 1	31.57 ± 1	36.81 ± 1	28.06 ± 1
n_{Whead}	13.1 ± 1	13.2 ± 1	13.1 ± 1	13.2 ± 1	13.27 ± 1	12.78 ± 1
η	0.068 ± 0.003	0.072 ± 0.003	0.076 ± 0.003	0.08486 ± 0.003	0.1130± 0.003	0.04092 ± 0.003
Nmean	55	9	9	7.040	9.000	8.395

References:

[1] Böckmann, R.A. and H. Grubmüller. 2004. Multistep binding of divalent cations to phospholipid bilayers: a molecular dynamics study. Angew. Chem. Int. Ed. 43: 1021-1024.

BAROTROPIC PHASE TRANSITION OF BINARY MIXTURES OF POPC AND STEROLS (CHOLESTEROL AND PLANT STEROLS)

M. Kriechbaum[1], B. Sartori[1], M. Steinhart[2], H. Amenitsch[1], M. Rappolt[1], S. Bernstorff[3] and P. Laggner[1]

1.) Institute of Biophysics and X-Ray Structure Research, Austrian Academy of Sciences, Graz, Austria
2.) Institute of Macromolecular Chemistry, Czech Academy of Sciences, Prague, Czech Republic
3.) Sincrotrone Trieste, Basovizza, Italy

We have studied the barotropic phase transition and the underlying changes in the structural and mechanical properties of biomembranes consisting of 1-palmitoyl-2-oleoyl-phosphatidyl-choline (POPC) and admixtures of cholesterol and plant sterols in low concentrations (POPC/cholesterol, POPC/sitosterol and POPC/stigmasterol, respectively). Reversible hydrostatic pressure scan experiments have shown hystheresis effects on the transition pressure depending on the sterol concentrations and scan-rate. The hystheresis effects in the barotropic gel-to-fluid phase transition might be also attributed to domain formations of cholesterol rich and cholesterol depleted regions and phase separations between liquid-disordered and liquid-ordered phases This results in locally different regions of compressibility in the membrane and also in changes of the membrane fluidity.

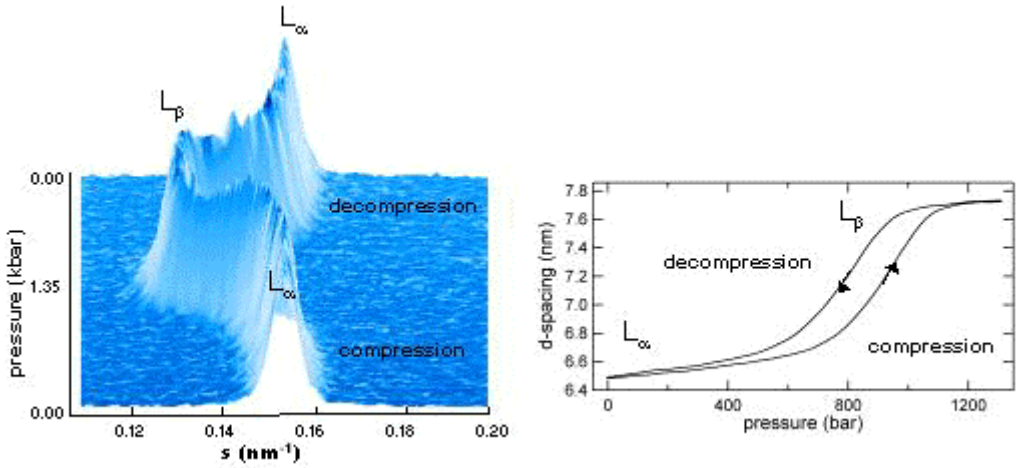

Figure 1. Left: Time-resolved SAXS patterns of a pressure-scanning SAXS experiment in a 3-dimensional representation (with the scattering vector *s* zoomed into the region of the first-order Bragg reflection of the lamellar repeat spacing, 3 s exposure time per frame) through the main-transition ($L_\alpha \leftrightarrow L_\beta$) during a reversible p-scan of POPC/sterol from 1 to 1350 bar and back to 1 bar (20 wt% POPC, 10 mol% sterol, 10°C). Right: Corresponding changes in the lamellar d-spacing and hystheresis effect in a pressurizing (compression) and subsequent depressurizing scan.

References:

[1] Rappolt, M., Vidal, M.F., Kriechbaum, M., Steinhart, M., Amenitsch, H., Bernstorff, S. & Laggner, P. (2003): Sturctural, dynamic and mechanical properties of POPC at low cholesterol concentration studied in pressure/temperature space. *Eur. Biophys. J.* 31, 575-585

ORIENTED CRYSTALLISATION OF COCOA BUTTER IN COUETTE-DSC-SWAXS COUPLED INSTRUMENT

M. Ollivon[1], C. Bourgaux[1], G. Keller[1], D. Kalnin[1] and H. Amenitsch[2]

1.) Physico-Chimie des Systèmes Polyphasés, UMR 8612, Univ. Paris-Sud, 5 rue JB Clément, Chatenay, France
2.) Institute of Biophysics and X-ray Structure Research, Austrian Academy of Sciences, Schmiedlstraße 6, A-8042 Graz, Austria

Following report about triglyceride crystallisation in emulsion, we present here the oriented crystallisation of an untempered sample of cocoa butter (CB) on cooling down to 15°C at low shear rate in the coupled DSC-SAXS-WAXS instrument (MICROCALIX®) equipped with the Couette cell described previously (Elettra, SAXS BL 5.2 report 2003) [1]. The picture has been taken under shear using image plate exposition during about 30 sec. Briefly, the Couette cell shown schematically on Figure below is made from a quartz capillary of $2r_1$ = 1 mm slowly rotating at (150 rpm) in a fixed quartz capillary of $2r_0$ = 1.5 mm sample thank to a torque limited and speed controled micromotor. The sample (about 10-15 mg) is placed in the vertical Couette device located in the reference cell which is of the calorimeter the temperature of which is computer controled to get first cooling from 35 to 20°C at fast rate then slow cooling (e.g. 0.1C.min^{-1}) until CB initial crystallisation. Oriented crystallisation occurred in several steps. The picture shows oriented crystallisation of form V ($3L\beta_2$) starting after oriented crystallisation of metastable forms of 2L type [2, 3]. Oriented crystallisation of CB has been already observed but the main advantage of such device over comparable Couette instruments installed at other synchrotron benches is the possibility to get images perpendicular and parallel to the flow then in perpendicular directions relatively to the crystal with no image analysis (Figure shows image as obtained) and its simplicity of use [4].

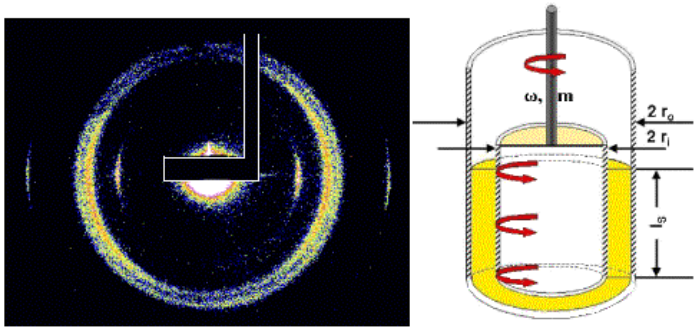

Figure 1. Oriented multiple crystallisations of cocoa butter in a new Couette cell as shown by raw image plate recording and device cut. Large opened circles show initial 2L crystallisation of CB in metastable forms while small elongates spots represents crystallisation of form V of CB. The beam stop shape is delimited for clarity (left). The coaxial quartz capilary Couette device is schematically shown as a 3D cut (right).

References:

[1] G. Keller, F. Lavigne, L. Forte, K. Andrieux, M. Dahim, C. Loisel, M. Ollivon, C. Bourgaux and P. Lesieur; DSC and X-ray diffraction coupling : specifications and applications; J. Therm. Anal., 51, 783-791 (1998)
[2] C. Loisel, G. Lecq, G. Keller, C. Bourgaux and M., Ollivon; Phase transitions and polymorphism of cocoa butter, J. Am. Oil Chem. Soc. , 75 425-439 (1998)
[3] R. Peschar, M.M. Pop, D.J.A. De Ridder, J.B. Van Mechelen, R.A.J. Driessen, H. Schenk, J. Phys. Chem. B. 108, 15450-15453 (2004)
[4] G. Mazzanti, S. E. Guthrie, E.B. Sirota, A.G. Marangoni and S.H.J. Idziak ; Orientation and Phase Transitions of Fat Crystals under Shear; Crystal Growth & Design, 3 7321-725 (2003)

EFFECTS ON THE QUATERNARY STRUCTURE OF BETA-LACTOGLOBULIN: HOW INTERACTIONS CAN BE AFFECTED BY TEMPERATURE AND SOLVENT MODIFICATIONS

M.G.Ortore[1,2], P.Mariani[1], F.Spinozzi[1], G.Onori[2], S. Bernstorff [3] and H. Amenitsch[4]

1.) Dipartimento di Scienze Applicate ai Sistemi Complessi, Universita' Politecnica delle Marche, via Ranieri 65, 60131 Ancona (Italy)
2.) Dipartimento di Fisica, Università degli Studi di Perugia, via A. Pascoli, 06123 Perugia (Italy)
3.) Sincrotrone Trieste, Area Science Park, 34012 Trieste, Italy
4.) Institute of Biophysics and X-ray Structure Research, Austrian Academy of Sciences, Schmiedlstr. 6, A-8042 Graz, Austria

β-lactoglobulin (BLG) is a well-known protein belonging to the lipocaline family, abundantly contained in the mammalian milk. BLG is constituted by two identical subunits of 18,400 Da and can be considered a model for understanding protein aggregation behaviour.
The monomer/dimer equilibrium of BLG is in fact affected by protein concentration, solvent features, temperature, pressure and pH. In particular, the fraction of monomers increases with decreasing protein concentration and pH, and with increasing temperature and pressure. The experimental landscape corresponding to each physical and chemical parameter has been investigated with different techniques, but the understanding of their combined effects is still not complete[1].
Here, in solution Small Angle X-Ray Scattering (SAXS) has been used to analyze how temperature and solvent modifications affect the quaternary structure of BLG. SAXS tecnique has been chosen since it is able to provide information between protein-protein interactions in a non-invasive way.
In order to investigate how dielectric features of the solvent may affect protein-protein interactions, different solutions containing water and water/ethylene-glycol (0-50% w/w EG), have been used. BLG was dissolved in sodium phosphate buffer (12 mM NaCl, pH 2.3) at 8 mg/ml. Kratky plots of our data confirm that even the presence of 50% w/w EG induces no protein denaturation at ambient temperature. Nonetheless EG effect is evident both on the unfolding process and on the interaction between proteins.
The experiments performed varying temperature (20°C-70°C) show that the unfolding process induced by temperature is influenced by the presence of EG (Fig.1). This effect is already detectable at 15% w/w of EG. EG destabilizes the protein inducing partial unfolding already at 40°C (50% w/w ethylene-glycol).
This observation suggests that the study of interactions between unfolded proteins in presence of EG should be carried out in a closer temperature range.
In Fig.2 it is shown how the presence of EG modifies the scattering curves of BLG at the same conditions of protein concentration, pH, ionic strenght and temperature. Curve fitting is the result obtained considering the contrast electron density of different solvents and different amounts of monomers/dimers, neglecting the interference contribute (fitting procedure consider $Q > 0.05$ Å). The calculation of the scattering form factor from the atomic coordinates of aminoacids constituing the protein has been performed using the cristallographic structure of BLG by means of Monte Carlo [2]. The presence of EG at room temperature seems to promote the dimeric structure.
The interference peak present at low Q could be reproduced using a model which describes the interaction potential among monomer and dimer. The calculation of the theoretical average structure factor, using a new approximation to the protein-protein correlation functions $g_{ij}(r)$ and screened electrostatic potential among charged monomer and dimer [3], has not been able to reproduce the interference peak. Thereby the interactions between

proteins cannot be explained considering only electrostatic contributions. EG modifies the dielectric features of the solvent and the interactions between proteins acting in a non-electrostatic way.
A thermodynamic description of the dissociation process can be assumed according to:

$$\Delta G_{dis} = -\Delta C_P \left[T\left(\log \frac{T}{T_0} - 1 \right) + T_0 \right] - \Delta S_0 \left(T - T_0 \right) + \Delta G_0$$

where Δ always means the change of the corresponding parameter during dissociation, G is the free energy, C_p is the heat capacity and S the entropy. In this way the thermodynamic parameters indicate how the presence of ethylene-glycol modifies the equilibria in solution.
This analysis is still in progress.

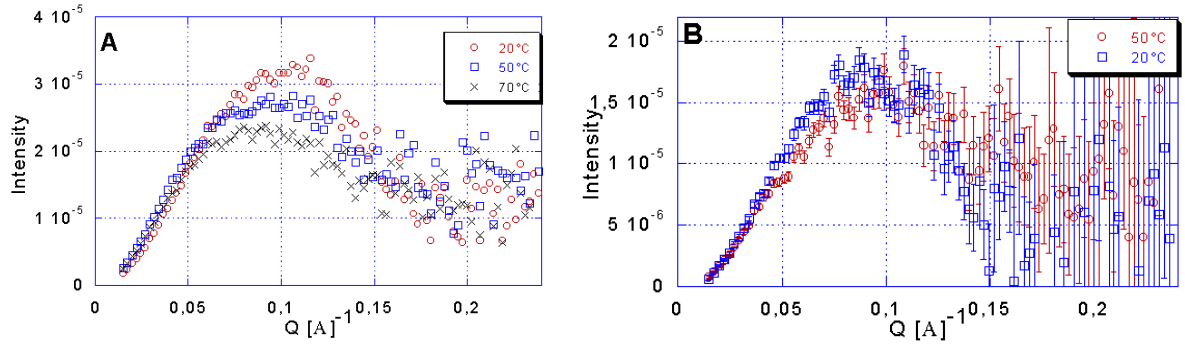

Figure 1. Kratky plots of scattering BLG curves. **A**: 0% w/w ethylene-glycol, t=20°C, 50°C, 70°C. **B**: 30% w/w ethylene-glycol, t=20°C, 50°C. Without ethylene glycol the loss of globular structural character begins toward 70°C, in presence of ethylene-glycol this process is evident since 50°C.

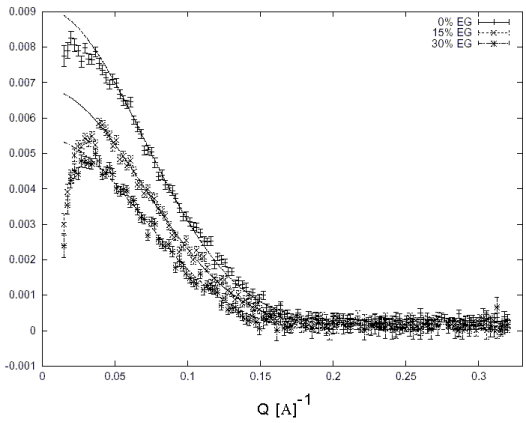

Figure 2. Scattering curves of BLG at different EG fractions: 0-15-30% w/w. pH=2.3, $C_{protein}$=8mg/ml, Ionic strenght:12mM, T=20°C.

References:

[1] Baldini G, Beretta, S. G. Chirico, E. Maccioni, F. Spinozzi, P. Mariani, H. Franz. 1999. Salt-Induced Association Of Beta-Lactoglobulin By Light And X-Ray Scattering. *Macromolecules*, 32:6128-6138

[2] S. Brownlow, J.H. Morais Cabral, R. Cooper, D.R. Flower, S.J.Yewdall, I. Polikarpov, A.C.T.North & L. Sawyer.1997. Bovine □-lactoglobulin at 1.8Å resolution - still an enigmatic lipocalin *Structure* 5(4) 481-495

[3] Spinozzi, F., D. Gazzillo, A. Giacometti, P. Mariani and F. Carsughi. 2002. Interaction of proteins in solution from small angle scattering: a perturbative approach. *Biophys. J.*, 82:2165–2175

EFFECT OF CHAIN LENGTH ON THE LATERAL ORGANIZATION OF CHARGED LIPID MEMBRANES.

G. Pabst[1], M. Rappolt[1], H Amenitsch[1], J. Katsaras[2] and A. Hickel[1]

1.) Institute of Biophysics and X-ray Structure Research, Austrian Academy of Sciences, Schmiedelstr. 6, 8042 Graz, Austria
2.) National Research Council, Steacie Institute of Molecular Sciences, Chalk River, Ontario K0J 1J0, Canada

We have studied the hydrocarbon chain packing in the gel phase of well aligned multibilayers composed of phosphatidylglycerol (PG) by grazing incidence x-ray diffraction. Hydration of the samples was achieved from water vapour in a sample chamber of special design [1]. The hydrocarbon chain length was varied between 16 hydrocarbons and 18 hydrocarbons per chain. We observe a transition from a orthorhombic packing with a tilt direction towards nearest neighbours for di16PG to a monoclinic chain packing with a tilt direction in-between nearest and next nearest neighbours for di18PG. This leads to an increase of packing density, which might affect the lipids affinity for interaction with membrane active compounds.

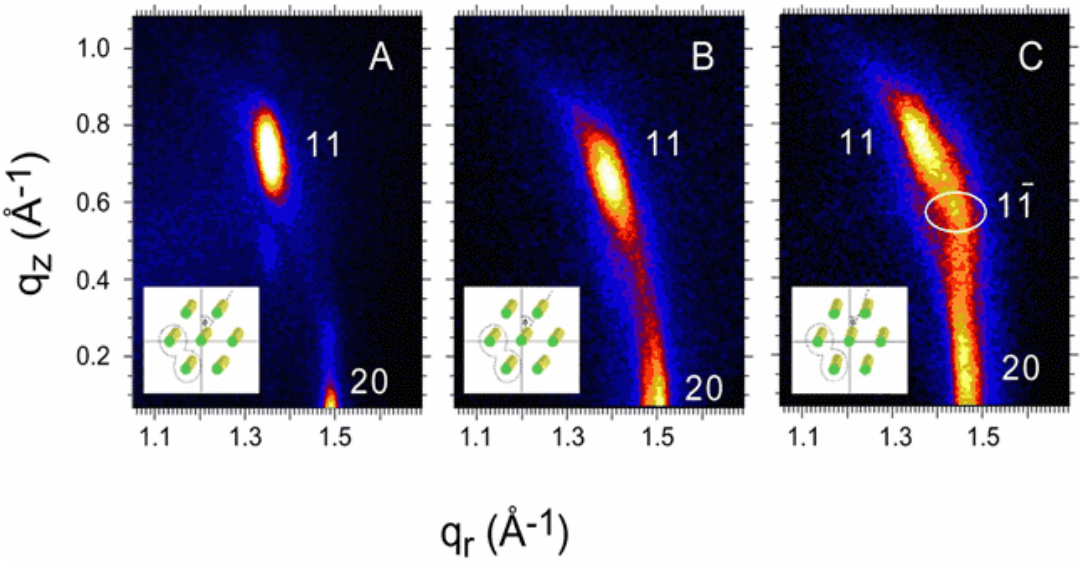

Figure 1. Wide-angle diffraction patterns of aligned (A) DPPC, (B) DPPG and (C) DSPG in the gel ($L_{\beta'}$) under grazing incidence conditions. The data shows that DPPC and DPPG chains are tilted towards nearest neighbors [2]. DSPG, in contrast exhibits a tilt direction intermediate between nearest and next nearest neighbors.

Table 1. Chain tilt with respect to bilayer plane (θ), tilt direction (ϕ) and lateral area (A) per lipid for DPPC, DPPG, and DSPG.

	θ [°]	**ϕ [°]**	**A [Å^2]**
DPPC	32.9	30	46.7
DPPG	29.3	30	44.7
DSPG	26.9	11	43.9

References:

[1] J. Katsaras and M. Watson; Rev. Sci. Instrum. 71, 1737 (2000)
[2] G.S. Smith, E.B. Sirota, C.R. Safinya, and N.A. Clark; Phys. Rev. Lett. 60, 813 (1988)

PRESSURE EFFECTS ON LIPID DIRECT PHASES: AN ANALYSIS OF THE DODECYL TRIMETHYL AMMONIUM CHLORIDE-WATER SYSTEM

M. Pisani[1], L. Paccamiccio[2], F. Spinozzi[2], H. Amenitsch[3], S. Bernstorff[4] and P. Mariani[2]

1.) Dipartimento di Scienze dei Materiali e della Terra, Marche Polytechnique University, Ancona (Italy).
2.) Department of Science Applied to Complex Systems, Physical Sciences Section, Marche Polytechnique University, Ancona (Italy).
3.) Institute of Biophysics and X-ray Structure Research, Austrian Academy of Sciences, Schmiedlstrasse 6, A-8042 Graz, Austria
4.) Sincrotrone Trieste, Area Science Park, 34012 Trieste, Italy

It is generally assumed that under compression, lipids adapt to volume restriction by changing their conformation and packing: since a delicate balance of competing energetic contributions is involved in stabilization of lipid phases in water, such small changes in conformation can determine large structural transformations. For example, the lamellar-to-gel phase transitions has been detected in some phosphatidyl choline-water dispersions under compression, while transition temperatures related to non-lamellar phases resulted very sensitive to pressure [1].
Remarkable structural effects have been in particular detected on lipid inverse systems (type II): pressure induces the transition from the hexagonal to the lamellar phase in DOPE [2], and the transition from the Pn3m cubic to the Ia3d cubic phase (or to the lamellar phase, depending on sample concentration) in monoolein [3,4]. However, the most intriguing result concerned the compressibility of the inverse phases, which resulted negative (i.e., under compression, the unit cell dimension increases) [2-5]. Simple molecular packing arguments, based on changes in the molecular shape, explained this behavior: by increasing pressure, the lipid chain order parameter increases, so that the wedge shape of the molecules reduces. Because of the consequent decreased curvature of the lipid layer, this results in an enlargement of the unit cell size [2]. Moreover, the increase in the lattice constant has been observed to be larger in lipid systems dispersed in excess of water: a change in the hydration level has been then associated to the variation of the basic geometrical shape of the lipid molecule [2,4,5].
Concerning direct phases, high-pressure structural investigations have been only sparingly performed [1]. Direct phases (type I) are constituted by cylindrical, spherical or quasi-spherical micelles, filled by lipid hydrocarbon chains and embedded in a water matrix. Because the topology, pressure effects are expected to be quite different from those observed in inverse phases. In this work, the dodecyl-trimethyl-ammonium chloride (DTAC) - water system was considered. The phase diagram of DTAC at atmospheric pressure shows in the middle region the occurrence of a direct hexagonal H phase, consisting of a hexagonal array of cylinders, filled by the hydrocarbon chains, coated with the DTAC polar head-groups and embedded in the water matrix [6]. A micellar Pm3n cubic phase extends between the hexagonal and the isotropic fluid phases, while a Ia3d cubic phase extends in the drier side of the phase diagram, between the hexagonal and a lamellar phase, which forms in very dehydrated conditions. The Pm3n cubic phase consists of two types of disjointed micelles of type I embedded in a continuous water matrix [7]. The Ia3d cubic phase is bicontinuous, and consists of two 3D networks of joined rods, mutually intertwined and unconnected [6]: the rods are filled by the hydrocarbon chains and are coplanarly joined 3 by 3.
Synchrotron X-ray diffraction was used to investigate the polymorphism of DTAC at different concentrations of water under hydrostatic pressure up to 3 kbar. For high-pressure measurements, the control system designed and constructed by M. Kriechbaum and M. Steinhart was used [8]. The pressure cell has two diamond windows (3.0 mm diameter and 1 mm thickness) and allows to measure diffraction patterns at hydrostatic pressures up to 300

MPa. X-ray diffraction measurements were performed at 25°C for different pressures, from 0.1 MPa to about 220 MPa, with steps of about 10 MPa. In each experiment, a number of sharp reflections and a diffuse band were detected in the low- and wide-angle X-ray diffraction regions, respectively, and their spacings measured following the usual procedure [6]. SAXS profiles were indexed considering the different symmetry systems commonly observed in lipid phases. A few of X-ray diffraction profiles are shown in Figure 1.

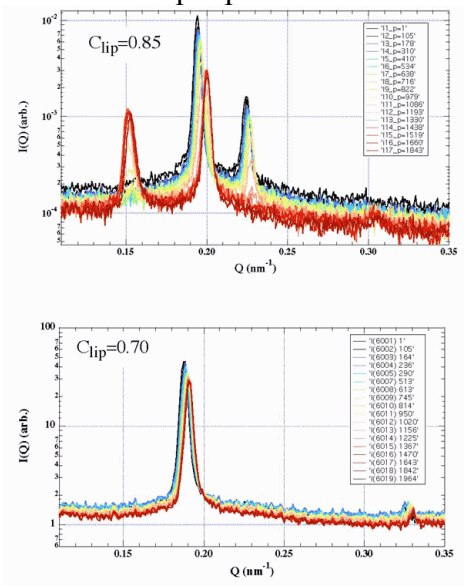

Figure 1. X-ray scattering pattern of DTAC samples investigated at different pressures and concentrations

From the diffraction profiles, a transition from the hexagonal phase to the micellar cubic phase Pm3n in hydrated samples (c=0.55 - 0.66) and from the bicontinuous cubic phase Ia3d to the hexagonal phase in dried samples (c>0.82) have been derived. The obtained phase diagram is reported in Figure 2.

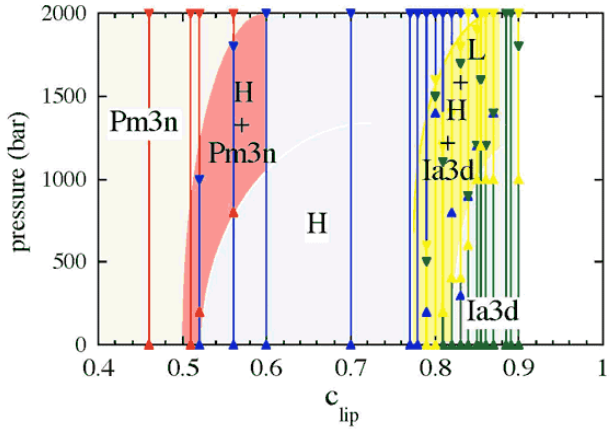

Figure 2. Concentration-pressure dependent phase diagram for the DTAC-water system

From the positions of the peak observed in the X-ray diffraction profiles, unit cell dimensions were then calculated: results show that the unit cell decreases during compression in all the different phases. Moreover, the pressure dependence is very week. It should be noticed that the behavior detected in inverse phases was basically opposite, where the unit cell dimensions increase under compression in both hexagonal and cubic phases [2,4]. The volume variations of the 2D hexagonal and 3D cubic phases under pressure were then used to derive the isothermal compressibility of the different phases and considering the structural properties of the lipid phases, the partial lipid and water molecular compressibilities were also derived.

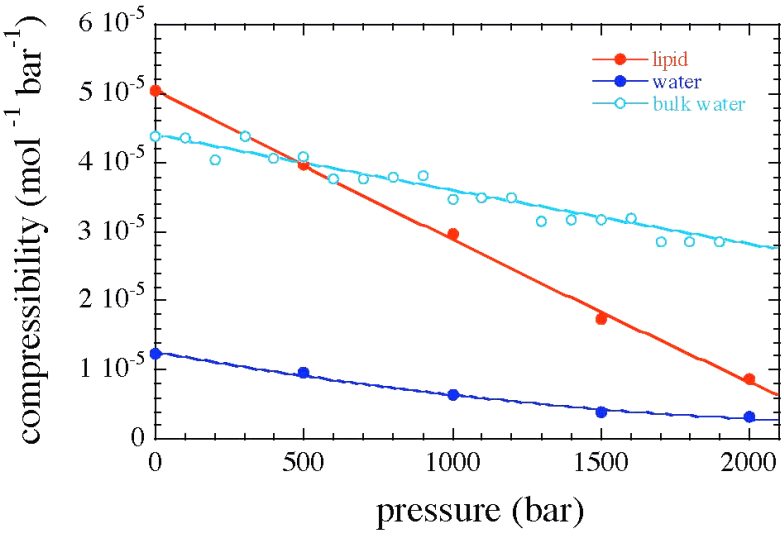

Figure 3. Pressure dependence of the coefficients of isothermal partial compressibility of the DTAC and water molecules

It is interesting to underline that the water confined within the lipid phase shows an unusual low compressibility, of about one sixth of the compressibility observed for bulk water. On the other side, the DTAC compressibility appears very dependent on pressure: as the lipid compressibility represents a measure of intermolecular interactions, this suggest that the observed behavior reflect the tightness of intrinsic hydrocarbon packing induced by pressure. Structural parameters were also determined: the average area-per-molecule at the polar/apolar interface and the hydrocarbon chain length decrease during compression. The variations are however small, and indicate that the conformational changes induced by pressure in the DTAC molecule are rather small. Finally, noticeable is the fact that the area-per-molecule at constant concentration slightly decreases during compression, indicating that pressure induces a some dehydration of the polar surfaces, in contrast with results obtained in inverse phases, suggesting different energy contributions to the stabilization and transformation of lipid phases.

References:

[1] R. Winter, Curr. Opin. Coll. Interf. Sci. 6, 303(2001)
[2] M. Pisani, T. Narayanan, G.M. Di Gregorio, C. Ferrero, S. Finet, P. Mariani: PRE, 68, 21924(1) (2003)
[3] P. Mariani, B. Paci, P. Bosecke, C. Ferrero, M. Lorenzen, R. Caciuffo. PRE, 54, 5840-5843 (1996)
[4] M. Pisani, S. Bernstorff, C. Ferrero, P. Mariani. Journal Phys. Chem. B, 105, 3109-3119 (2001)
[5] P.T.C. So, S.M. Gruner, S. Erramilli, Phys. Rev. Lett. 70, 3455 (1993)
[6] P. Mariani, V. Luzzati, H. Delacroix. J. Mol. Biol., 204, 165-189 (1988)
[7] R. Vargas, P. Mariani, A. Gulik, V. Luzzati. J. Mol. Biol., 225, 137-145 (1992)
[8] M. Steinhart, M. Kriechbaum, K. Pressl, H. Amenitsch, P. Laggner, S. Bernstorff Rev. Sci. Instr. 1999, 70, 1540-1545

COMPOSITION DEPENDENCE OF AGGREGATION FORM AND MIXING PROPERTIES IN A BACTERIAL MODEL MEMBRANE SYSTEM

B. Pozo Navas, K. Lohner, G. Deutsch, E. Sevcsik, and G. Pabst

Institute of Biophysics and X-ray Structure Research, Austrian Academy of Sciences, Schmiedlstraße 6, A-8042 Graz, Austria

We have determined the mixing properties and aggregation behavior of bacterial (POPE) and -phosphatidylglycerol (POPG) at various molar ratios applying differential scanning calorimetry and small and wide-angle x-ray scattering. Combining the experimental thermodynamic data with a simulation of the liquidus and solidus lines we were able to construct a phase diagram. Using this approach we find that the lipids mix in all phases non-ideally in the thermodynamic sense. As expected, pure POPE aggregates into multilamellar and pure POPG into unilamellar vesicles, respectively, which are stable within the studied temperature range. In contrast, mixtures of the two components form oligolamellar vesicles consisting of about three to five bilayers. The layers within these oligolamellar liposomes are positionally correlated within the gel phase, but become uncorrelated within the fluid phase exhibiting freely fluctuating bilayers, while the vesicles as a whole remain intact and do not break up into unilamellar aggregates. X-ray, as well as DSC data, respectively reveal a miscibility gap due to a lateral phase segregation at POPG concentrations above about 70 mol%, similar to previously reported data on mixtures composed of disaturated PEs and PGs. Hence, the existence of a region of immiscibility is a general feature for PE/PG mixtures and the mixing properties are dominated by PE/PG headgroup interactions, but are largely independent on the composition of the hydrocarbon chains. This is in accordance with a recent theoretical prediction.

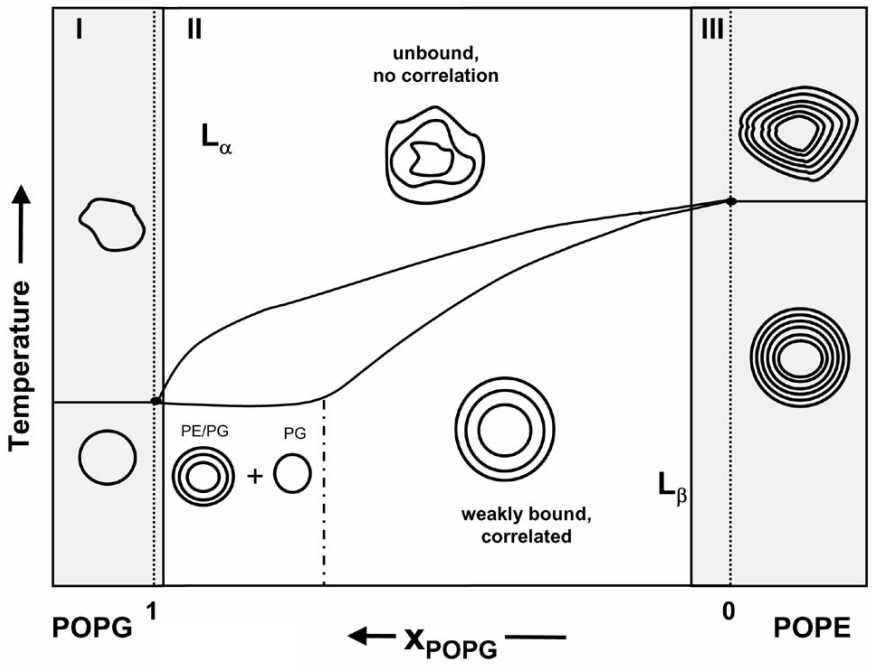

Figure 1. Schematic representation of the vesicle morphology as a function of POPE/POPG composition and phase state. The phase diagram exhibits a miscibility gap at $x_{POPG} > 0.70$ indicated by the straight solidus line in this composition range. (I) corresponds to the existence range of unilamellar vesicles, (II) to oligolamellar vesicles and (III) to multilamellar vesicles.

IN SITU TENSILE TESTING OF HUMAN AORTAS BY TIME-RESOLVED SMALL ANGLE X-RAY SCATTERING

F. Schmid[1,2], G. Sommer[2], M. Rappolt[1], C.A.J. Schulze-Bauer [2], P. Regitnig[3], G.A. Holzapfel[2,4], P. Laggner[1] and H. Amenitsch[1]

1.) Austrian Academy of Sciences, Institute of Biophysics and X-ray Structure Research, Graz, Austria
2.) Graz University of Technology, Computational Biomechanics, Graz, Austria
3.) Medical University Graz, Institute of Pathology, Graz, Austria
4.) Royal Institute of Technology, Department of Solid Mechanics, Stockholm, Sweden

Cardiovascular Diseases (CVDs), i.e. diseases concerning the heart and the circulatory system, have become a worldwide issue. In the so called „developed countries“ the situation is particularly alarming, as meanwhile CVDs account for around half of the total deaths. The most important CVD in terms of numbers is atherosclerosis, at which biochemical and biomechanical changes in the wall of a blood vessel (“calcifications”) cause a narrowing or even an obstruction. This narrowing of the blood vessel is the cause for “classic” diseases such as ischemic stroke and heart attack. The reasons for atherosclerosis are well known, terms like cholesterol, smoking or sedentary lifestyle – to name but a few – have become omnipresent buzzwords.

A common therapy to increase the diameter of a blood vessel is balloon angioplasty, where a balloon is inserted into the narrowed section of the blood vessel and inflated. Simultaneously, quite often a cylindrical wire mesh (a “stent”) is inserted into the vessel in order to keep it open after deflation of the balloon. Thus the diameter of the blood vessel is usually restored sufficiently to provide proper blood flow.

Despite the high success rate of this intervention the detailed mechanisms of the procedure are not yet fully investigated. There is still a lack of knowledge about the structure and the mechanical behavior of the involved biological tissues as well as the interaction between balloon, stent and the individual tissues. Such data need to be implemented into new mathematical models to simulate and improve long term success of this interventional treatment.

A major mechanical component of blood vessels is the network of collageneous fibers in the tissue. Its behavior under mechanical load is important to understand the coupling of the nano- and macroscopical responses. There have been considerable numbers of studies on collagen itself or collagen rich tissue. However, many of these studies have been performed on animal tissue, the samples underwent histological fixation processes and/or were performed under non-physiological conditions or they provided only “snaphots” and no continuous information.

In this in situ study at the Austrian Small Angle X-ray Scattering beamline at Elettra, structural changes of the collagen network in human aortas were investigated. The artery was dissected into its layers and sample strips were cut out in circumferential and longitudinal directions of the blood vessel. They were kept in a semi-physiological environment during uniaxial tensile tests (in circumferential and longitudinal direction). The beam was set radially with respect to the axis of the blood vessel. Simultaneously with the diffraction patterns representative parameters such as force, displacement and the lateral contraction were recorded. Analysis of the diffraction patterns yielded extension dependent changes in the orientation and d-spacing of the collagen fibers.

The results show a direct relation between the orientation and extension of the collagen fibers on the nanoscopic level and the macroscopic stress/strain. This is attributed first to a straightening of collagen fiber bundles where no significant increase in macroscopic force is observed. Upon further increase of load the fibers start to reorient towards the tensile axis and an increase in stress can be observed. After this reorientation of the fibers has completed the macroscopic stress increases and the fibers themselves are being stretched, i.e. the change of an increase in d-spacing can be observed. These three distinctable regions are marked as Phase I-III in Figure 1.

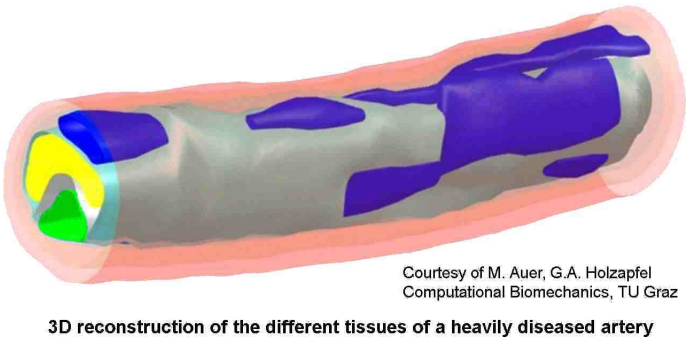

Figure 1: Mechanical macroscopic stress over strain. The nonlinear mechanical behavior is typical for soft biological tissues.

In Phase I – commonly referred to as “toe region” – no significant increase in macroscopic stress is observed, only kinks in collagen fiber bundles are being straightened. The according diffraction pattern on the left shows broad arcs, representing a wide angular distribution of the fibers in the tissue. After that (Phase II) the fibers start to reorient towards the tensile axis, the tissue starts to bear stress. This is called the “heel region”. Finally the fibers have reached their maximum orientation and do not turn any further, they are “locked” in Phase III. This is clearly seen in the diffraction pattern on the right: the angle of the arcs has decreased significantly, the fibers are clearly oriented around the vertical, which is the tensile axis. Here they take over a significant amount of stress from the tissue, which leads to a stretching of the fibers.

Reference:

[1] F. Schmid, G. Sommer, M. Rappolt, C.A.J. Schulze-Bauer, P. Regitnig, G.A.Holzapfel, P.Laggner and H. Amenitsch, J. Synchr. Rad., 2005, in press

PROTEIN-PROTEIN INTERACTIONS IN THE HUMAN PYRUVATE DEHYDROGENASE COMPLEX

M. Smolle[1], J.G. Lindsay[1] and O. Byron[2]

1) Division of Biochemistry & Molecular Biology, Institute of Biomedical & Life Sciences, University of Glasgow, Glasgow G12 8QQ, United Kingdom
2) Division of Infection & Immunity, Institute of Biomedical & Life Sciences, University of Glasgow, Glasgow G12 8QQ, United Kingdom

The pyruvate dehydrogenase complex (PDC) is a large, highly ordered multi-enzyme complex that plays an important role in cellular metabolism by linking glycolysis with the TCA cycle. It also serves as a model system for the investigation of protein-protein interactions, enzyme cooperativity and active site coupling. The human complex consists of four different proteins: dihydrolipoamide acetyltransferase (E2) and E3 binding protein (E3BP, X) form the icosahedral core that allows association of pyruvate decarboxylase (E1) and dihydrolipoamide dehydrogenase (E3). The PDC core consists of 60 E2 and 12 E3BP molecules, and provides binding sites for 30 E1 and 6 E3 molecules, respectively [1]. In contrast to the bacterial complexes where E1 and E3 compete for mutually exclusive binding sites on E2, specific subcomplexes between E1 and E2, as well as E3 and E3BP are formed in eukaryotes [2,3]. We are particularly interested in the formation of so-called "cross-bridges" (Fig. 1) by E3/E3BP and E1/E2 respectively – 1:2 stoichiometric subcomplexes whose existence has been shown by previous experiments using analytical ultracentrifugation, isothermal titration calorimetry, and native polyacrylamide gel electrophoresis (manuscript in preparation). The aim of this experiment was to gain insights into the structural arrangement of proteins within the E3/E3BP subcomplex which in conjunction with the E1/E2 subcomplex is thought to influence profoundly PDC function and regulation.

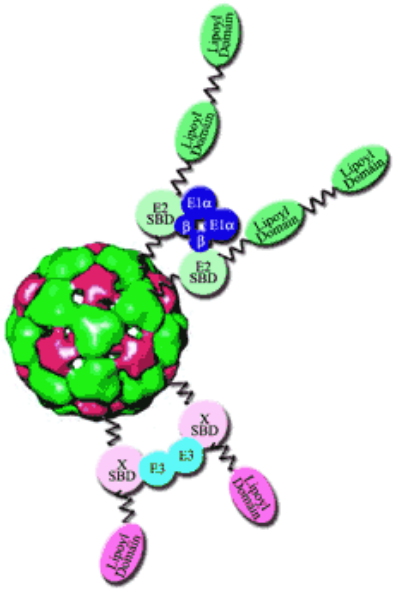

Figure 1. Schematic representation of protein-protein interactions within the PDC E2 (green) and E3BP (pink) are multi-domain proteins, consisting of two or one N-terminal lipoyl domains, a subunit binding domain (SBD) and a C-terminal core-forming domain respectively, all of which are interconnected by flexible linker regions. Diagram partially adapted from [4].

Scattering experiments for E3, a special didomain construct of E3BP (E3BP-DD) consisting of the protein's lipoyl and subunit binding domains, as well as their complex (DD/E3) were performed at two different sample-to-detector distances, 1.6 m and 0.75 m covering a range of momentum transfer of $0.01 < s < 0.8$ Å^{-1} ($s = 4\pi \sin\theta/\lambda$, where 2θ is the scattering angle and λ the x-ray wavelength of 1.5 Å). The scattering of at least three different concentrations of each E3, E3BP-DD and the DD/E3 complex were recorded at 10ºC using a 1D gas detector and covering a concentration range of 2-30 mg/ml. The data were normalised to the intensity

of the incident beam and corrected for the detector response. The scattering of the buffer was subtracted and the difference curves scaled for concentration. Final scattering curves (Fig. 2) were obtained by merging data recorded at different concentrations and camera lengths using PRIMUS [5]. The particle maximum dimensions, D_{max}, and radius of gyration, R_g, were obtained using GNOM [6]. Because we obtained relatively few data at low scattering angles for the DD/E3 complex we could not fit the scattering curve with GNOM. We have overcome this by merging the scattering curve with low angle data for the same complex previously obtained at beamline BM26 at the ESRF, Grenoble.

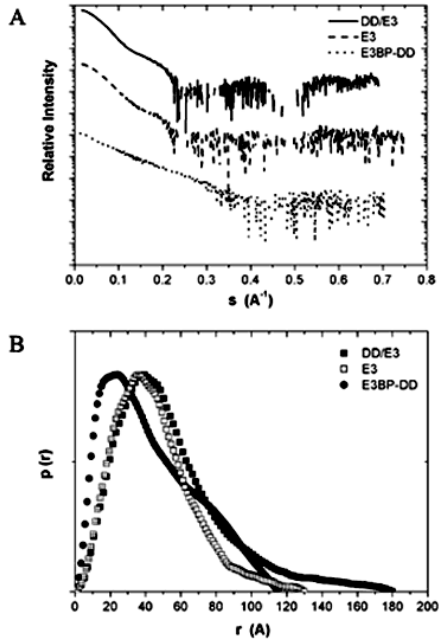

Figure 2. Scattering curves (A) and distance distributions (B) of E3, E3BP-DD and the DD/E3 complex

The D_{max} and R_g values determined experimentally agree well with those obtained for homology models of the two proteins and their complex (not shown) using the program CRYSOL [7] (Table 1). The values for E3 are larger than predicted, but these can be explained by the absence of ca. 70 amino acids from the N- and C-termini that could not be modeled and/or hint at a slightly different structural conformation for human E3 when compared with the yeast template used for modeling. The data also confirm the existence of a 2:1 stoichiometric complex of E3BP-DD and E3. The difference in the experimentally determined and calculated values of D_{max} for the DD/E3 complex is presumably caused by a different arrangement of E3BP-DD and E3 than that assumed in the model. Unfortunately, *ab initio* modeling proved to be difficult because of the relatively poor statistics of the low angle region of the scattering curves and no reliable models were obtained.

Table 1. Comparison of experimentally determined and calculated particle dimensions

Protein	Experimental		Calculated	
	R_g (Å)	D_{max} (Å)	R_g (Å)	D_{max} (Å)
E3	35.1	130	31.1	116
E3BP-DD	35.2	115	34.4	110
DD/E3 complex	43.9	180	44.8	165

References:

[1] S.J. Sanderson, C. Miller and J.G. Lindsay; Stoichiometry, organisation and catalytic function of protein X of the pyruvate dehydrogenase complex from bovine heart; *Eur. J. Biochem*. 236, 68-77 (1996)

[2] A.H. Harris, M.M. Bowker-Kinley, P. Wu, J. Jeng and K.M. Popov; Dihydrolipoamide dehydrogenase-binding protein of the human pyruvate dehydrogenase complex - DNA-derived amino acid sequence, expression, and reconstitution of the pyruvate dehydrogenase complex; *J. Biol. Chem*. 272, 19746-19751 (1997)

[3] Q.D. Yang, J.S. Song, T. Wagenknecht and T.E. Roche; Assembly and full functionality of recombinantly expressed dihydrolipoyl acetyltransferase component of the human pyruvate dehydrogenase complex; *J. Biol. Chem.* 272, 6361-6369 (1997)

[4] Z.H. Zhou, D.B. McCarthy, C.M. O'Connor, L.J. Reed, J.K. Stoops; The remarkable structural and functional organization of the eukaryotic pyruvate dehydrogenase complexes; *PNAS* 98, 14802-14807 (2001)

[5] P.V. Konarev, V.V. Volkov, A.V. Sokolova, M.H.J. Koch and D.I. Svergun; PRIMUS: a Windows PC-based system for small-angle scattering data analysis; *J. Appl. Crystallography* 36, 1277-1282 (2003)

[6] D.I. Svergun, A.V. Semenyuk and L.A. Feigin; Small-angle-scattering-data treatment by the regularization method; *Acta Cryst.* A44, 244-250 (1988)

[7] D.I. Svergun, C. Barberato and M.H.J. Koch; CRYSOL: a program to evaluate x-ray solution scattering of biological macromolecules from atomic structures; *J. Appl. Crystallography* 28, 768-773 (1995)

3. Chemistry

INFLUENCE OF SYMMETRICAL TRI-BLOCK COPOLYMERS TO THE STRUCTURE DEVELOPMENT IN POLYMER BLENDS

J. Baldrian[1], M. Steinhart[1], A. Sikora[1], H. Amenitsch[2], S. Bernstorff[3] and M. Staneva[4]

1.) Institute of Macromolecular Chemistry, A.S. CR, Heyrovsky Sq.2, 162 06 Prague, Czech Republic
2.) Institute of Biophysics and X-ray Structure Research, A.A.S., Schmiedlstrasse 6, 8010 Graz, Austria
3.) Sincrotrone Trieste, Area Science Park, 34012 Trieste, Italy
4.) Institute of Polymers, Bulgarian Academy of Sciences, 1126 Sofia, Bulgaria

Introduction

Block copolymers are of great scientific interest due to their self-assembled supramolecular structures formed under various conditions. In crystalline/amorphous copolymer systems, there are three factors that determine the final phase and crystalline morphology, i.e. the microphase separation of block copolymer, crystallization of crystallizable blocks and the vitrification of the amorphous blocks. The phase separation behavior of block copolymers results in creation of lamellar (L), hexagonal (H) and cubic (C) structures depending on the different environments of the assembling copolymer molecules.

The aim of this work was to study structural phenomena occurring in the series of two-component symmetrical tri-*block*-copolymers and their blends with the neat polymer during crystallization and melting.

Experimental

The series of block-copolymers PEO-*b*-PPO-*b*-PEO (BCP) and two narrow molecular weight fractions of neat polymer PEO were selected for the study (Table I.). Chains of P2 fraction (M_w ~ 2000) are "stiff", as they can crystallize as EC only; the second fraction P3 is flexible, the chains can be folded in lamellae. The structure development was studied by simultaneous WAXS/SAXS/DSC measurements during cooling from the melt and during subsequent heating (70 °C → 30 °C → 70 °C, rate 1°C/min.).

Results and discussion

Typical changes of periodicities (LP) in studied blends are shown on Fig.1 (for P105/P2, P3 blends). Starting *melt* LPs abruptly change at temperature of crystallization to the new LPs value in solid (partially crystalline) state and L, H and C structures are developed depending on blend compositions. Periodicities LPs developed during cooling [166 Å - 192 Å] are in relatively narrow interval and they are proportional to the molecular weight of pure PEO admixtures. PEO tails of BCPs are embedded into lamellae in 1F or 2F conformations. Pure P2 chains are in lamellae in extended form and in P3 are in 1F form. This LPs are stabile, they do not change during cooling and subsequent heating. Relatively steep increase of the LPs starts near melting point of blends and at melting point return LPs to the starting *melt* value.

The crystallization of blends during cooling from melt causes formation of very stable high temperature structure and therefore are the LPs stabile during temperature treatment. The steep growth of LPs, proceeding in studied systems during heating approaching the melting point, can be explained partly by the structure inprovement of crystalline phase and mainly by the thickening of amorphous interlayers caused by partial melting of the shortest PEO chains in blends and their diffusion into amorphous regions.

The components of copolymers are not compatible; they are phase separated also in the melt, which is demonstrated by periodical structure (LP_M) observed by SAXS (Table 1.). BCPs and their blends clearly demonstrate order/disorder/crystallization effect. The melt-periodicities are proportional to the molecular weight of copolymers and their values increase with increasing content of homopolymer admixture. The growing periodicities in melted blends are shown on Fig.2. This growth points out to the dilution of phase separated PPO regions in the melt.

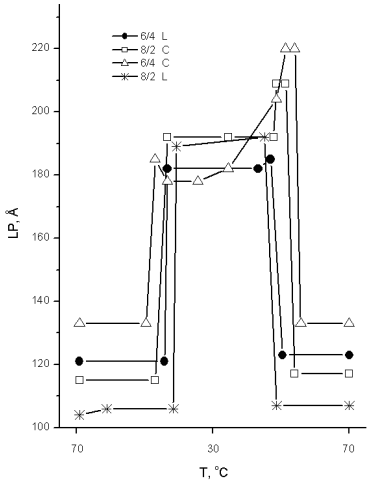

Figure 1. Changes of periodicities in blends of BCPs P105 with P2 and P3 during heat treatment

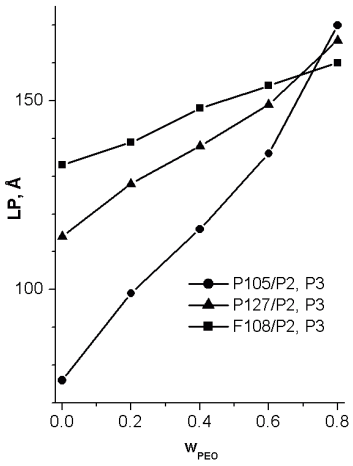

Figure 2. Changes of periodicities in melted BCPs and in their blends

Table 1. Parameters of studied polymers (M_w^E, l_E, and M_w^P, l_P – mol. weights and lengths of PEO and PPO blocks resp.; Cr – crystallinity; LP_M – periodicity in melt)

	M_w^E	M_w^P	E, %	l_E, Å	l_P, Å	Cr	LP_M, Å
P 105	2x1625	3250	50	103	196	.29	84
P 6800	2x3500	1750	80	221	105	.45	86
F 127	2x4410	3780	70	278	228	.41	116
F 108	2x5840	2920	80	369	176	.47	134
PEO 2000	2000	–	100	125	–	.78	–
PEO 3000	3000	–	100	190	–	.78	–

Acknowledgment
Research was supported by the Grant Agency of the Czech Republic (grant No. 203/03/0611)

SAXS-INVESTIGATIONS OF NANOPARTICLE/POLYMER HYBRIDS

W. H. Binder[1], D. Farnik[1], C. Kluger[1], L. Petraru[1] and S. Bernstorff[2]

1.) Institute of Applied Synthetic Chemistry, Division of Macromolecular Chemistry, Vienna University of Technology, Getreidemarkt 9 / 163 / MC, A-1060 Wien, Austria
2.) Sincrotrone Trieste SCpA, Strada Statale 14, km 163.5, in Area, Science Park, I-34012 Basovizza / Trieste, ITALY

The projects aims to investigate the structuring behavior of materials held together by noncovalent bonds. To this purpose, we are using complex hydrogen bonding systems to achieve defined hydrogen bonding patterns, which are used to connect functional building blocks in a regular and defined manner. [1, 2] Two different sets of materials were investigated : (a) Block copolymers, [3] where hydrogen boding patterns were located purely in one block, acting in accordance with the phase separation of the strongly differing blocks and (b) the aforementioned polymers in junction with nanoparticles bearing matching functional groups. The nanoparticles (NPs) were designed with a surface structure that either a specific interaction with one of the blocks of the block copolymer was possible or impossible. The resulting materials were subjected to temperature-variable measurements to investigate the changes in microphase structure of the resulting block-copolymer. SAXS-measurements represent the only possibility to study phase effects in the solid state by dynamic measurements in a reasonable time scale, therefore measurements were performed at ELETTRA using a holder cell with a variable heating element, controllable with an external control element. Specimen were applied as powders in 2 mm glass capillaries, using approximately 10 mg of powdered material. The temperature was varied in steps of 10 – 60 °C, depending on the effects observed. The measurement time for each sample was about 3 minutes, which - after equilibration of temperature – allowed a fast and steady measurement of all samples required. Unfortunately, the irradiation during the measurements led to an irreversible crosslinking of the material, such as to impede effects upon cooling the sample. Thus an investigation of cooling/heating cycles was not possible. Figure 1 shows the temperature resolved changes of the calculated spacings (d) within the different polymeric materials in nm: the native block copolymer (”Cleft/F-BCP”) shows a regularly ordered structure with a d-spacing of approx. 22 nm. Different block copolymers with varying chain lengths and composition were investigated with this method, yielding unabigously defined scattering values. The incorporation of nanoparticles (NPs) into these block copolymers causes only a slight change in the scattering curves (“Cleft/F-BPC + OD”). There are small changes in the spacing (d) within several nanometers (with variations between 1 – 3 nm’s). The significant change however lies in the temperature behavior (see Figure 1): The pure block-copolymers start to change their spacing (d) at a temperature of about ~ 110 °C, the same is observed for the material incorporating the noninteracting nanoparticles (displaying a octadecyl-surface). In contrast, the material incorporating the barbiturate-modified NPs (i.e.: those able to interact with one block of the block-copolymer - “Cleft/F-BPC + OD”) showed a distinctly higher order/disorder temperature of the material (starting at significantly elevated temepratures of about 130 °C). All materials retained a certain level of structural integrity and order up to temperatures above 200 °C.

The behavior of the “nanoparticle/polymer composite materials” can be clearly interpreted as follows (Figure 2): In case of a matching interaction between the NPs and one block of the block-copolymer, the NPs act as crosslinkers between the chains of the block-copolymer in one phase of the material. In case of the nonmatching interaction or the absence of the NPs only the phase separation within the block-copolymer remains. Clearly this crosslinking-effect

is reflected in the material behavior visualized in Figure 1, demonstrating that the matching hydrogen bonding interaction between the NPs and the matrix can exert an extremely strong effect on the stabilization of the microphases within the material. The method thus offers two important findings: (a) the possibility to incorporate appropriately capped NPs into specific polymeric phases and (b) the crosslinking effect, leading to a reduced diffusion of the NPs within the matrix and – most importantly – also the crosslinking and thus stabilization of the polymeric matrix.

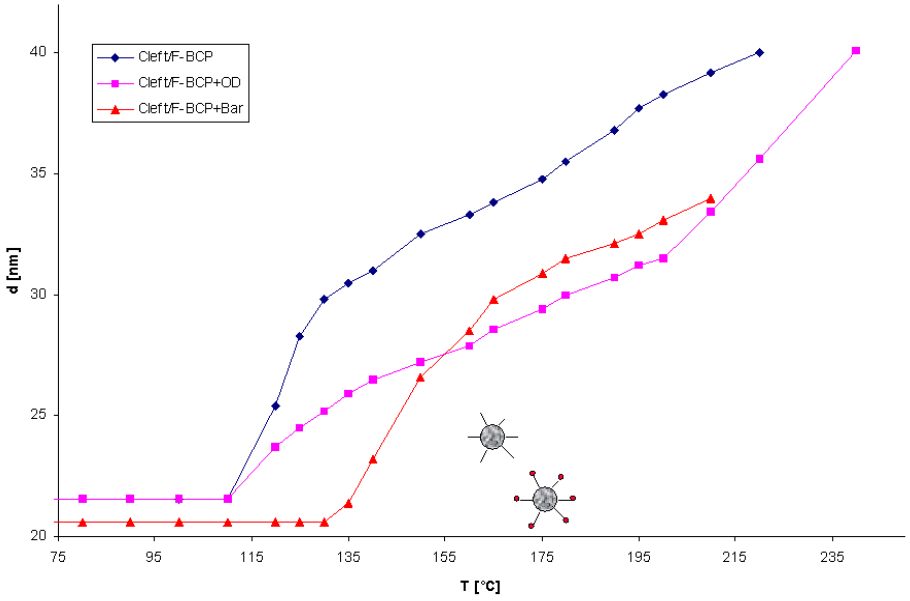

Figure 1. Temperature dependent SAXS-measurements on three samples without ("Cleft/F-BCP"); with octadecyl capped NPs ("Cleft/F-BCP+OD") and with barbiturate capped NPs ("Cleft/F-BCP+Bar").

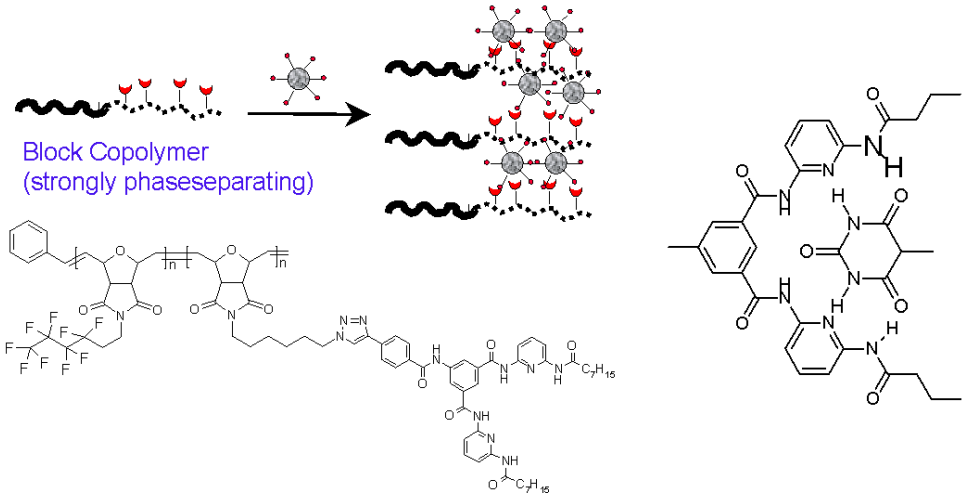

Figure 2. Schematic picture of the observed material behavior

In conclusion, the measurements by SAXS [4] reveal a unique material behavior, consisting of phase-separation as well as intermolecular interactions. Thus nanostructured composite polymers can be constructed, whose thermal behavior can be correlated with a defined nanostructure featuring modulative behavior. Additionally, the combination of strongly differing materials (including surface modified nanoparticles and polymers) featuring multiple material properties can be combined down to the nanoscale.

References:

[1] (a) D. Farnik, C. Kluger, M. J. Kunz, D. Machl, L. Petraru, W. H. Binder, Synthesis and Self Assembly of Hydrogen-Bonded Supramolecular Polymers, Macromol. Symp. 247 - 266 (2004). (b) W. H. Binder, M. J. Kunz, C. Kluger, R. Saf, G. Hayn, Synthesis and Analysis of Telechelic Polyisobutylenes for Hydrogen-Bonded Supramolecular Pseudo-Block Copolymers, Macromolecules 37, 1749 – 1759 (2004). (c) M. J. Kunz, G. Hayn, R. Saf, W. H. Binder, Hydrogen Bonded Supramolecular Poly(etherketones), J. Polym. Sci. 42, 661 – 674 (2004). (d) W. H. Binder, Polymeric Ordering by H-Bonds : Mimicking Nature by Smart Building Blocks, Monatshefte f. Chemie 1 – 19 (2005).

[2] W. H. Binder, M. J. Kunz, E. Ingolic, Supramolecular Poly(etherketone)-Poly(isobutylene) Pseudo-Block Copolymers, J. Polym. Sci. 42, 162 – 172 (2004).

[3] W. H. Binder, C. Kluger, Combining Ring-Opening Methatesis Polymerization (ROMP) with Sharpless-Type "Click" Reactions : An Easy Method for the Preparation of Side Chain Functionalized Poly(oxynorbornenes), Macromolecules 9321 – 9330 (2004).

[4] (a) W. H. Binder, C. Kluger, L.- Petraru, C. Kunz, D. Machl, V. Torma, H. Peterlik, S. Bernstorff, Temperature Dependent SAXS-Measurements of Supramolecular Polymers, Annual Report 2003 of the Austrian SAXS beam line at Elettra (2004).
(b) W. H. Binder, S. Bernstorff, C. Kluger, L. Petraru, M. J. Kunz, V. Torma, Polym. Prepr, 620 - 621 (2004).

SYNTHESIS OF LEAD SULFIDE NANOCRYSTALS USING MESOSTRUCTURED SILICA FILMS AS NANOREACTORS

S. Costacurta[1], D. Buso[1], P. Falcaro[2], L. Malfatti[3], H. Amenitsch[4], G. Mattei[5], C. Sada[5], A. Martucci[1], M. Guglielmi[1] and P. Innocenzi[6]

1.) Dipartimento di Ingegneria Meccanica, Settore Materiali, Università di Padova, Via Marzolo 9, 35131 Padova, Italy.
2.) Associazione CIVEN, Nano Fabrication Facility, via della Libertà 12, 30175 Marghera, Venezia, Italy.
3.) Dipartimento di Scienze Chimiche, Università di Padova, via Marzolo 1, 35131 Padova, Italy.
4.) Institute of Biophysics and X-ray Structure Research, Austrian Academy of Sciences, Schmiedelstraße, A-8042, Graz, Austria.
5.) Dipartimento di Fisica "Galileo Galilei", Università di Padova, Via Marzolo 8, 35131 Padova, Italy.
6.) Laboratorio di Scienza dei Materiali e Nanotecnologie, Nanoworld Institute, Dipartimento di Architettura e Pianificazione, Università di Sassari, Palazzo Pou Salid, Piazza Duomo 6, 07041 Alghero, Sassari, Italy.

Mesoporous materials have been intensively studied since their first successful synthesis in 1992 [1]. Many interesting applications have been prospected, such as electrochemical and optical sensors [2], ultralow-*k* materials for microelectronics and low refractive index materials [3-5]. Another interesting function of mesostructured materials is in nanoparticle synthesis, where the nanoparticles can be obtained through a one-pot synthesis or be grown in already formed nanopores [6]. Metal [7-10], metal oxide [11, 12] or semiconductor [11, 13] nanocrystals embedded in mesoporous materials have been studied, the most common examples being Au, Ag, Pt, CdS, CdSe, GaN, InP, Mn_3O_4. In the present report a study on mesoporous silica films employed as nanoreactors for the growth of lead sulfide (PbS) nanoparticles is presented.

The mesoporous films were synthesized via Evaporation-Induced Self Assembly (EISA) using surfactant Pluronic F-127 (PEO_{106}-PPO_{70}-PEO_{106}) as templating agent according to a recipe used in previous works: a stock solution was prepared following the molar ratio TEOS: ETOH : HCl : H_2O = 1 : 2.78 : 1.45×10^{-2} : 1.17. A templating solution was prepared dissolving 1.3 g Pluronic F127 in 15 ml EtOH and adding 1.5 ml HCl 0.005M. The stock solution was stirred for one hour to allow a slight prehydrolisis, and 7.7 ml from the stock solution were added to the templating solution. The calcination was performed in three steps: @150°C for 20 min, @250°C for 20 min and @350°C for 1 h. As pointed out by preventive FTIR studies (not reported here) this thermal treatment yields a partially densified SiO_2 network. Therefore the silica matrix is porous enough to allow the diffusion of the lead and sulphur precursors throughout the whole thickness.

The mesoporous films were first immersed into a solution containing acetic acid (HAc, Ac=CH_3COO^-), lead acetate ($PbAc_2\cdot3H_2O$) and methanol, with molar ratio MeOH : PbAc : HAc = 1 : 0.01 : 0.05, for 24 hours at 25°C. The films were then washed with methanol to remove the lead acetate residuals. After drying, the films were immersed in a solution with molar ratio MeOH : CH_3CSNH_2 (thioacetamide) = 1 : 0.04, for one hour. The colour of the films changed from transparent to dark brown. The films were then washed in methanol and dried in air.

The ordered mesostructure of the host silica matrix was investigated using the high-flux grazing incidence small angle X-ray scattering (GI-SAXS) apparatus at the Austrian high-flux beamline of the electron storage ring ELETTRA (Trieste, Italy) [14]. Images of samples (before and after impregnation, see Figure 1) were acquired with exposition times ranging from 200 ms to 24 s. The selected incident radiation energy was 8 KeV, corresponding to a wavelength of 1.54 nm. The instrumental grazing angle was set maintaining an incident X-ray beam smaller than 3° The images were collected with the CCD detector and processed using the "fit2d" programme (A. P. Hammersley / ESRF) [15]. Before analysis, the collected

images were corrected with fit2d: the intensity of the images was normalized, the spatial distortion was corrected and instrumental errors (background noise and dark current) were subtracted.
The position of the diffraction maxima in the image allowed us to identify the phase of the mesostructure and to calculate the cell parameters, exploiting the same procedure reported in previous works [16, 17]. Diffraction patterns were acquired for a sample that underwent impregnation and PbS growth, and an untreated sample used as a reference. In both samples the diffraction pattern is consistent with a face-centered orthorhombic (FCO) phase (space group *Fmmm*). The cell parameters were calculated using the following formula:

$$\frac{1}{d_{hkl}^2} = \frac{h^2}{a^2} + \frac{k^2}{b^2} + \frac{l^2}{c^2}$$

where d_{hkl} is the interplanar distance of the plane family *hkl*, and *a*, *b*, *c* are the cell parameters of the FCO structure. The calculated values are a = 21.0 nm, b = 14.8 nm, c = 29.7 nm. Since the results are the same for both treated and untreated samples, we can infer that the mesostructure is retained after the impregnation process, with no variations in both cell symmetry and lattice parameters.

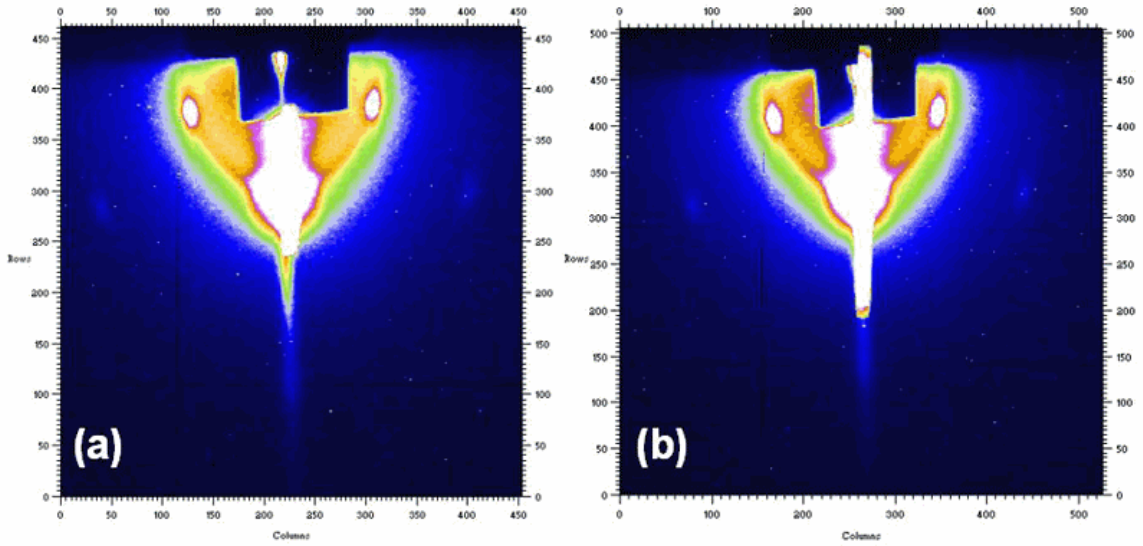

Figure 1. GI-SAXS diffraction pattern of mesostructured silica films: (a) before and (b) after impregnation.

Secondary Ions Mass Spectroscopy (SIMS) spectrum of a PbS-doped sample (not shown) reveals the homogeneous dispersion of the lead and sulphur atoms through the entire silica matrix thickness, this being a proof of the complete penetration of the PbS constituents inside the silica mesostructured film.
TEM image of Figure 2a shows PbS nanoparticles precipitated close to the interface between the film and the silicon substrate. This gives a further direct evidence of the penetration of the impregnating solutions through the whole film thickness. Furthermore TEM together with the SIMS plot images give an indirect proof that the pores inside the silica matrix are interconnected, allowing a homogeneous diffusion of the solutions throughout the film thickness. EDS analysis was performed on several regions of the sample section, pointing out that the Pb to S molar ratio has a value constantly around 1 in all the volumes investigated, as it was expected considering the stoichiometric composition of lead sulfide. Moreover, Pb to Si ratio evaluated by EDS analysis performed scanning only the silica film area resulted to be 0.08. Assuming that the Si signal detected is referable unambiguously to the silica SiO_2

matrix (and not to the Si substrate), the molar concentration of PbS inside the film is therefore 8%.
Figure 2b is a HRTEM image showing a spherical PbS monocrystal, with diameter of 5 nm. Considerations on the nanocrystals growth can be made observing TEM images and considering that no capping agent was employed in order to tailor PbS nanoparticles shape and dimensions. PbS nanocrystal growth is first controlled by the surface energy of the nuclei that are forming, and the particles assume spherical shape in order to minimize it. Secondly, the pore walls impede them to aggregate into bigger clusters, therefore conditioning their final shape and dimensions.

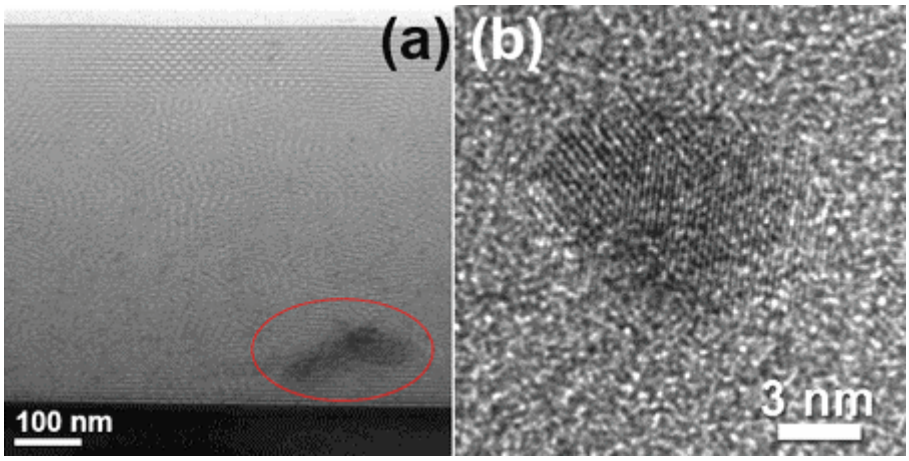

Figure 2. TEM (a) and HRTEM (b) images of a mesostructured silica film after impregnation and subsequent PbS growth.

The films were characterized after the impregnation process by X-Ray diffraction (XRD) using a diffractometer equipped with glancing-incidence X-Ray optics. The analysis was performed using CuK_{α}-Ni filtered radiation at 40 kV and 40 mA. The average crystallite size was calculated using the Scherrer correlation after fitting the experimental profiles with a pseudo-Voigt function. XRD spectrum (Figure 3) confirms the presence of crystalline lead sulfide, precipitated during the impregnation process. Peaks are consistent with a *Fm*3*m* face centered cubic structure. The average diameter of PbS nanoaparticles evaluated from line broadening of the three main diffraction peaks ranged from 4,5 to 6 nm, in good agreement with the average diameter evaluated from TEM measurements. Furthermore both particles diameter and pores dimension are of the same order of magnitude.

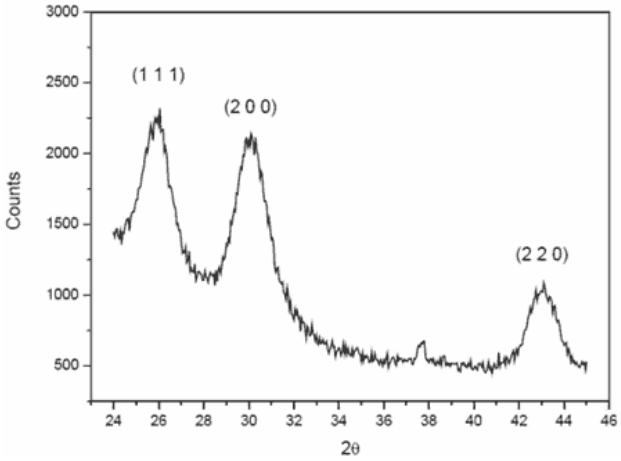

Figure 3. XRD diffraction pattern of a PbS-doped mesostructured silica sample.

With the present work we have shown the possibility to use the pores of mesoporous silica films as nanoreactors for nanoparticle synthesis. The precursors penetrate through the film allowing the growth of semiconductor nanoparticles, which do not break or modify the mesostructure.

References:

[1] C.T. Kresge, M.E. Leonowicz, W.J. Roth, J.C. Vartuli, and J.S. Beck; Nature. 359, 710-712 (1992).
[2] G. Wirnsberger, B.J. Scott, and S.G. D.; Chem. Commun., 119 (2001).
[3] A. Jain, S. Rogojevic, S. Ponoth, N. Agarwal, I. Matthew, W.N. Gill, P. Persans, M. Tomozawa, J.L. Plawsky, and E. Simonyi; Thin Solid Films. 513, 398-399 (2001).
[4] S. Baskaran, J. Liu, K. Domansky, N. Kohler, X. Li, C. Coyle, F.G. E., T. Suntharampillai, and R.E. Williford; Adv. Mater. 12, 291 (2001).
[5] A.R. Balkenende, F.K. de Theije, and J.C. Kriege; Adv. Mater. 15, 139 (2003).
[6] R. Köhn and M. Fröba; Catal. Today. 68, 227-236 (2001).
[7] Z. Liu, Y. Sakamoto, T. Ohsuna, K. Hiraga, O. Terasaki, C.H. Ko, H.J. Shin, and R. Ryoo; Angew. Chem. Int. Ed. 39(17), 3107 (2000).
[8] A. Fukuoka, H. Araki, Y. Sakamoto, S. Inagaki, Y. Fukushima, and M. Ichikawa; Inorg. Chim. Acta. 350, 371 (2003).
[9] Y. Wu, L. Zhang, G. Li, C. Liang, X. Huang, Y. Zhang, G. Song, J. Jia, and C. Zhixiang; Mater. Res. Bull. 36, 253 (2001).
[10] J. Arbiol, A. Cabot, J.R. Morante, F. Chen, and M. Liu; Appl. Phys. Lett. 81, 3449 (2002).
[11] M. Wark, H. Wellmann, and J. Rathousky; Thin Solid Films. 20, 458 (2004).
[12] B. Folch, J. Larionova, Y. Guari, C. Guérin, A. Mehdi, and C.J. Reyé; Mater. Chem. 14, 2703 (2004).
[13] H. Winkler, A. Birkner, V. Hagen, I. Wolf, R.A. Fisher, R. Schmechel, and H.V. Seggern; Adv. Mater. 11, 1444 (1999).
[14] H. Amenitsch, M. Rappolt, M. Kriechbaum, H. Mio, P. Laggner, and S. Bernstorff; J. Sync. Rad. 5, 506 (1998).
[15] Available at www.esrf.fr/computing/expg/subgroups/data_analysis/FIT2D/index.html
[16] P. Falcaro, D. Grosso, H. Amenitsch, and P. Innocenzi; J. Phys. Chem. B. 108(30), 10942-10948 (2004).
[17] P. Falcaro, S. Costacurta, G. Mattei, H. Amenitsch, A. Marcelli, M.C. Guidi, M. Piccinini, A. Nucara, L. Malfatti, T. Kidchob, and P. Innocenzi; J. Am. Chem. Soc. 127, 3838-3846 (2005).

IN SITU SAXS INVESTIGATION ON THE PHASE BEHAVIOR OF SELECTED NON-IONIC SURFACTANT LIQUID CRYSTALLINE SYSTEMS

C. Fritscher[1], N. Hüsing[2], S. Bernstorff[3], D. Brandhuber[4], T. Koch[1], S. Seidler[1] and H. C. Lichtenegger[1]

1.) Institute of Materials Science and Technology, Vienna University of Technology, Favoritenstrasse 9-11/308, A-1040 Vienna, Austria
2.) Institute of Inorganic Chemistry I, Ulm University, Albert-Einstein-Allee 11, 89069 Ulm, Germany
3.) Sincrotrone Trieste, Strada Statale 14, Km. 163.5, in AREA Science Park 34012 Basovizza/Trieste, Italy
4.) Institute of Materials Chemistry, Vienna University of Technology, Getreidemarkt 9/165, A-1060 Vienna, Austria

The amphiphilic properties of surfactant molecules are responsible for their distinct tendency to self assemble into larger liquid crystalline (LC) structures such as hexagonal, cubic or lamellar arrangements depending on their concentration in a given solvent. This lyotropic LC systems are commonly used in sol-gel-chemistry as structure directing agents [1].

The aim of this SAXS-study was to continuously follow changes and reordering effects in the structure of different liquid crystalline surfactant/water systems *in situ*, while under thermal treatment. For this purpose a furnace was built that could be placed in the beam. The furnace was furthermore designed to heat the sample capillaries inside a low magnetic field (0.3-0.7 T). The experimental setting is described in more detail in [2].

Typically the samples were heated up to 60°C (above the order/disorder transition temperature of the LC systems) and kept at this temperature for at least 10 minutes to equilibrate. Subsequently, they were cooled down with a rate of 1 K/min, in order to allow the LC-order to reform. SAXS patterns were recorded continuously during the process.

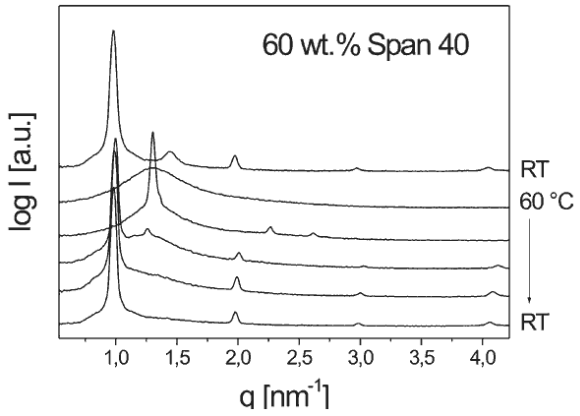

Figure 1. The LC system sorbitan monopalmitate (Span 40) in water cooling down from 60°C to room temperature

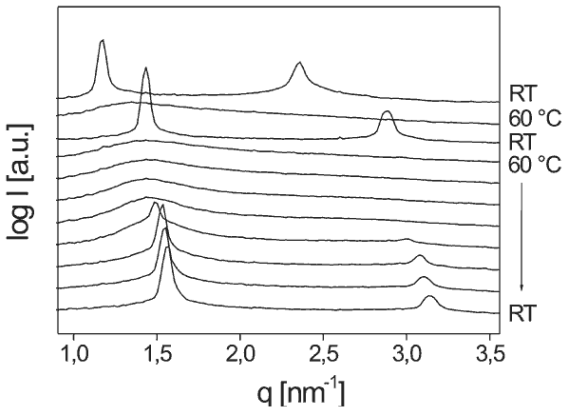

Figure 2. Decrease in d-spacing after two heating cycles in the system 50 wt.% Triton X-45 in water

An example for the ordering of the non-ionic surfactant sorbitan monopalmitate (Span 40) into a lamellar structure after heating the sample to 60°C is given in Fig. 1. In the beginning the scattering pattern is consistent with two coexisting lamellar phases. At 60°C the structural order is destroyed indicated by a broad distribution of the measured intensity. A transition from hexagonal to lamellar was observed with decreasing temperature (in the temperature regime 60°C > T > 40°C the system exhibits a hexagonal structure with d_{100}=4.8 nm and below a lamellar structure with d_{100}=6.4 nm).

Results for 50 wt.% of the non-ionic surfactant Triton X-45 (Polyethylene glycol 4-tert-octylphenyl ether) in water are depicted in Figure 2, which shows again the scattering intensity plotted versus q. The peak positions can be indexed according to a lamellar LC phase, with the d_{100} and d_{200} reflections clearly visible. The topmost curve was recorded at room temperature before heating and gives an initial *d*-spacing of d_{100}=5.38 nm. Upon heating the sample up to 60°C, the long-range order vanished and the diffraction peaks disappeared (second curve from the top) indicating that the order – disorder transition was passed at this temperature. Upon slow cooling of the system, the lamellar phase was restored, but with a smaller *d*-spacing of 4.41 nm (decrease by 18 %). A second heating-cooling cycle resulted in a further decrease of the *d*-spacing by another 7 % to d=4.01 nm (four forefront curves in Figure 2). In the case of 60 wt.% Triton X-45 in water the observed decrease in *d*-spacing was around 13.5 % from 5.03 nm to 4.35 nm. Since no additional peaks evolved, a formation of ripple phases can be excluded.

Whereas heating and slow cooling of 50 % and 60 % Triton X-45 in water showed a considerable decrease of the *d*-spacing, no decrease of the *d*-spacing upon heating and cooling was observed in the samples with 20 % Triton X-45 in water. Here, the *d*-spacing was constantly as small as d=4.55 nm from the beginning. Faster cooling of externally heated samples with 50 % surfactant showed also no decrease of the *d*-spacing (d is constant with a value of 5.2 nm).

Furthermore measurements of different concentrations of Triton X-45 show an alignment of the lamellar liquid crystalline structure close to the wall of the glass capillaries. Scanning of the 2 mm capillary by a 0.5 mm beam in steps of 0.1 mm allowed a clear distinction between the regions close to the capillary wall and the bulk material. In the bulk, no preferential orientation of the liquid crystalline domains was observed, whereas the liquid crystalline domains tended to align parallel to the walls of the glass capillary. The preferential alignment was observed after heating in the system with 50 wt.% surfactant. For the system with a concentration of 20 wt.% the alignment was already present before heating but became much more pronounced after heating and cooling the sample (Figure 3 a and b).

Measurements were made with and without magnetic field, but no effect due to the magnetic field was observed.

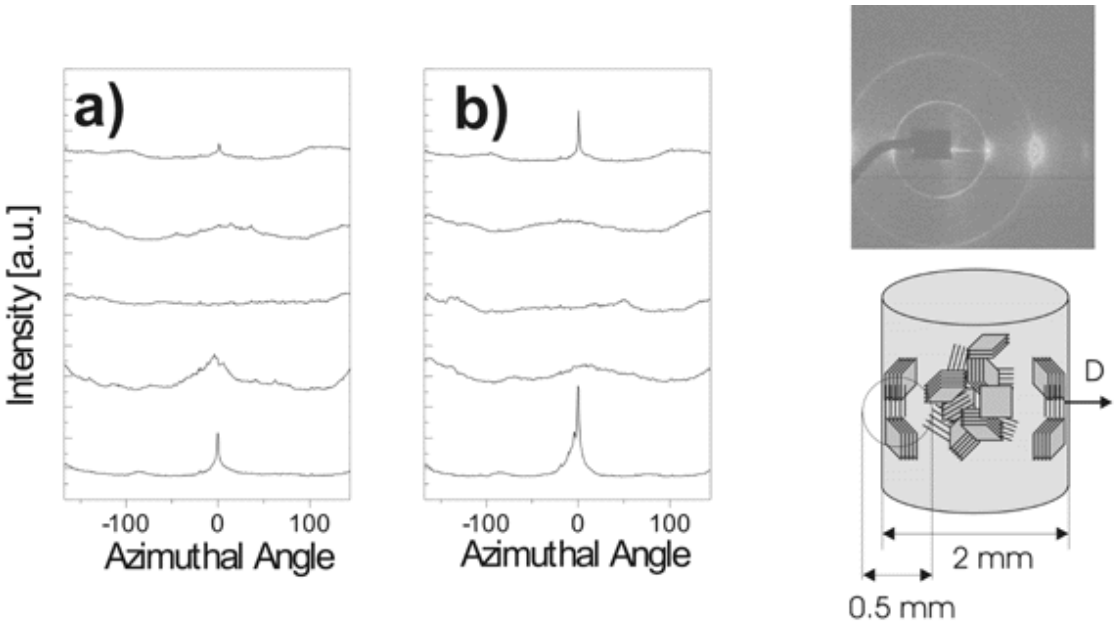

Figure 3. Reordering effect of the lamellae along the wall of the glass capillary in the Triton X-45/water system, a) before heating, b) after heating and cooling in the system with 20 wt.% surfactant. To the right: scattering image of the region close to the wall; below a schematic sketch of the aligned lamellae close to the wall and the randomly oriented domains in the bulk.

References:

[1] Beck, J. S., Vartuli, J. C., Roth, W. J., Leonowicz, M. E., Kresge, M. E., Schmitt, K. D., Chu, C. T W., Olson D. H. & E. W. Sheppard; A New Family of Mesoporous Molecular Sieves Prepared with Liquid Crystal Templates; J. Am. Chem. Soc. 114, 10834-10843 (1992)

[2] C. Fritscher, N. Hüsing, S. Bernstorff, D. Brandhuber, T. Koch, S. Seidler and H. Lichtenegger; In-situ SAXS study on cationic and non-ionic surfactant liquid crystals using synchrotron radiation; Journal of Synchrotron Radiation (2005) in press

SWELLING OF TRIBLOCK COPOLYMER TEMPLATES USING PRESSURISED FLUIDS

J. P. Hanrahan[1], M. P. Copley[1], J. M. O'Callaghan[1], J. D. Holmes[1], M. Steinhart[2] and H. Amenitsch[3]

1.)Department of Chemistry, Materials Section and Supercritical Fluid Centre, University College Cork, Cork, Ireland
2.) Institute of Macromoleculear Chemistry, Academy of Sciences of the Czech Republic, Heyrovsky Sq. 2, 16206 Prague 6, Czech Republic
3.) Institute for Biophysic and X-ray Structure Research, Austrian Academy of Science, Schmiedlstr. 6, 8042 Graz, Austria

Mesoporous materials with uniform and tailorable pore dimensions are expected to play a vital role in many applications that range from catalysis, to molecular separations, and even semiconductor and low k dielectric devices [1]. Traditionally, tailoring the pore dimensions of mesoporous silicas prepared from triblock co-polymer surfactants has been achieved either through synthesising surfactants of various tail lengths or by adding organic swelling agents, such as decane, or co-surfactants. Even though mesoporous silicas have been prepared with pore diameters ranging from 20-300 Å, it has proven difficult to tailor the pore diameters to specific sizes within this broad range. We have recently developed a novel approach for preparing large pore calcined mesoporous silicas with tunable pore dimensions, wall widths and pore densities using a mixed surfactant direct templating method. We have utilised supercritical carbon dioxide (sc-CO_2) to produce large pore mesoporous silicas, with pore dimensions > 10 nm, and manipulate pore dimensions with high precision. In particular, mesoporous templates formed using sc-CO_2 processing techniques are highly ordered with superior thermal stability [2].In effect, our method, using only commercially available triblock copolymer surfactants, allows mesopore dimensions to be engineered on an Ångström-level scale.

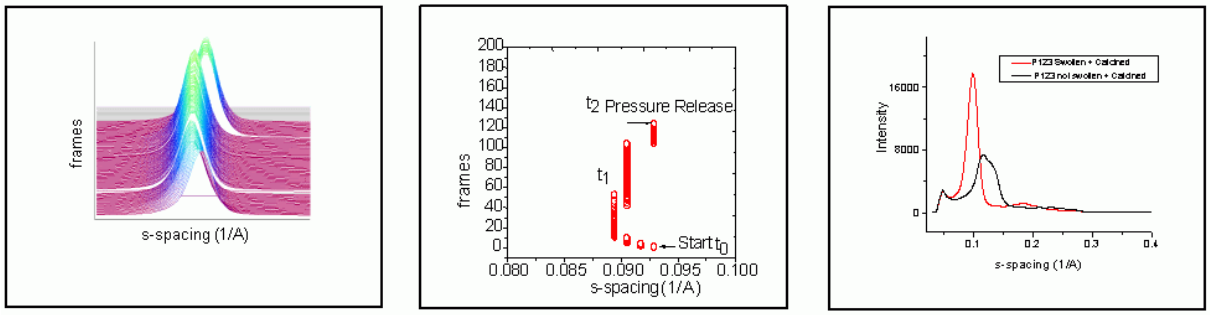

Figure 1. (a) SAXS profiles of the swelling procedure, (b) peak position for the (100) reflection during swelling and (c) SAXS data for swollen and non-swollen sample of P123-templated mesoporous silica templated.

Figures 1a and 1b illustrate SAXS data taken on the Austrian Small Angle X-ray Scattering Beam-line at Elettra of a P123-templated mesoporous silica sample formed in the presence and absence of sc-CO_2 during the silica condensation process. The position of the intense (100) peak can be seen to shift dramatically from 0.092 (s-spacing) at t_0 to 0.0894 on application of CO_2 at 200 bar pressure. This shift represents a swelling of the d-spacing by approximately 10 Å. At a time, t_1, there is another marked change in the position of the (100) reflection (from 0.090 to 0.089). This shift may be due to a phase transition. An epitaxial

cubic to hexagonal phase transition, observed when the same solution is deposited as a thin film, could explain this shift. At a time, t_2, there is again a substantial shift in the position of the (100) peak due to the release of CO_2 from the system. Upon depressurizing the system this 'de-swelling' effect is almost instantaneous. Silica samples swelled by sc-CO_2 and subsequently calcined showed an increased mesoporous ordering as depicted by the SAXS data shown in figure 1(c).

Conclusions

Using sc-CO_2 swelling protocols the diameters of silica mesopores, and the spacing between the pores, can be tuned with Ångström-level precision. SAXS proved to be a useful technique for probing the in-situ swelling of the liquid crystal templating phases. All of the liquid crystal phases studied were found to be highly ordered and acted as excellent templates for mesoporous silica formation.

References:

[1] Ryan, K. M.; Erts, D.; Olin, H.; Morris, M. A.; Holmes, J. D. *J. Am. Chem. Soc.* 2003, *125*,6284
[2] Hanrahan, J.P.; Copley, M.P.; Holmes, J.D.; *Chem. Mater* 2004, 16, 424

900°C STABLE NANOCRYSTALLINE γ-ALUMINA LAYERS WITH HIGHLY ORDERED 3D MESOPOROSITY

Monika Kuemmel[1], David Grosso[1], Cédric Boissière[1], Bernd Smarsly[2], Torsten Brezesinski,[2] Pierre A. Albouy[3], Heinz Amenitsch[4] and Clement Sanchez[1]

1.) Chimie de la Matière Condensée, UMR UPMC-CNRS 7574, 4 place Jussieu, 75252 Paris 05, France.
2.) Max Planck Institute of Colloids and Interfaces, Research Campus Golm,D-14424 Potsdam, Germany.
3.) Laboratoire de Physique des Solides, Université Paris-Sud, 91405 Orsay, France.
4.) Institute of Biophysics and X-ray Structure Research, Austrian Academy of Sciences, Schmiedlstr.6, A8042, Graz, Austria

Mesostructured materials can be obtained by combining ionic surfactants [1] or block copolymers [2] with the synthesis of metallic oxides through soft chemistry. Amongst the non-silicates mesoporous materials, alumina (Al_2O_3 with perfectly controlled mesoporosity associated to the hardness, hydrolytic stability, amphoteric character, and thermal stability of the γ transition oxide phases) is very attractive. The present work describes the characterisation of nanocrystalline γ-Al_2O_3 layers with contracted *fcc* mesoporosity stable up to 900°C. Because of the very low quantity of matter associated with thin films, the evolution of the mesostructure during thermal treatment was assessed using 2D Small Angle X-ray Scattering (SAXS) in transmission with an angle of 5° with respect to the X ray incident beam.

Figure 1 represents the evolution of *in situ* 2D-SAXS patterns, performed during thermal treatment. Indexation of the diffraction spots, reported on Figure 1b), reveals that the initial structure at 25°C is a perfect fcc structure with lattice parameter of 36 and 60 nm when the KLE 22 template (Figure 1a) and the KLE 23 template (Figure 1d) are respectively used. The diffraction rings (Figure 1c inset) are characteristic of the preferential monoorientation with the [111] direction normal to the surface (direction of shrinkage). Figures 1c displays the diffraction pattern of a KLE 22 templated alumina film calcined 20 min at 900°C. For clarity, diffraction points corresponding to these contracted systems are indexed with the original *fcc* structure.

Despite the significant lattice contraction found in Figure 1, diffraction peaks are still very intense and well-resolved. The initial contraction of 68% takes place between room temperature and 400°C, while the remaining 6% occurred between 400 and 900°C. The cubic structure is clearly confirmed by TEM analysis (see Figure 2), where the [111] view plane of the contracted-fcc arrangement of pores exhibits the expected hexagonal arrays (a and b). The film side view in Picture c) confirms the *fcc*-based structure. It also reveals that pores are highly anisotropic due to the high degree of contraction induced by the thermal treatment.

In summary, in-situ SAXS experiment is highly appropriated to follow the evolution of mesostructured thin films during annealing. More than all it allows to deduce the optimise thermal treatment conditions to crystallise the network without collapsing the mésostructure.

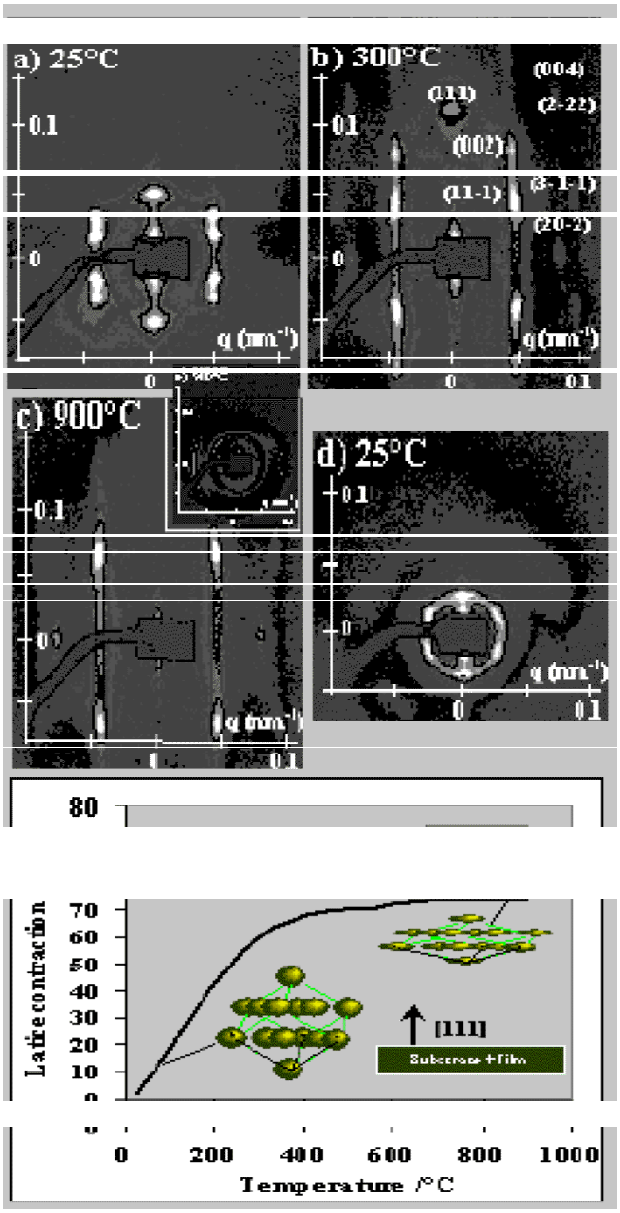

Figure 1. a), **b)** and **c)** 2D-SAXS patterns of KLE22-templated alumina layers treated at various temperatures, **d)** 2D-SAXS patterns of KLE23-templated alumina layer at room temperature.

Bottom: Evolution of the *fcc* lattice contraction in the direction normal to the layer surface ([111] direction of the *fcc* domains) versus the temperature.

References:

[1] C.T. Kresge, M.E. Leonowicz, W.J. Roth, J.C. Vartuli, J.S. Beck, *Nature* 1992, *359*, 710
[2] P. Yang, D. Zhao, D.I. Margolese, B. Chmelka, G. Stucky, *Nature* 1998, *396*, 512

STRUCTURE EVALUTION OF ALUMINOSILICATE NANOCOMPOSITE

K. Sinko[1] and V. Torma[2]

1.) L. Eotvos University, Pazmany P. 1/a, Budapest, Hungary
2.) Technical University, Budafoki ut, Budapest, Hungary

Aluminosilicate amorphous materials as porous ceramics with high surface areas and small pore sizes may be exploited in applications such as filtration, separation, catalysis, and chromatography. The role of the Al content in the aluminosilicate systems is to provide the glass or ceramics product with high chemical, electric and heat resistance, and low thermal expansion. The purpose of the present work is to prepare homogeneous aluminosilicate systems with as high as possible, *i.e.* higher aluminum content as that can be achieved by traditional high-temperature melting methods. Maximum 0.1 mole ratio of Al/(Si+Al) may be obtained by traditional process in fused silicate glass. Higher Al content results in a phase separation during the cooling of the hot aluminosilicate melt. A new preparation method has been developed for procedure of aluminosilicate systems with high aluminum content [1-3]. The new method can produce optically clear, homogeneous aluminosilicate gels in one step from tetraethoxysilane (TEOS) and $Al(NO_3)_3 \cdot 9H_2O$ in organic medium at 80 ºC. This new method resulted in new structures (*e.g.* fractals) and new properties (*e.g.* piezoelectricity or in wide range variable porosity) for aluminosilicate materials comparing with that of fused glass or ceramic [4-8,]. The disadvantage of this aluminosilicate system is the fragility in wet as well as aerogel states. The other problem of the use of Al nitrate is the release of nitrous gases noxious to the environment.

Experimentals

Another newly developed sol-gel procedure got rid of these disadvantages. It starts from in the respect of environmental advantageous Al acetate and from cheap water glass solution. Gel samples can be obtained only in basic condition (pH = ≥ 12). In acidic medium a phase separation of (poly)silicic acid occurred. Directly after mixing the aqueous solutions, an opaque monolith gel structure formed. At 2.5 mole ratio of Al/Si, monolith gel structure with extremely large stiffness was obtained comparing with the other wet aluminosilicate gel samples. Thus, this preparation method suits the requirements of the environmental protection and the hardness of gel systems. According to the ^{27}Al MAS NMR measurements, the large hardness may be induced by a separated crystalline alumina phase inserted in the aluminosilicate network. The main aim of the present work is to study the structure evolution of the separated Al-containing crystalline phase during the gelation of the gel systems prepared from Al acetate and water glass solutions.

Results

SAXS measurements prove the presence of an amorphous aggregate phase in the sample (Fig 1). Since the slope of the SAXS curves just after the gelation are about -3, the kinetics of the aggregation might be a reaction limited process. The size evolution of the aggregate particles, similarly to the most sol-gels systems, turned out to be an exponential growth in time. In the sol system aggregate particles formed during the heat treatment at 80°C and the size increase from a couple of nanometers to above 50 nm. This is the largest size, which can be detected by our SAXS measuring arrangement.

WAXS measurements indicate the presence of a crystalline phase in the sample (Fig. 2). The Bragg reflections (at 5.66, 8,48 Å) verified aluminum (oxide) hydroxide (e.g. bayerite) as crystalline particles. These crystalline particles are inserted in the amorphous aluminisilicate network to form an extremaly hard nanocomposite. The determination of the size of crystalline particles needs further scattering investigation at an other measuring arrangement. The crystallization process could be very well followed by WAXS detector during the heat treatment at 80 °C (Fig. 2).

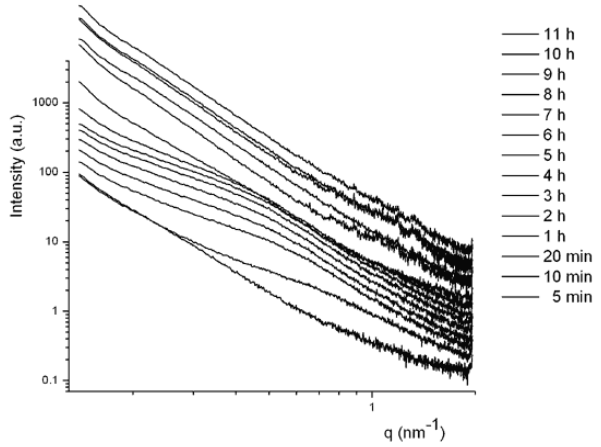

Figure 1. SAXS measurements on crystallization kinetics

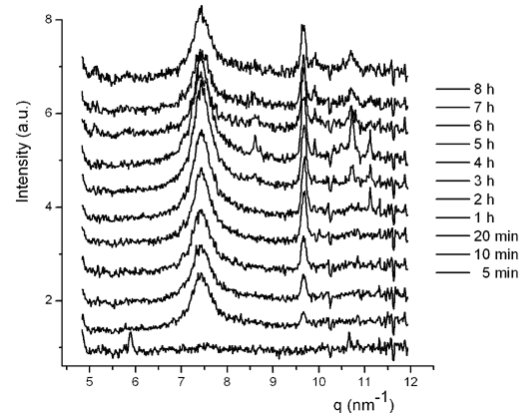

Figure 2. WAXS measurements on crystallization kinetics

References:

[1] K. Sinkó, R. Mezei: "Preparation effects on sol-gel derived aluminosilicate gels", J. Non-Cryst. Solids 231/1-2. 1-9 (1998)

[2] K. Sinkó, R. Mezei, J. Rohonczy, P. Fratzl: "Gel structures containing Al(III)", Langmuir 15. 6631-6639. (1999)

[3] R. Mezei, K. Sinkó, J. Rohonczy, O. Paris, P. Fratzl: "Short- and intermediate-range structure in Al(III)-containing gels prepared from aluminum nitrate" Chem. Phys. 246. 295-301. (1999)

[4] K. Sinkó, L.Cser, R. Mezei, M. Avdeev, H. Peterlik, G. Trimmel, U. Schubert, P. Fratzl: "Structure investigation of intelligent aerogels" Physica B 276-278. 392. (2000)

[5] K. Sinkó, K. Fél, J. Rohonczy, N. Hüsing: "Chemical processing of new piezoelectric materials" Smart Mat. Struc. 10. 1078. (2001)

[6] K. Sinkó, K. Fél, J. Rohonczy, N. Hüsing: "Piezoelectric property of sol-gel derived composite gels" Proceeding of SPIE`s 8th International Symposium on Smart Structures and Materials, 4333. 151-158. (2001)

[7] K. Sinkó, L. Pöppl: "Transformation of aluminosilicate wet gel to solid state" J. Sol. State Chem. 165. 1. 111. (2002)

[8] K. Sinkó, K. Fél, M. Zrínyi: "Preparation possibilities of Al- and Si-containing hybrid systems" Polymers for Advanced Technologies 14. 776. (2003)

GISAXS CHARACTERIZATION OF TRANSITION METAL – OXIDE DOPED MESOSTRUCTURED SILICA FILMS

R. Supplit[1], N. Hüsing[2] and S. Bernstorff[3]

1.) Institute of Materials Chemistry, Vienna University of Technology, Getreidemarkt 9/ 165, A-1060 Vienna, Austria
2.) Inorganic Chemistry I, University of Ulm, Albert-Einstein-Allee 11, D-89069 Ulm, Germany
3.) Sincrotrone Trieste, Strada Statale 14, Km. 163.5, in AREA Science Park 34012 Basovizza/ Trieste, Italy

Thin silica films doped with transition metal oxides (Ti, Fe, Hf) are of special interest for application such as sensors, membranes or catalysts. The focus of our work is on the preparation of mesostructured silica films doped with transition metal oxides relying on a combination of ligand-assisted templating and evaporation-induced self-assembly [1,2]. By this approach, the surfactant not only serves as structure directing agent, but also acts as an agent to control and slow down the hydrolysis and condensation rate of the transition metal alkoxide and to position the latter at the template-silica interface to achieve high homogeneity and dispersion within the silica matrix [3, 4].
In this study we investigated the mesostructures formed from the metal-coordinated surfactants in thin silica-metal oxide films and the structural evolution upon heat treatment up to 1000°C by GISAXS.

The grazing-incidence SAXS (GISAXS) measurements were performed with a photon energy of 8 keV, and at a grazing angle between the beam and the film surface close to the critical angle of total external reflection of silicon (0.18-0.21°). Therefore, additional spots corresponding to out-of-diffraction plane reflections were sometimes observed. 2D-diffraction patterns were recorded with a CCD detector (Photonic Science) in a distance of 107cm from the sample. A partially absorbing beam attenuator was used close to the central beam position. The detector was calibrated with silver behenate as a reference standard. The *d*-spacings were determined from the diffraction spots by analysis of the CCD images with the FIT2D program (A.P. Hammersley/ESRF).

The metal-coordinated surfactants were produced according to reference [5]. Films were deposited on single side polished silicon wafers by dip coating from solutions of the compositions TEOS : M-P123: H_2O : HCl : EtOH = 1 : M : 5 : 0.016 : 10 and TEOS: M-Brij-56: H_2O: HCl: EtOH = 1 :M: 15: 0.005: 42. The films were labelled as M-P123(M) and M-Brij(M).

The variation of the molar ratio of the modified surfactant resulted in the formation of different mesostructures. With increasing amount of M-Brij (M) 2d-centered rectangular, mixed lamellar – 2d centered rectangular and lamellar mesostructures were formed. A sequence of typical diffraction patterns for Brij containing samples is displayed for Hf-Brij (M) films in figure 1. The presence of diffraction spots instead of rings shows that the mesostructure is aligned with respect to the substrate plane. The unit cell parameters for the 2d centered rectangular (M=0.10) structure were calculated from the *d*-spacings of the 02 and the -11 spot: a= 6.5nm, b= 10.0nm. The lamellar structure (M=0.17) has a *d*-spacing of 6.0nm.

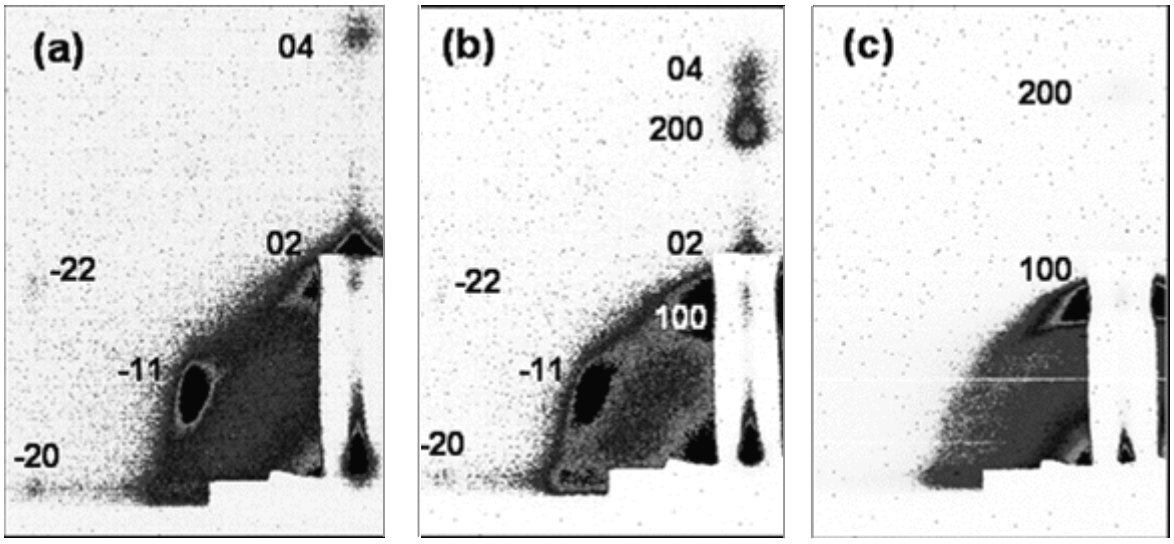

Figure 1. GISAXS diffraction pattern of as synthesized films: (a) Hf-Brij (0.10), (b) Hf-Brij (0.12), and (c) Hf-Brij (0.170)

Samples prepared with M-P123 surfactant exhibit larger unit cells. Typical diffraction pattern are given in figure 2a and 2b for Fe-P123(M) films. The use of this surfactant resulted in the formation of mesostructures with larger unit cells. 2d-centered rectangular (a = 13.5nm, b=18.5m) were formed with M = 0.011 and lamellar structures (d_{100}= 10.5 nm) with M=0.018.

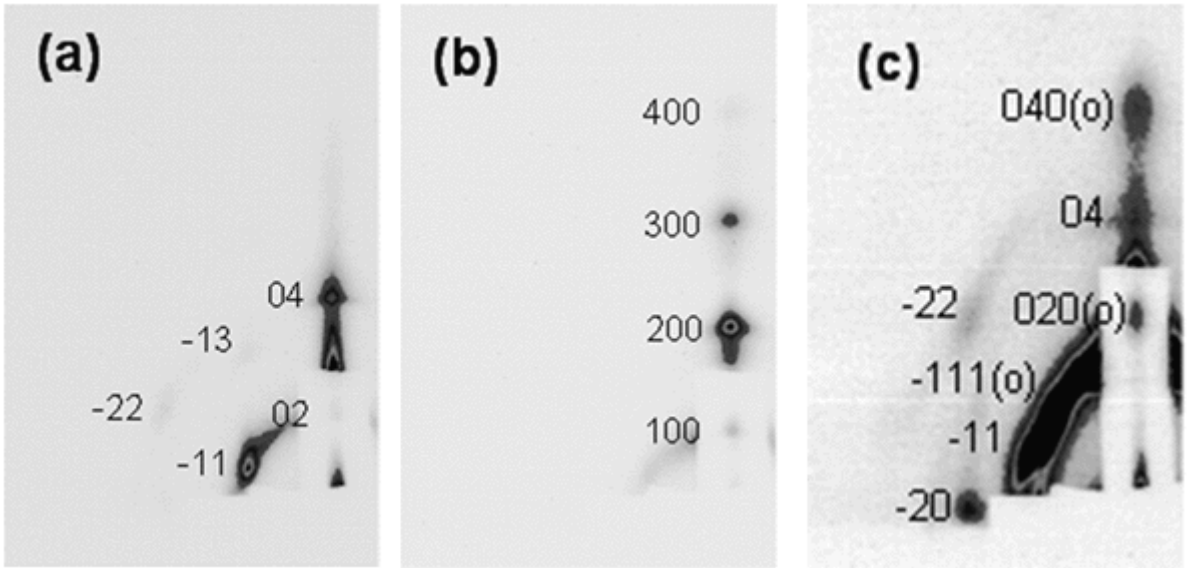

Figure 2. GISAXS diffraction pattern of as synthesized films: (a) Fe-P123 (0.011), (b) Fe-P123 (0.018) and (c) Fe-P123 (0.011) treated at 700°C

The influence of the heat treatment on the mesostructures was studied. In general lamellar structures were not stable at temperatures above 200°C since degradation of the surfactant results in collapse of the lamellae. 2d centered rectangular mesophases undergo shrinkage during the heat treatment. The high temperature stability of M-P123(M) samples (> 1000°C) was superior to M-Brij samples (≈ 700°C). After the heat treatment of specific M-P123(M) samples like Fe-P123(0.011) additional diffraction spots were detected at temperatures above 200°C (figure 2c) and assigned to an orthorhombic mesostructure. The occurrence of this mesostructure is addressed in more detail in reference [5].

References:

[1] C.J. Brinker, Y. Lu, A. Sellinger, H. Fan, Evaporation-induced self-assembly. Nanostructures made easy, Adv. Mater. 11, 579-585 (1999).

[2] D. Grosso, A.R. Balkenende, P.A. Albouy, A. Ayral, H. Amenitsch, F. Babonneau, Two-Dimensional Hexagonal Mesoporous Silica Thin Films Prepared from Block Copolymers: Detailed Characterization and Formation Mechanism, Chem. Mater. 13, 1848-1856 (2001).

[3] N. Hüsing, B. Launay, G. Kickelbick, S. Gross, L. Armelao, G. Bottaro, M. Feth, H. Bertagnolli, F. Hofer and G. Kothleitner Transition metal oxide-doped mesostructured silica films, Appl. Catal. 254, 297-310 (2003).

[4] N. Hüsing, B. Launay, F. Hofer and G. Kickelbick, Silica-Titania Mesostructured Films, J. Sol-Gel Sci. Technol. 26, 615-619 (2003).

[5] R. Supplit, N. Hüsing, C. Fritscher, P. Jakubiak, V. G. Kessler, G. A. Seisenbaeva and S. Bernstorff; Iron Oxide – Doped Mesostructured Silica Films; MRS Proceedings Mater. Res. Soc. Symp. Proc., 847, EE9.13 (2005).

INFLUENCE OF SALTING-IN AND SALTING-OUT EFFECTS ON THE FORMATION OF MESOSCOPICALLY ORDERED SILICATE-SURFACTANT MATERIALS SYNTHESIZED IN THE PRESENCE OF NON-IONIC SURFACTANTS

C.V. Teixeira[1], V. Alfredsson[2], H. Amenitsch[3] and M. Lindén[1]

1.) Department of Physical Chemistry, Abo Akademi University, Porthansgatan 3-5, Turku, Finland
2.) Physical Chemistry 1, Lund University, P.O. Box 124, SE- 221 00, Lund, Sweden
3.) Institute of Biophysics and X-Ray Structure Research, Austrian Academy of Sciences, Schmiedlstrasse 6, A-8042 Graz, Austria

The initial stages of the formation of SBA-15, 2D hexagonally ordered surfactant-silicate material, have been studied under acidic conditions in the presence of added salts by *in situ* SAXS/XRD using synchrotron radiation. This is an extension of our previous work on the formation of SBA-15 under standard conditions, i.e. without the addition of salts.[1] The salts studied were NaCl, NaBr, and NaI, in order to study the effect of salt induced hydration/dehydration of the EO units, which is mainly an effect of the anions present. Cl^- and Br^- are considered to be dehydrating ions, while I^- is considered to be hydrating, i.e. one would expect the influence of the two groups of anions on the silicate-surfactant mesophase formation to be different. The influence of the self-evident formation of cylindrical micelles as one step in the formation of the 2D hexagonally ordered material can thus be followed, since the formation of cylindrical micelles should be easier in the presence of dehydrating salts, if the surfactant micelles are globular in the absence of added salt. Thus, we chose to study a synthesis where the hydrophilic tri-block-co-polymer P104 ($EO_{27}PO_{61}EO_{27}$) was used as the structure-directing agent. The synthesis temperature was kept constant at 45^oC in all cases, where the P104 micelles are globular in under the synthesis conditions applied without salt addition, and the salt concentration was the variable.

The addition of salt to the synthesis lead to a shortening of the time needed for the formation of the 2D hexagonal phase in all cases, as shown in Table 1. The precipitation time at a given salt concentration decreased with increased salt concentration for all salts, and the precipitation time decreased in the order $Cl^- > Br^- > I^-$ for a given salt concentration. Thus, the salt concentration and the anion has a great influence on the formation kinetics, and the anions follow the order expected from the Hofmeister series.

Table 1. Time in minutes corresponding to the time where the (10) reflection of the 2D hexagonal mesophase appeared.

Concentration [M]	NaCl	NaBr	NaI
0	40	40	40
0.5	24	33	32
1.0	14	19	30
1.5	8.5	15	

Analysis of the diffuse micellar scattering region of the time-resolved SAXS patterns (results not shown) revealed that the micelles elongate faster in the presence of Cl^- and Br^-as compared to the no added salt case, and thus the kinetics of formation of the mesophase is clearly influenced by the kinetics of elongation of the micelles. Unfortunately, analysis of the micellar scattering region was not possible in the case of I^- containing compositions, due to a very low scattering intensity. This is probably due to a more even electron density distribution

in the system rather than an effect of the absence of micelles, since the presence of micelles in the I^- containing sols were independently checked by NMR and TEM. However, since the precipitation time decreased in all cases, there is not a straightforward linking between the expected "salting-in" and "salting-out" behavior of the ions and the time of precipitation. In this respect, we cannot exclude that the added salt also will influence the hydrolysis and condensation kinetics of TEOS used as the source for silica, but such studies are scarce in the literature for acidic sols. However, the ionic strength is high also in the absence of added salt, so at least the electrostatic interactions between charged species should be effectively screened in all cases.

The influence of added salt on the kinetics of precipitation of the 2D phase is also seen at times longer than that where the first signs of order is seen in the diffractograms. As an example, the integrated intensity of the main reflection is shown in Figure 1 as a function of time.

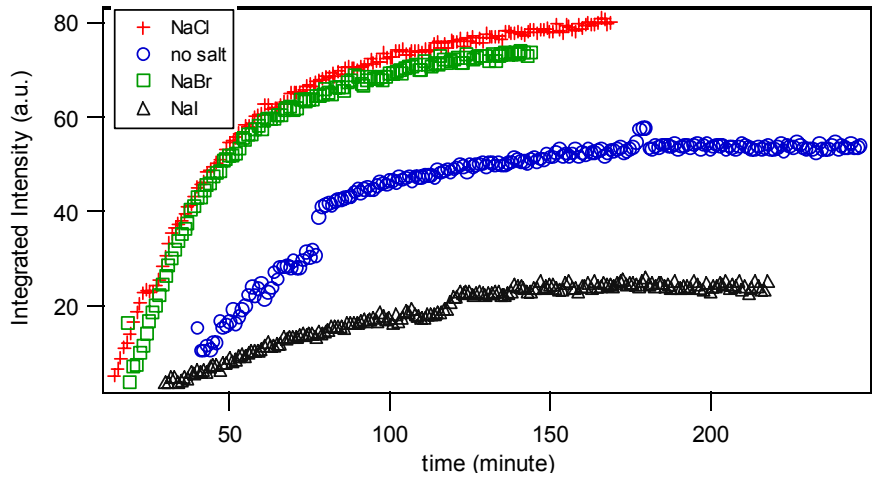

Figure 1. Integrated intensity of the main reflection as a function of reaction time for SBA-15 synthesis in the presence of added salts. The concentrations of the added salts were 1 M in all cases.

While the overall shape of the curves are similar, the integrated intensities follow the order NaCl ≈ NaBr > no added salt > NaI, which is corresponding to what is expected from a salting-in/salting-out effect of the anions. It should be stressed that this difference cannot be rationalized solely based on the difference in X-ray absorption of the different sols, and thus includes information about the rate of growth of the 2D hexagonal domains, both in size and number. Furthermore, the micellar scattering intensity observed after the precipitation of the 2D hex phase decreased in with time in the same order, (note, no analysis possible for NaI) which gives further support for this claim. Thus, we have been able to show that the Hofmeister concept is valid also for the influence of anions on the formation kinetics of mesoscopically ordered non-ionic surfactant-silicate materials, although the influence of the added salts on silica solution chemistry should be taken into account as well.

References:

[1] K. Flodström, C.V. Teixeira, H. Amenitsch, V. Alfredsson, and M. Lindén; In Situ Synchrotron Small-Angle X-ray Scattering/X-ray Diffraction Study of the Formation of SBA-15 Mesoporous Silica; Langmuir **20**, 4885-4891 (2004)

STUDY OF THE GROWTH OF SEMICONDUCTING ZnO NANOCRYSTALS USING SAXS TECHNIQUE

R. Viswanatha[1], H. Amenitsch[2] and D.D. Sarma[1]

1.) Solid State and Structural Chemistry Unit, Indian Institute of Science, Bangalore-560012, India
2.) Institute of Biophysics and X-ray Structure Research, Austrian Academy of Sciences, Schmiedlstr. 6, 8042 Graz, Austria

The solution route synthesis of nanocrystals has been used extensively to prepare a wide range of systems so far. However, the primary difficulty of this method is the strong interplay between various factors like temperature, concentration and by the addition of a capping agent in a way that is very little understood; though these very processes controls the size along with the size distribution of the generated particles. Besides the fact that an understanding of the growth mechanism will be useful to improve the quality and the control of such nanocrystals, at a fundamental view point there is little known about the growth mechanisms of these nanocrystals. The issues regarding the growth processes in these nanocrystals are largely debatable, mainly due to probe, i.e., UV-absorption spectroscopy used to study the growth processes. The major drawbacks of this method are the highly indirect nature of obtaining the size and the difficulty in carrying out a short time scale *in-situ* measurement. Recent experiments in our group on ZnO nanocrystals using UV-absorption spectroscopy suggests that the growth mechanism deviates strongly from the 'Ostwald Ripening', the generally accepted mechanism of growth. In this work we have used *in-situ* SAXS measurements to study the growth of ZnO by varying the temperature, concentration of the reactants using dynamic stopped flow technique [1] to determine the mechanism of growth.
The precursors were prepared by dissolving fixed amount of zinc acetate in iso-propanol and the required amount of sodium hydroxide in iso-propanol. The sodium hydroxide solution was quickly injected into zinc acetate solution at different temperatures. The time resolved evolution of the scattering patterns were monitored initially with a resolution of 1 second for 100 seconds and then with a resolution of 10 seconds for the next 1000 seconds and then eventually with a resolution of 30 seconds. The high time resolution at initial time is necessary to study the fast growth of the nanocrystal. The time resolved patterns were normalized and background subtracted and a typical resulting pattern is shown in Figure. 1.

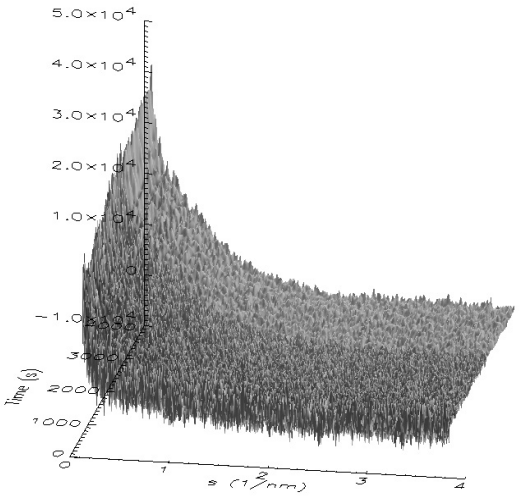

Figure 1. Time resolved scattering pattern of a typical growth of ZnO nanocrystals.

From the figure, it is clear that the ZnO nanocrystals are growing as a function of size. In order to get more detailed information regarding the dependence of the size of the nanocrystal

with time, we fitted the scattering patterns with the equation of the form I(q) = B. exp (-$q^2R_g^2/3$), B is any arbitrary constant and R_g is the Guinier Radius of the particle. The diameter of the particle is related to the Guinier radius by the relation $D^2 = 20. R_g^2/3$. The diameter of the nanocrystal was thus obtained for different concentrations of sodium hydroxide and at different temperatures. Typical variations in diameter of the nanocrystals by varying the concentrations are shown in Figure. 2(a) and by varying the temperatures are shown in Figure. 2(b).

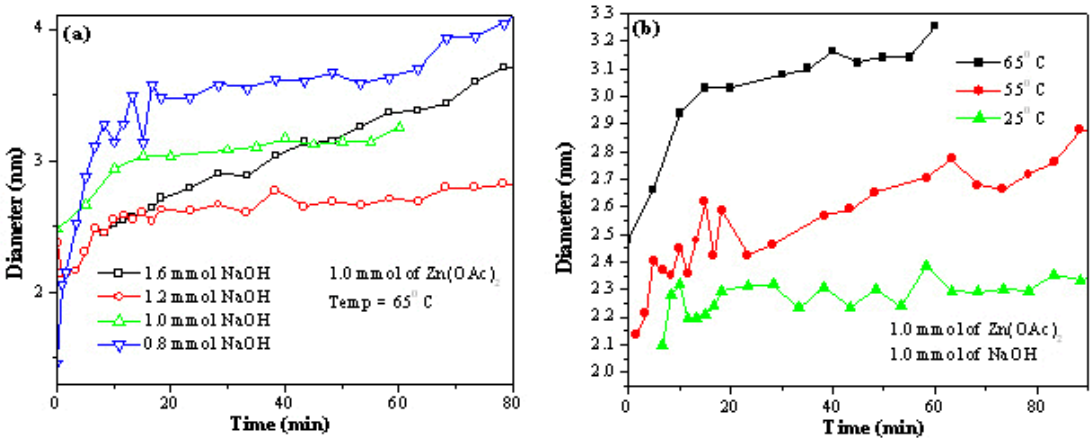

Figure 2. Variation of the diameters of ZnO as a function of time at (a) different concentrations and (b) different temperatures.

From the figure, it can be seen that there exists a strong dependence of the size variation on sodium hydroxide concentration which suggests that the growth mechanism cannot be Ostwald ripening. Also it is been observed that the diameter of the nanocrystal does not have a cubic dependence on time. These results clearly suggest that the growth of ZnO nanocrystals follows a different model of growth. Thus having analyzed these scattering patterns, we are now in the process of developing a growth model that can explain these observations and hence determine the mechanism of growth.

References:

[1] Agren,P., M.Linden, J.B.Rosenholm, R.Schwarzenbacher, M.Kriechbaum, H.Amenitsch, P.Laggner, J.Blanchard, and F.Schuth. 1999. Kinetics of cosurfactant-surfactant-silicate phase behavior. 1. Short-chain alcohols. *Journal of Physical Chemistry B* 103:5943-5948

STUDY OF THE GROWTH OF SEMICONDUCTING CdS AND ZnS NANOCRYSTALS USING SAXS TECHNIQUE

R. Viswanatha[1], S. Sapra[1], H. Amenitsch[2] and D.D. Sarma[1]

1.) Solid State and Structural Chemistry Unit, Indian Institute of Science, Bangalore-560012, India
2.) Institute of Biophysics and X-ray Structure Research, Austrian Academy of Sciences, Schmiedlstr. 6, 8042 Graz, Austria

The chemical approach to the synthesis of such nanocrystals, owing to its simplicity, flexibility and tunability, has been used extensively to prepare a wide range of systems so far [1,2,3]; this method depends basically on stopping the reaction process leading to the formation of the semiconductor in a solution by adding a capping agent that binds to the surface of the growing nanocrystal and stops it from growing any further. The primary difficulty of this method is that the size, along with the size distribution of the generated particles are determined primarily by the concentrations of the reactants and temperature in a way that is very little understood. Thus, the techniques of synthesis of high quality nanocrystals, indicated by the ability to grow a pre-defined size with a narrow size distribution, has remained largely in the realm of empiricism based on large number of hit-and-trial methods to fine-tune the synthesis parameters. In this work, we have used *in-situ* Small Angle X-ray scattering (SAXS) technique to study the thermal induced growth of CdS and ZnS nanocrystals by varying the temperatures as well as the capping agent concentrations. Using the results obtained from these experiments, we are trying model and understand the growth mechanism in these nanocrystals, thus being able to predict the size as well as the size distribution of the nanocrystals depending on the synthesis conditions. These can also be used in optimizing the various parameters for their synthesis.

The precursors were freshly prepared at room temperature using Dimethyl Sulphoxide (DMSO) as the solvent and then sealed in 1.5 mm quartz capillary and the samples were quickly heated to different temperatures. The evolution of the scattering pattern was monitored with a time resolution of 1 minute. The low time resolution is necessary to study initial growth that contains the most characteristic features of the growth mechanism involved in any case. The time resolved scattering patterns for CdS nanocrystals were normalized and background subtracted. A similar procedure was carried out also for the ZnS nanocrystals. A typical CdS pattern at 150°C is shown in Figure 1.

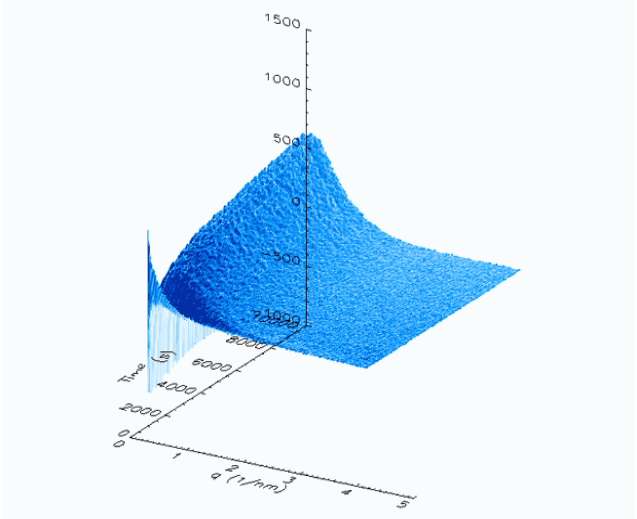

Figure 1. Scattering pattern of CdS at 150°C.

In order to obtain more detailed information we obtain the forward intensity and the invariant. The diameter of the particles and thus the trends associated by varying the temperature as well as the capping agent are obtained by dividing the forward intensity by the invariant. The

growth trends at different temperatures as well as different capping agent concentrations for CdS nanocrystals are shown in figure 2.

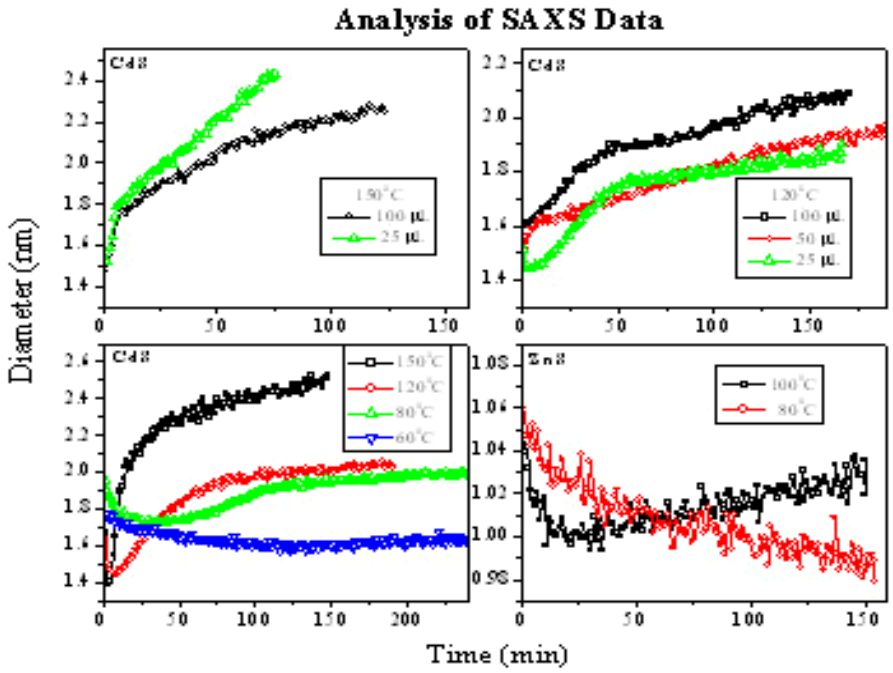

Figure 2. Growth of the nanocrystals at different temperatures and capping agent concentrations.

From the figure it can be seen that the temperature plays a major role in deciding the size of the nanocrystals, especially in case of CdS. However the capping agent concentration can be used to fine tune the size of the nanocrystals. Also from the figure, we observe some interesting features like the initial rapid decrease in the sizes of the nanocrystal. The rate of decrease of size increases with increasing temperature. Further analysis of the scattering plots using the software GNOM presented a quantitative measure of the size as well as the size distribution. These analyses in combination with the UV-absorption studies provide conclusive evidence that the decrease in the size of the nanocrystal is from dissolving the particle that was precipitated at room temperature that increases with increasing temperature. Also we find that the size of the dissolved particle increases monotonically with time. Thus having analyzed these scattering patterns, we are now in the process of developing a growth model that can explain these observations. Thus, from these measurements we have not only studied the variation of size but also obtain an insight into the mechanism of growth of these nanocrystals.

References:

[1] T. Vossmeyer, L. Katsikas, M. Giersig, I. G. Popovic, K. Diesner, A. Chemseddine, A. Eychmuller, H. J. Weller, J. Phys. Chem., **98**, 7665 (1994)
[2] C. B. Murray, D. B. Norris, M. G. Bawendi, J. Am. Chem. Soc. **115**, 8706 (1993)
[3] J. Nanda, S. Sapra, D. D. Sarma, N. Chandrasekharan and G. Hodes, Chem. Mater. **12**, 1018 (2000)

Publications

Publications in 2004

Amenitsch, H., C. Bombelli, S. Borocci, F. Ceccacci, G. Mancini, and M. Rappolt.
Elucidation of the isomeric domains formed by sodium N-dodecanoyl-L-prolinate
Journal of Colloid and Interface Science 280, 212-218 (2004)

Amenitsch, H., M. Rappolt, C. V. Teixeira, M. Majerowicz, and P. Laggner
In situ sensing of salinity in oriented lipid multilayers by surface X-ray scattering
Langmuir 20, 4621-4628 (2004)

V.K. Aswal, P.S. Goyal, H. Amenitsch and S. Bernstorff
Counterion condensation in ionic micelles as studied by a combined use of SANS and SAXS
Pramana-Journal of Physics 63(2), pp. 333-338 (2004)

P. Ausili, M. Pisani, S. Finet, H. Amenitsch, C. Ferrero and P. Mariani
Pressure effects on columnar lyotropics: anisotropic compressibilities in guanosine mono-phosphate four-stranded helices
J. Phys. Chem. B 108, 1783-1789 (2004)

Josef Baldrian, Milos Steinhart, Antonin Sikora, Jana Kasparova, Heinz Amenitsch, Sigrid Bernstorff
SWAXS and DSC Study of PEO Cocrystalline Structures Development in Polymer Blends
Conference Proceedings of MACRO 2004, Long Abstract (2004)

Andrea Bearzotti, Johnny Mio Bertolo, Plinio Innocenzi, Paolo Falcaro, Enrico Traversa
Humidity Sensors Based on Mesoporous Silica Thin Films Synthesized by Block Copolymers
J. European Ceram. Soc., 24, 1969-1972, 2004

L. Benes, V. Zima, K. Melanova, M. Steinhart, M. Kriechbaum, H. Amenitsch and S. Bernstorff
In situ high pressure phase transition of alcohol intercalated zirconium phosphate observed by synchrotron X-ray scattering
Journal of Physics and Chemistry of Solids 65 (2-3) pp. 615-618 (2004)

W.H. Binder, S. Bernstorff, C. Kluger, L. Petraru, M.J. Kunz and V. Torma
Poly(ether ketone)-Poly(isobutylene) Pseudo Block Copolymers : Phase Behavior via SAXS
Polym. Preprints 45(2), 620 – 621 (2004)

W.H. Binder, M.J. Kunz, E. Ingolic
Supramolecular Polyetherketone-Polyisobutylene pseudo block-Copolymers
J. Polym. Sci. 42, 162 – 172 (2004)

M. Cócera, O. López, R. Pons, H. Amenitsch, and A. de la Maza
Effect of the electrostatic charge on the mechanism inducing liposome solubilization: a kinetic study by synchrotron radiation SAXS
Langmuir 20(8), 3074 - 3079 (2004)

Z. Crnjak Orel, D. Kuščer, M. Kosec and A. Turkovic
Characterization of nanocrystalline V2O5 and mixed V2O5/Ce oxide
Progress in Colloid and Polymer Science 128, pp.120-125 (2004)

G. Croce, A. Frache, M. Milanesio, L. Marchese, M. Causa, D. Viterbo, A. Barbaglia, V. Bolis, G. Bavestrello, C. Cerrano, U. Benatti, M. Pozzolini, M. Giovine and H. Amenitsch
Structural characterization of siliceous spicules from marine sponges
Biophysical Journal 86(1), pp. 526-534 (2004)

U.V. Desnica, M. Buljan, I.D. Desnica-Frankovic, P. Dubcek, S. Bernstorff, M. Ivanda and H. Zorc
Direct Ion Beam Synthesis of II-VI Nanocrystals
Nucl. Instrum. & Methods B 216, pp. 407-413 (2004)

P. Dubcek, B. Pivac, O. Milat, S. Bernstorff and I. Zulim
Study of structural changes in krypton implanted silicon
Nucl. Instrum. & Methods B 215, Issue 1-2, pp. 122-128 (2004)

P. Dubcek, A. Turkovic, Z. Crnjak Orel, B. Etlinger and S. Bernstorff
Synchrotron Light Scattering on Nanostructured V/Ce Oxide Films Intercalated with Li+ Ions
Journal of Chemical Information & Computer Sciences. 44, pp. 290-295 (2004)

P. Falcaro, P., D. Grosso, H. Amenitsch, and P. Innocenzi
Silica orthorhombic mesostructured films with low refractive index and high thermal stability
Journal of Physical Chemistry B 108, 10942-10948 (2004)

P. Falcaro, J.M. Bertolo, P. Innocenzi, H. Amenitsch, A. Bearzotti
Ordered mesostructured silica films: effect of pore surface on its sensing properties
J. Sol-Gel Science and Tech., 32, 107 (2004)

D. Farnik, C. Kluger, M.J. Kunz, D. Machl, L. Petraru, W.H. Binder
Synthesis and Self Assembly of Hydrogen Bonded Supramolecular Polymers
Macromolecular Symposia 217, 247 – 266 (2004)

K. Flodström, C. V. Teixeira, H. Amenitsch, V. Alfredsson, and M. Linden
In situ synchrotron small-angle X-ray scattering/X-ray diffraction study of the formation of SBA-15 mesoporous silica
Langmuir 20, 4885-4891 (2004)

K. Flodström, H. Wennerstrom, C. V. Teixeira, H. Amenitsch, M. Linden, and V. Alfredsson
Time-resolved in situ studies of the formation of cubic mesoporous silica formed with triblock copolymers
Langmuir 20, 10311-10316 (2004)

D. Gracin, P. Dubcek, H. Zorc and K. Juraic
Mediun Range Ordering of Amorphous Silicon-Carbon Alloys Studied by GISAXS, Spectroscopy and IBA
Thin Solid Films 459, 1-2; 216-219 (2004)

P.J. Griffiths, M.A. Bagni, B. Colombini, H. Amenitsch, S. Bernstorff, C.C. Ashley, and G. Cecchi
S1 structure under conditions of hypo- and hypertonicity
J. Physiol., 555P**,** C169 (2004)

D. Grosso, F. Cagnol, G.J. de A. A. Soler-Illia, E.L. Crepaldi, P.A. Albouy, H. Amenitsch, A. Brunet-Bruneau, and C. Sanchez
Fundamental of mesostructuration through evaporation-induced self-assembly
Advanced Functional Materials 14, 309-322 (2004)

D. Grosso, C. Boissière, B. Smarsly, T. Brezesinski, N. Pinna, P. A. Albouy, H. Amenitsch, M. Antonietti and C. Sanchez
Periodically ordered nanoscale islands and mesoporous films composed of nanocrystalline multimetallic oxides
Nature Materials, Vol. 3, 787-792 (2004)

H. S. Gupta, P. Messmer, P. Roschger, S. Bernstorff, K. Klaushofer, and P. Fratzl,
Synchrotron Diffraction Study of Deformation Mechanisms in Mineralized Tendon
Phys. Rev. Lett., 93, No. 15, pp. 158101-1 / 158101-4 (2004)

Harroun, T. A., M.-P. Nieh, M. J. Watson, V. A. Raghunathan, G. Pabst, M. Morrow, and J. Katsaras
The relationship between the unbinding and the main phase transition temperature under pressure
Phys. Rev. E 69, 031906 (2004)

P. Innocenzi, P. Falcaro, S. Schergna, E. Menna, M. Maggini, H. Amenitsch, JAA Soler-Illia, D. Grosso and C. Sanchez
One-Pot Self-Assembling of Mesostructured Silica Films and Membranes Functionalised with Fullerenes Derivatives
J Mater Chem, 14, pp. 1838-1843, 2004

D. Kalnin, O. Schafer, H. Amenitsch, and M. Ollivon
Fat crystallization in emulsion: Influence of emulsifier concentration on triacylglycerol crystal growth and polymorphism
Crystal Growth & Design 4, 1283-1293 (2004)

O. López, M. Cócera, J. Pereira, H. Amenitsch, J. Caelles, L. Coderch, J.L. Parra, A. de la Maza and R. Pons
Processing stopped-flow saxs data to study the kinetic of liposome-surfactant systems
Biophys. J, 86(1), 76a, (2004)

J. Morell, C.V. Teixeira, M. Cornelius, V. Rebbin, M. Tiemann, H. Amenitsch, M. Froeba and M. Linden
In situ Synchrotron SAXS/XRD Study on the Formation of Ordered Mesoscopic Hybrid Materials with Crystal-Like Walls
Chemistry of Materials 16 (26), 5564-5566 (2004)

A. Orthen, H. Wagner, S. Martoiu, H. Amenitsch, S. Bernstorff, H.J. Besch, R.H. Menk, K. Nurdan, M. Rappolt, A.H. Walenta and U. Werthenbach
Development of a two-dimensional virtual-pixel X-ray imagining detector for time-resolved structure research
J. Synchrotron Rad. 11, 177-186 (2004)

D. Ortis, C. Boissière, D. Grosso, P.A. Albouy, H. Amenitsch**,** and C. Sanchez
Preparation of multi nano-crystalline transition metal oxide (TiO_2-$NiTiO_3$) thin films with cubic mesostructure
New Journal of Chemistry 29, 141 (2004)

G. Pabst, H. Amenitsch, P. Laggner, and M. Rappolt
Pretransitional swelling is not linked to ripple phase formation in phosphatidylcholines
Biophysical Journal 86, 350A (2004)

G. Pabst
SAXPD Studies of Phospholipid Modelmembranes
IUCr CPD Newsletter 31, 41-44 (2004)

G. Pabst, H. Amenitsch, D. P. Kharakoz, P. Laggner, and M. Rappolt
Structure and fluctuations of phosphatidylcholines in the vicinity of the main phase transition
Phys. Rev. E 70, 021908 (2004)

L. Petraru, D. Farnik, R. Saf, W.H. Binder
Supramolecular, Telechelic Poly(etherketones) Bearing Barbituric Acid as Hydrogen Bonding Unit
Polym. Preprints 45(2), 690 – 691 (2004)

B. Pivac, P. Dubcek, S. Bernstorff, F. Corni and R. Tonini
GISAXS study of hydrogen implanted silicon
Journal of Alloys and Compounds, Volume 382, Issues 1-2, 17.11.2004, pp. 75-77 (2004)

G. Principi, A. Maddalena, M. Meyer, S. Dal Toe, A. Gupta, P. Sharma, B.A. Dasannacharya, N. Paul, S. Bernstorff and H. Amenitsch
Structural Evolution of the Amorphous Grain Boundary Phase during Nanocrystallization of $Fe_{72}Cu_1Nb_{4.5}Si_{13.5}B_9$
Journal of Magnetism and Magnetic Materials 272-76: 1441-1442 Part 2 Sp. Iss. SI May 2004

N. Radic, A. Tonejc, J. Ivkov, P. Dubcek, S. Bernstorff, Z. Medunic
Sputter-deposited amorphous-like tungsten
Surface and Coatings Technology Vol 180-181, pp 66-70 (2004)

Rappolt, M., H. Amenitsch, J. Strancar, C. V. Teixeira, M. Kriechbaum, G. Pabst, M. Majerowicz and P. Laggner
Phospholipid mesophases at solid interfaces: in-situ X-ray diffraction and spin label Studies
Advances in Colloid Interface Sciences 111, 63-77 (2004)

Rappolt, M., P. Laggner and G. Pabst
Structure and elasticity of phospholipid bilayers in the L •phase: A comparison of phosphatidylcholine and phosphatidylethanolamine membranes
In: Recent Res. Devel. Biophys. Vol. 3, Part II, Transworld Research Network, editor S. G. Pandalai, Trivandrum, pp 363-392 (2004)

A. Raudino, F. Lo Celso, A. Triolo, and R. Triolo
Pressure-induced formation of diblock copolymer "micelles" in supercritical fluids. A combined study by small angle scattering experiments and mean-field theory. I. The critical micellization density concept
J. Chem. Phys. 120, 3489 (2004)

A. Raudino, F. Lo Celso, A. Triolo, and R. Triolo
Pressure-induced formation of diblock copolymer "micelles" in supercritical fluids. A combined study by small angle scattering experiments and mean-field theory. II. Kinetics of the unimer-aggregate transition
J. Chem. Phys. 120, 3499 (2004)

Th. Schmidt, T. Clausen, J. Falta, S. Bernstorff, G. Alexe, T. Passow and D. Hommel
Investigation of CdSe/ZnSSe quantum dot ordering by grazing incidence small angle X-ray scattering
Phys. stat. sol. (b) 241 (3), 523-526 (2004)

Th. Schmidt, T. Clausen, J. Falta, G. Alexe, T. Passow, and D. Hommel and S. Bernstorff
Correlated stacks of CdSe/ZnSSe quantum dots
Appl. Phys. Lett. 84(22) 4367-4369 (2004) and
Virt. J. Nanoscale Sci. Techn. **9** (2004)

E.Schafler, K. Simon, S.Bernstorff, P. Hanak, G. Tichy, T. Ungar and M.J. Zehetbauer
A second-order phase-transformation of the dislocation structure during plastic deformation determined by in situ synchrotron X-Ray diffraction
Acta Materialia Vol 53/2 pp 315-322 (2004)

V. Torma, N. Hüsing, H. Peterlik, U. Schubert
Small Angle X-Ray Scattering Investigation of the cluster Distribution in Inorgani-Organic Hybrid Polymers Prepared from Organically Substituted Metal Oxid Clusters
Comptes rendus Chimie 7, 495-502 (2004)

A. Turkovic'
Grazing-incidence small-angle X-ray scattering and reflectivity on nanostructured oxide films
Materials Science & Engineering B. 110, 1; 68-78 (2004)

A. Turkovic and M. Gabercek
Impedance Spectroscopy of Nanostructured TiO2 films on Glass Substrate as Electrode for Dye-Sensitized Solar Cell
Proceedings 3rd Croatian Symposium on Electrochemistry, Gojo, Miroslav (ed.). Zagreb, pp. 101-104, (2004)

H. Wagner, A. Orthen, H.J. Besch, S. Martoiu, R.H. Menk, A.H. Walenta, U. Werthenbach
On image reconstruction with the two-dimensional interpolating resistive readout structure of the Virtual-Pixel detector
Nucl. Instr. & Meth. A523, 287-301 (2004)

H. Wilhelm, A. Paris, E. Schafler, S. Bernstorff, J. Bonarski, T. Ungar, M. J. Zehetbauer
Evidence of dislocations in melt-crystallised and plastically deformed polypropylene
Mater.Sci.Eng.A 387-389,pp. 1018-1022 (2004)

I. Winter, G. Pabst, K. Lohner, and S. M. Melnikov
Vesicles formed by non-phospholipid selfassembly
Chem. List. 98, 27-28 (2004)

Publications from January to June 2005

W.H. Binder, D. Machl
Poly(etherketone)-Poly(isobutylene) Block Copolymers : Synthesis and Phase Behavior
J. Polym. Sci. Polym. Chem Part A, 188 – 202 (2005)

G. Caracciolo, H. Amenitsch, C. Sadun and Ruggero Caminiti
In situ formation of solid-supported lipid/DNA complexes
Chem. Phys. Lett. 405 252-257 (2005)

Z. Crnjak Orel, M. Gabercek and A. Turkovic
Electrical and spectroscopical characterization of nanocrystalline V/Ce oxides
Solar Energy materials & Solar Cells. 86, pp.19-32 (2005)

V. Erokhin, S. Carrara, C. Paternolli, L. Valkova, S. Bernstorff and C. Nicolini
X-ray stduy of structural reorganization in phthalocyanine containing Langmuir-Blodgett heterostructures
Applied Surface Science 245, 369-375 (2005)

P. Falcaro, S. Costacurta, G. Mattei, H. Amenitsch, A. Marcelli, M. Cestelli Guidi, M. Piccinini, A. Nucara, L. Malfatti, T. Kidchob, and P. Innocenzi
Highly ordered "defect-free"self-assembled hybrid films with a tetragonal mesostructure
J. Am. Chem. Soc., 127, 3838-3846 (2005)

J.I. Flege, T. Schmidt, G. Alexe, T. Clausen, S. Bernstorff, I. Randjelovic, V. Aleksandrovic, A. Kornowski, H. Weller and J. Falta
CoPt3 nanoparticles adsorbed on SiO2: a GISAXS and SEM study
Mater. Res. Soc. Symp. Proc. 840, pp. Q6.10.1 – Q6.10.6 (2005)

P. J. Griffiths, M. A. Bagni, B. Colombini, H. Amenitsch, S. Bernstorff, C. C. Ashley, and G. Cecchi
Myosin lever disposition during length oscillations when power stroke tilting is reduced
Am J Physiol Cell Physiol. 289, 177-186 (2005)

P. Innocenzi, L. Malfatti, T. Kidchob, P. Falcaro, MC. Guidi, M. Piccinini, A. Marcelli
Kinetics of polycondensation reactions during self-assembly of mesostructured films studied by in situ infrared spectroscopy
Chem Commun (Camb). 2005 May 14;(18):2384-6. Epub 2005 Mar 18

E. Schafler, K. Simon, S. Bernstorff, P. Hanak, G. Tichy, T. Ungar, M.J. Zehetbauer
A Second Order Phase Transformation During Plastic Deformation Determined by In Situ X-Ray Synchrotron Diffraction
Acta mater. 53 (2005) 315-322

R. Supplit, N. Hüsing, C. Fritscher, P. Jakubiak, V. G. Kessler, G. A. Seisenbaeva and S. Bernstorff
Iron Oxide – Doped Mesostructured Silica Films
Mater. Res. Soc. Symp. Proc. 847, EE9.13 (2005)

Viktoria Torma, Herwig Peterlik, Ulrike Bauer, Wolfgang Rupp, Nicola Hüsing, Sigrid Bernstorff, Milos Steinhart, Günter Görigk and Ulrich Schubert
Mixed Silica Titania Materials Prepared from a Single-Source Sol-Gel Precursor: A Time-Resolved SAXS Study of the Gelation, Aging, Supercritical Drying, and Calcination Processes
Chem. Mater. 17, 3146-3153 (2005)

B. Toury, R. Blum, V. Goletto, F. Babonneau
Thermal Stability of Periodic Mesoporous SiCO Glasses
J. Sol-Gel Sci. Techn. 33, pp 99-102 (2005)

R. Triolo, F. Lo Celso, V. Benfante, A. Triolo, A. Wiedenmann and S. Bernstorff
Small angle scattering study of poly(methylmethacrylate)-blockpoly(ethylene oxide) block co-polymer in aqueous solution
Progress in Colloid and Polymer Science 130, p. 79 (Published Online: June 2005)

Publications in print (June 2005)

S. Areva, C. Boissière, D. Grosso, T. Asakawa, C. Sanchez, M. Lindén
One-pot aerosol synthesis of ordered hierarchical mesoporous core-shell silica nanoparticles
Chem. Commun.

Baldrian J., Steinhart M., Sikora A., Amenitsch H., Bernstorff S.
Phase structure of symmetric tri-block-copolymers and their blends
Fibres & Text. East. Eur.

S. Bernstorff, P. Dubcek, B. Pivac, I. Kovacevic, A. Sassella, A. Borghesi
GIXR and GISAXS study of silicon oxinitride films
Applied Surface Science

U.V. Desnica, P. Dubcek, K. Salamon, I.D. Desnica-Frankovic, M. Buljan, S. Bernstorff, U. Serincan, R. Turan
The evolution of the morphology of Ge nanocrystals formed by ion implantation in SiO_2
Phys. Res. B

P. Dubcek, B. Pivac, S. Bernstorff, F. Corni, C. Nobili and R. Tonini
Grazing incidence small angle X-ray scattering study of He irradiation induced defects in monocrystalline silicon
NIM B

P. Dubcek, B. Pivac, S. Bernstorff, F. Corni, R. Tonini, G. Ottaviani
Grazing incidence X-ray reflectivity study of hydrogen implanted silicon
Applied Surface Science

D. Farnik, W.H. Binder, N. Hüsing
Novel Carbohydrate Based Surfactants for the Preparation of Imprinted Silica
Polym. Preprints

J. I. Flege, Th. Schmidt, V. Aleksandrovic, G. Alexe, T. Clausen, B. Gehl, A. Kornowski, H. Weller, S. Bernstorff, J. Falta
Grazing-incidence small-angle x-ray scattering investigation of spin-coated CoPt3 nanoparticle films
NIMB

C. Fritscher, N. Hüsing, S. Bernstorff, D. Brandhuber, T. Koch, S. Seidler, H. C. Lichtenegger
In-situ SAXS study on cationic and non-ionic surfactant liquid crystals using synchrotron radiation
Journal of Synchrotron Radiation

D.Gracin, K.Juraic, P.Dubcek, A.Gajovic, S.Bernstorff
Analysis of the Nano-structural Properites of Thin Film Silicon-Carbon Alloys
Vacuum

A. Gupta, P. Rajput, A. Saraiya, V. R. Reddy, M. Gupta, S. Bernstorff, H. Amenitsch
Depth profiling of marker layers using x-ray waveguide structures
Phys. Rev. B

Plinio Innocenzi, Luca Malfatti, Tongjit Kidchob, Paolo Falcaro, Stefano Costacurta, Massimo Guglielmi, Giovanni Mattei, Heinz Amenitsch
Thermal induced phase transitions in self-assembled mesostructured films studied by small angle X-rays scattering
J. Sync. Rad.

M. Kerber, E. Schafler, P. Hanak, G. Ribàrik, S. Bernstorff , T. Ungàr , M. Zehetbauer
Spatial Fluctuations of the Microstructure during deformation in Cu Single Crystals
Z. Kristallographie

I. Kovacevic, B. Pivac, P. Dubcek, N. Radic, S. Bernstorff, A. Slaoui
A GISAXS study of SiO/SiO_2 superlattice
Thin Solid Film

M. Kuemmel, D. Grosso, C. Boissière, B. Smarsly, T. Brezinski, P. A. Albouy, H. Amenitsch, and C. Sanchez
Nanocrystalline γ-alumina layers with highly ordered fcc cubic mesoporosity stable up to 900°C
Angewandte Chemie

B. Pivac, I. Kovacevic, P. Dubcek, N. Radic, S. Bernstorff, A. Slaoui
Self-organized growth of Ge islands on Si(100) substrates
Thin Solid Film

E. Schafler, K. Nyilas, S. Bernstorff , L. Zeipper , M. Zehetbauer, T. Ungàr
Microstructure of post deformed ECAP-Ti investigated by Multiple X-Ray Line Profile Analysis Z. Kristallographie
A. Turkovic, P. Dubcek and N.D. Fox
Self-Organization of Nanoparticles in TiO2 Thin Film on the Glass Substrate
Vacuum

T. Ungár, E. Schafler, P. Hanák, S. Bernstorff, M. Zehetbauer
Vacancy concentrations determined from the diffuse background scattering of X-rays in plastically deformed copper
Zeitschrift fuer Materialkunde

M. Zehetbauer, E. Schafler, T. Ungar
Quantification of Nanocrystallization by Means of X-Ray Line Profile Analysis
Arch. Metall.

International Conferences and Workshops in 2004

H. Amenitsch, M. Rappolt, B. Sartori, G. Pabst, D. Grosso and P. Laggner
In-situ self-assembly of phospholipids studied with surface diffraction
8th International Conference on Surface X-Ray and Neutron Scattering
Bad Honnef (Germany), June 28 - July 2 2004 (talk)

H. Amenitsch and P. Laggner
Characterization of pharmaceutical nanophase formulations by synchrotron SWAXS
Workshop at the NLSL Users-meeting: "Pharmaceutical Applications of Synchrotron Radiation", Brookhaven, USA, 17.5.04 (invited lecture)

H. Amenitsch
Introduction to SAXS and WAXS
ICTP school for Synchrotron Radiation, Trieste, IT, 7.-13.5.04 (invited lecture)

H. Amenitsch
SAXS under extereme conditions
ICTP school for Synchrotron Radiation, Trieste, IT, 7.-13.5.04 (invited lecture)

H. Amenitsch
Small angle X-ray scattering with synchrotron radiation used as tool in material science and biology
National University of Singapore, 22.5.04 (invited lecture)

H. Amenitsch
In-situ tensile testing of blood vessels
6 th ELBA Forum, Porto Conte, Sardinia, IT, 9.-12.9.04 (invited lecture)

H. Amenitsch
New generation of tools for advanced materials characterization
Workshop in Nanotechnology and Nanoscience, Ministry of Science and Technology, Brazil – European Commission, São Paulo, Brazil, 12.-14.12.04 (invited lecture)

H. Amenitsch, S. Bernstorff, M. Rappolt, P. Laggner
Small angle X-ray scattering with synchrotron radiation used as tool in material science and biology
3. SESAME Users' Meeting, Antalya, Turkey, 11.-13.10.04 (invited lecture)

H. Amenitsch, M. Rappolt, B. Sartori, G. Pabst, D. Grosso and P. Laggner
In-situ self-assembly of phospholipids studied with surface diffraction
Associazione Italiana di Cristallografia, XXXIV Congresso Nazionale Roma 2004, 26.-29.09.04 (talk)

H. Amenitsch, M. Rappolt, C. Teixeira, M. Majerowicz, P. Laggner
In-situ sensing of salinity in oriented lipid multilayers by surface X-ray scattering.
Associazione Italiana di Cristallografia, XXXIV Congresso Nazionale Roma 2004, 26.-29.09.04 (poster)

V.K. Aswal, S. Chodankar, J. Kohlbrecher and S. Bernstorff
Entropy driven self-association of block copolymers in presence of selective additives
49th DAE Solid State Physics Symposium, Amritsar, India, Dec. 26-30, 2004

F. Babonneau
Organosilices à Porosité Contrôlée
20èmes Journées du Groupe Francais de Zeolithes, Dijon, France, 17-19 March 2004 (invited talk)

F. Babonneau
Structural chemistry of sol-gel derived organic/inorganic materials
International Conference on Glasses (ICG XX), Kyoto, Japan, September 26 -October 1, 2004 (invited talk)

F. Babonneau
Structural investigations of organic-inorganic and organic-organic interactions in mesostructured silicas and organosilicas powders
Department of Chemical Engineering, University of California, Santa Barbara (USA), 2.8.2004 (seminar)

F. Babonneau
Structural investigations of organic-inorganic and organic-organic interactions in mesostructured silicas and organosilicas powders
Advanced Materials Laboratory, University of New Mexico/Sandia National Laboratories, Albuquerque (USA), 11.8.2004 (seminar)

N. Baccile, A. Riley, H. Amenitsch, S. Tolbert, M. Linden and F. Babonneau
On the mechanism of formation of SBA–1, SBA–2 and SBA–3 mesostructured silicas as studied by in situ XRD
Fall Meeting of the Materials Research Society, Boston, MA, USA, 29.-11.- 3.12.2004

Josef Baldrian, Milos Steinhart, Antonin Sikora, Jana Kasparová, Heinz Amenitsch, Sigrid Bernstorff
SWAXS and DSC Study of PEO Cocrystalline Structures Development in Polymer Blends
40th IUPAC International Symposium on Macromolecules, World Polymer Congress MACRO, Paris, France, July 4-9, 2004 (poster)

Baldrian J., Steinhart M., Sikora A., Amentisch H., Bernstorff S.
Phase structure of symmetric tri-block-copolymers and their blends
6th International Conference on X-Ray Investigation of Polymer Structure XIPS'2004, Ustron, Poland, December 8-11, 2004 (Invited lecture)

S. Bernstorff
Synchrotron Radiation Scattering Methods in Condensed Matter Investigation
Seminar, Institute of Atomic Energy, Swierk (Warsaw), Poland, May 5, 2004 (invited lecture)

S. Bernstorff
Synchrotron Radiation Scattering Methods in Condensed Matter Investigation
11th International Seminar on "Neutron Scattering Investigation in Condensed Matter"
Institute of Physics, Adam Mickiewicz University, Poznan, Poland, May 6-8, 2004 (invited plenary lecture)

S. Bernstorff
GISAXS in materials science
ICTP school for Synchrotron Radiation, Trieste, IT, 7.-13.5.04 (invited lecture)

Wolfgang, H Binder, Sigrid Bernstorff, Dominique Farnik, Christian KLuger, Michael, J. Kunz, Laura Petraru
Supramolecular Poly(ether ketone)-Polyisobutylene Pseudo-Block Copolymers: Hydrogen Bonding versus Phase Separation
MACRO 2004 - 40th IUPAC World Polymer Congress, Paris, France, July 4-9, 2004 (talk)

W. H. Binder, M. J. Kunz, C. Kluger, L. Petraru, S. Bernstorff, V. Torma
Poly(etherketone)-poly(isobutylene) pseudo block-copolymers : Phase behavior via SAXS
228th National Meeting of the American Chemical Society, Philadelphia, PA (22-27.8.2004) (talk)

W. H. Binder
Nanostrukturen aus supramolekularen Polymeren : Phasenseparationseffekte und Wasserstoffbrückenbindungen als strukturdirigierende Faktoren zum Aufbau supramolekularer Materialien
Universität Erlangen/Nürnberg, 15. November 2004 (invited talk)

W. H. Binder
Supramolecular Chemistry with Polymers : New Approaches Towards Functional Materials and Surfaces
Hungarian Academy of Sciences, 8. October 2004, Budapest (invited talk)

W. H. Binder
Modulative Materials from Supramolecular Polymers : Creating Two- and Threedimensional Order
Universität Linz, 2004 (invited talk)

W. H. Binder
Nanostructured Membranes and Materials from Designed Polymers
Novartis Forschungsinstitut Wien, 2004 (invited talk)

W. H. Binder
Synthese und Applikation massgeschneiderter Makromoleküle für nanostrukturierte Polymere und funktionale Polymere
Universität Stuttgart, 2004 (invited talk)

W. H. Binder
Nanostrukturen aus supramolekularen Polymeren : Phasenseparationseffekte und Wasserstoffbrückenbindungen als strukturdirigierende Faktoren zum Aufbau „weicher" Materie
Universität Münster, 2004 (invited talk)

W. H. Binder
Selbstanordnung von Polymeren in Nanostrukturen : Die Wasserstoffbrückenbindung als strukturdirigierendes Element
GDCh – Chemiedozententagung, Dortmund 2004

C. Boissoire, D. Grosso, B. Smarsly, T. Brezesinski, S. Lepoutre, J.C. Valle Marca, L. Nicole, M. Antonietta and C. Sanchez
From Hybrid Films to Mesoorganized Multi-Metal-Oxide Meso-Organized Nanocrystalline Films (M3NF), Preparation and Characterization
Fall Meeting of the Materials Research Society, Boston, MA, USA, 29.-11.- 3.12.2004 (talk)

M. Buljan
Primjena raspršenja X-zračenja pod malim kutom za vrlo mali upadni kut na proučavanje geometrijskih svojstava CdS nanokristala dobivenih ionskom implantacijom, // in Croatian// (GISAXS studies of the shape of CdS nanocrystals obtained by ion implantation)
Seminar, Zagreb University, Croatia, 12.10.2004

Z. Crnjak Orel and A. Turkovic
Preparation and characterization of nanocrystalline V2O5 and mixed V/Ce oxide
The 8th Arab International Solar Energy Conference & Regional World Renewable Energy Congress, 8-10 March 2004, University of Bahrain, Kingdom of Bahrain. Bahrain (invited lecture)

Z. Crnjak Orel, A. Turkovic and M. Ivanda
Preparation and Characterization of Nanocrystalline V/Ce Oxides
NANO 2004, 7th International Conference on Nanostructured Materials (poster)

G. Croce
Structural organization in siliceous spicules from marine sponges
Riunione annuale del gruppo di biochimica marina e dell'ambiente, Rapallo, Italy, 27-28 May 2004 (oral)

Croce G., Viterbo D., Milanesio M., Marchese L., Amenitsch H.
Structural organization in siliceous spicules from marine sponges
XXXIII Congresso Nazionale della Divisione di Chimica Fisica - Società Chimica Italiana, Napoli, Italy, 21-25.6.2004 (oral)

Croce G., Viterbo D., Milanesio M., Amenitsch H.
Structural organization in siliceous spicules from marine sponges
22nd European Crystallographic Meeting – ECM22, Budapest, Ungary 26-31.8.2004 (poster)

Croce G., Viterbo D., Milanesio M., Amenitsch H.
A mesoporous pattern created by nature in siliceous spicules from marine sponges
Micro and mesoporous mineral phases meeting, Roma, Italy, 6-7 December 2004 (oral)

I.D. Desnica-Frankovic, P. Dubcek, M. Buljan, U.V. Desnica, S. Bernstorff, H. Karl, I. Großhans and B. Stritzker
Influence of stoichiometry deviations on properties of ion-beam synthesized CdSe QDs
4th Conference on "Synchrotron Radiation in Materials Science (SRMS-4)", Grenoble, France, 23-25 August 2004 (talk)

U. V. Desnica, P. Dubcek, M. Buljan, I.D. Desnica-Frankovic, S. Bernstorff
From atoms to nanoparticles: changing the shape
The Briuni Conference, Exploring the fundamental problems in science: "Matter under extreme conditions", Briuni Island, Croatia, 30. 08 – 03- 09.2004 (poster)

U.V. Desnica, P. Dubcek, K. Salamon, I.D. Desnica-Frankovic, M. Buljan, S. Bernstorff, U. Serincan, R. Turan,
The evolution of the morphology of Ge nanocrystals formed by ion implantation in SiO_2
4th Conference on "Synchrotron Radiation in Materials Science (SRMS-4)", Grenoble, France, 23-25 August, 2004 (poster)

P. Dubcek, I. Kovacevic, N. Radic, H. Zorc, B. Pivac, S. Bernstorff, A. Campione and A. Borghesi
GISAXS and AFM study of germanium islands on silicon
16th International Vacuum Congress (IVC-16)/ 12th International Conference on Solid Surfaces (ICSS-12)/ 8th International Conference on Nanometer-Scale Science and Technology (NANO-8)/ 17th National Vacuum Symposium (AIV-17), Venice, Italy, June 28-July 2, 2004

P. Dubcek, A. Turkovic and N.D. Fox
Self-organisation of nanoparticles in TiO^2 thin film on the glass substrate
10th Joint Vacuum Conference, 11th Meeting of Slovenian and Croatian Vacuum Scientists, 24th Slovenian Vacuum Symposium, September 28-October 2, 2004, Portoros, Slovenia (poster)

P. Dubcek, N. Radic, S. Bernstorff, K. Salamon, A. Furlan, P. Panjan, M. Čekada
Surface of sputter-deposited tungsten films
Joint Vacuum Conference JVC10, Portoroz, September 2004

Jens Falta, Thomas Schmidt, Torben Clausen, Jan Ingo Flege, Sigrid Bernstorff, Gabriela Alexe and Detlef Hommel
Small Angle X-Ray Scattering Reveals CdSe/ZnSSe Quantum Dot Ordering
Fall Meeting of the Materials Research Society, Boston, MA, USA, 29.-11.- 3.12.2004 (talk)

J.I. Flege, Th. Schmidt, R. Kröger, I. Randjelovic, V. Aleksandrovic, G. Alexe, T. Clausen, S. Bernstorff, H. Weller and J. Falta
Characterization of 2-dimensional CoPt3 Overlayers With Grazing Incidence Small Angle X-Ray Scattering and Electron Microscopy
Fall Meeting of the Materials Research Society, Boston, MA, USA, 29.11.- 3.12.2004 (talk)

C. Fritscher, H. C. Lichtenegger, J. Stampfl, N. Hüsing, R. Liska, S. Bernstorff, T. Koch, D. Brandhuber, S. Seidler
Sol-Gel-Synthese: Ein Weg zu bioinspirierten Materialien
1. Wiener Biomaterialsymposium, Vienna, Austria, 04.-05.11.2004 (talk)

C. Fritscher, H. C. Lichtenegger, J. Stampfl, N. Hüsing, R. Liska, S. Bernstorff, T. Koch, D. Brandhuber, S. Seidler
Fabrication of Bio-inspired Silica Composites
2004 MRS Fall Meeting, Boston, USA, 29.11.-03.12.2004 (poster)

D.Gracin, K. Juraic, P. Dubcek, I. Bogdanovic Radovic, A. Gajovic, S. Bernstorff
The nano-structural properties of hydrogenated silicon-carbon alloys by optical methods 16th IVC, 12th ICSS, 8th NANO & 17th AIV, Venice, Italy, June 28-July 2, 2004

D. Grosso, C. Boissière, G. J. de A. A. Soler-Illia, E. L. Crepaldi, and C. Sanchez.
XRD analyses applied to mesoporous materials
MCRM 2004, Stockholm, Sweden (invited talk)

H. S. Gupta
In-situ measurement of fibrillar deformation in parallel fibered bone using synchrotron radiation
Micro-Mechanical Properties of Biomaterials, Hotel dos Templários, Lg. Candido dos Reis, 1, 2300, Tomar, Portugal, September 26-30, 2004 (Oral presentation)

H. S. Gupta, W. Wagermaier, P. Roschger, P. Messmer, S. S. Funari, and P. Fratzl *Fibrillar Deformation Mechanisms in Parallel Fibred Bone and Mineralized Tendon using In-situ Tensile Testing Combined with Synchrotron Small Angle X-ray Diffraction*
The 8th International Conference on Chemistry and Biology of Mineralized Tissues, Banff Centre, Alberta, Canada, October 17-22, 2004 (poster)

P. Hanák, E. Schafler, S. Bernstorff, T. Ungár, M. Zehetbauer
The dislocation structure in polycrystalline Cu determined in-situ at an ELETTRA synchrotron source
European Powder Diffraction Conference (EPDIC9), Prague, Czech Republic, Sept. 2004 (poster)
N. Hüsing, D. Brandhuber, C. Raab, V. Torma, H. Peterlik, M. Steinhart, M. Kriechbaum, S. Bernstorff
In-situ SAXS Investigations on the Formation of Mesostructured Spider-Web Like Silica Monoliths
Symposium on the "Use of Synchrotron Radiation in Austria", Theatersaal Austrian Academy of Sciences, Vienna, Austria, 15.3.2004 (poster)

N.K. Huesing and D. Brandhuber
Hierarchically Structured Silica Monoliths Carrying Organic Functions
2004 MRS Fall Meeting, Boston, USA, 29.11.-03.12.2004 (poster)

N.K. Huesing, D. Brandhuber, C. Raab, V. Torma and H. Peterlik
Hierarchically Structured Silica Monoliths
2004 MRS Fall Meeting, Boston, USA, 29.11.-03.12.2004 (talk)

D. Kalnin, M. Ouattara, F. Artzner, M. Ollivon
A new Method for the Determination of the Surface Composition in Sodium Caseinate containing Model Emulsions
European Conference on Drug Delivery and Pharmaceutical Technology, Sevilla, Spain, May 10-12, 2004 (Poster)

D. Kalnin, O. Schafer, H. Amenitsch and M. Ollivon
Fat Crystallization in Emulsion: Influence of emulsifier concentration on triacylglycerol crystal growth and polymorphism
Conférence invitée at 2nd Lipid Structural Properties Symposium, Colworth House, Unilever, 17-18 Novembre 2004, proceedings, p. 43-47 (invited lecture)

M. Kerber, E. Schafler, P. Hanak, G. Ribàrik, S. Bernstorff, T. Ungàr, M. Zehetbauer
Spatial fluctuations of the microstructure during deformation in Cu single crystals
Poster at the 9. European Powder Diffraction Conference (EPDIC9), Prague, Czech Republic, September 2004

I. Kovacevic, P. Dubcek, H. Zorc, N. Radic, B. Pivac, S. Bernstorff
GISAXS characterization of Ge islands on Si(100) substrates
JVC-10, Portoroz, Slovenia, Sept 2004

P. Laggner
In-situ diffraction and spin-label ESR studies on membranes at solid surfaces
2 nd DARPA-MOLDICE-Workshop, Max-Planck Inst. for Polymer Research, Mainz, Germany, 2.2.04, (invited lecture)

P. Laggner
The Austrian synchrotron activities at ELETTRA: record and perspectives
Symposium on the "Use of Synchrotron Radiation in Austria", Theatersaal Austrian Academy of Sciences, Vienna, Austria, 15.3.2004 (talk)

P. Laggner
Looking at small holes: Cross-validation of SAXS- and BET- porosimetry
53 rd Annual Denver X-ray Conference, Steamboat Springs, Colorado, USA
2.-6.8.04 (invited lecture)

P. Laggner
Membranes – self-assembly in natural and artificial systems
Nanoforum Summer School, Cambridge, UK, 6.-10.9.04 (invited lecture)

P. Laggner
Nanostruktur und Dynamik von A(orta) bis Z(eolith) – Röntgenkinematographie an Biomaterialien
1.Wiener Biomaterialsymposium, Wien, Austria, 4.-5.11.04 (invited lecture)

P. Laggner
In-situ SWAXS on transformations of porous and nanostructured solids
XII. Workshop über die Charakterisierung von feinteiligen und porösen Festkörpern, POROTEC, Bad Soden, Germany. 16.11.04 (invited lecture)

P. Laggner
Möglichkeiten der Röntgenstreuung zur In-Situ Charakterisierung nanoporöser Materialien und ihrer Dynamik
XII. Workshop über die Charakterisierung von feinteiligen und porösen Festkörpern, POROTEC, Bad Soden, Germany. 16.11.04 (lecture)

P. Laggner
SWAXS – new perspectives for an old method
Institute of Chemical Technology, ETH Zürich, Valbella, CH, 29.2.04 (seminar talk)

P. Laggner
Combined SAXS and powder diffraction: A powerful tool for nanostructure characterization in pharmaceutical solids
Department of Pharmaceutics, Univ. of Minnesota, Minneapolis, USA, 27.7.04 (seminar talk)

P. Laggner
SWAXS and related techniques at synchrotron sources – benefits and drawbacks
Univ. of Minnesota, USA, 12.-14.10.04 (seminar talk)

M. Linden, C. V. Teixeira, H. Amenitsch, V. Alfredsson and F. Kleitz
In situ SAXS/XRD Investigations of the Formation of Mesoscopically Ordered Surfactant-Silica Mesophases
Fall Meeting of the Materials Research Society, Boston, MA, USA, 29.11.-3.12.2004 (talk)

O. López, M. Cócera, J. Pereira, , H. Amenitsch, J. Caelles, A. de la Maza, R. Pons
Procesamiento de datos obtenidos mediante SAXS acoplado a una celda de flujo interrumpido: estudio cinético de sistemas liposoma-tensioactivo
Reunión Nacional Usuarios de Radiación Sincrotron y constitución de AUSE, Málaga, Spain, 5-6 Febraury 2004 (poster)

O. López, M. Cócera, J. Pereira, H. Amenitsch, J. Caelles, L. Coderch, JL Parra, A. de la Maza, R. Pons
Processing stopped-SAXS data to study the kinetic of liposome-surfactant systems
48th Annual Meeting of the Biophysical Society, Baltimore (MA), USA, 14 -18.02.2004 (poster)

M. Ollivon, C. Lopez and D. Kalnin
How crystallisation in emulsion may be used to report on interface composition and curvature?
3rd Euro Fed Lipid Congress and Expo: Oils, Fats and Lipids in a Changing World, Edinburgh, 5-8 September 2004 (invited lecture)

M. Ollivon, C. Lopez and D. Kalnin
Monitoring crystallisation in emulsion by coupled DSC and X-ray diffraction reports on interface composition and curvature?
13th Int. Congress of Thermal Anal. and Calorimetry 12-19 sept 2004, Chia Laguna, Sardinia (invited lecture)

G. Pabst, H. Amenitsch, D.P. Kharakoz, P. Laggner and M. Rappolt
Structure and Fluctuations of Phosphatidylcholines in the Vicinity of the Main Phase Transition
The 5th International Conference on Biological Physics ICBP 2004, Göteborg, Sweden, August 23-27, 2004 (poster)

G. Pabst, H. Amenitsch, P. Laggner, M. Rappolt
Pretransitional Swelling is not linked to ripple phase formation in phosphatidylcholines
48 th Annual Meeting of Biophysical Society, Baltimore, USA, 14.-18.2.04 (lecture)

G. Pabst, H. Amenitsch, P. Laggner, M. Rappolt
Structure and interactions of weakly ordered lipid model membranes
9 th European Powder Diffraction Conference, Prague, Cech Republic, 2.-5.9.04 (lecture)

G. Pabst
Discontinuous unbinding of two-component lipid membranes
NPMR, NRC, Chalk River Labs., Chalk River, Canada, 08.7.04 (seminar talk)

G. Pabst
Discontinuous unbinding of two-component lipid membranes
Steacie Institute of Molecular Sciences, NRC, Ottawa, Canada, 15.7.04 (seminar talk)

L. Petraru, D. Farnik, G. Hayn, R. Saf and Wolfgang H.Binder
Supramolecular, telechelic poly(etherketones) bearing barbituric acid as hydrogen bonding unit
Fall National Meeting of the American Chemical Society, Philadelphia, PA, 22-27.8.2004 (Lecture)

B. Pivac, P. Dubcek, S. Bernstorff, F. Corni, R. Tonini, and G. Ottaviani
GISAXS comparative study of H and D implanted Si
ECM-95/IVC-16/ICSS-12/NANO-8/AIV-17, Venice, Italy, June 2004

R. Pons, J. Caelles, I.Carrera, H. Amenitsch
Emulsificación por cambio de temperatura seguida por dispersión de Rayos-X con resolución temporal (Emulsification by temperature change followed by time resolved SAXS
Reunión Nacional Usuarios de Radiación Sincrotron y constitución de AUSE (National Meeting of the Synchrotron Users), Málaga (Spain), 5-6 February 2004 (poster)

B. Pozo Navas
Biological Relevance of the thermal unbinding
Max-Planck-Institut für Kolloid- und Grenzflächenforschung, Golm, Germany, 4.2.04 (seminar talk)

N. Radic, P. Dubcek, S. Bernstorff, K. Salamon, A. Tonejc, A. Furlan, P. Panjan, M. Cekada
Tungsten Multilayers
IVC-16 / ICSS-12 / (NANO-8 / AIV-17, Venice, Italy, June 2004

M Rappolt
Model membrane studies at the Austrian SAXS beamline of ELETTRA
Satellite Workshop of BSR2004: "SAXS in the 21st Century", SPring-8, Japan, 5-7 September 2004 (talk)

M. Rappolt, H. Amenitsch, C. V. Teixeira, M. Majerowicz and P. Laggner
In-Situ Sensing of Salinity in Oriented Lipid Multilayers by Surface X-ray Scattering
BSR 2004 (8th International Conference on Biology and Synchrotron Radiation), Himeji, Japan, September 7 – 11, 2004 (poster)

P. Roschger, B.M. Misof, A. Valenta, W. Tesch, O. Paris, S. Bernstorff, H. Amenitsch, K. Klaushofer and P. Fratzl
Detection of a bimodal relationship between mineral content and particle size in individual bone packets
8th International conference on the chemistry and biology of mineralized tissues, Banff Centre, Alberta, Canada, October 17-22, 2004

E. Schafler, M. Kerber and M. Zehetbauer
Vom Einkristall zum Nanokristall: Charakterisierung der Mikrostruktur von Metallen w¨ahrend plastischer Verformung mittels Synchrotron Linienprofil-Analyse
54. Annual Meeting of the Austrian Physical Society, Linz, Austria, 28-30. Sep. 2004 (talk)

E. Schafler, K. Nyilas, S. Bernstorff, L. Zeipper, M. Zehetbauer, T. Ungàr
Microstructure of post deformed ECAP-Ti investigated by Multiple X-Ray Line Profile Analysis
9. European Powder Diffraction Conference (EPDIC9), Prague, Czech Republic, Sept. 2004 (poster)

E. Schafler, K. Simon, S. Bernstorff, H. Amenitsch, G. Tichy, T. Ungár, and M.J. Zehetbauer
A Second-Order Phase-Transformation During Plastic Deformation Determined by In-Situ Synchrotron X-Ray Diffraction
Symposium on the "Use of Synchrotron Radiation in Austria", Theatersaal Austrian Academy of Sciences, Vienna, Austria, 15.3.2004 (poster)

E. Schafler, T. Ungar
*The method of X-ray Bragg Profile Analysis as a Tool to determine Grain sizes and Lattice Defects in nanomaterials*7.
Int. Conference on Nanostructured Materials, Wiesbaden, Germany, June 2004 (talk)

S. di Stasio, V. Dal Santo, B. Caruso, G. Verrengia
Microscopy, light scattering and IR-spectroscopy characterization Of Zn/ZnO nanoparticles fabricated by aerosol route
PARTEC 2004, International Congress for Particle Technology, Nuremberg, Germany 16-18 March 2004

R. Supplit, N. Hüsing and S. Bernstorff
Metal Oxide Doped Mesostructured Silica Films
MRS Fall Meeting, Boston (MA), USA, 30.11.2004 - 04.12.2004 (poster)

R. Supplit, N. Hüsing, C. Fritscher, P. Jukabiak, V. Kessler, G.A. Seisenbaeva, S. Bernstorff
Iron-oxide doped mesostructured silica films
MRS Fall Meeting, Boston, USA, 29.11.-03.12.2004 (talk)

B. Toury, F. Babonneau
Periodic mesoporous SiCO glasses from Sol-Gel templating approach
E-MRS 2004 Spring Meeting, Symposium on Polymer-derived Ceramics, Strasbourg, France, May 25-28 2004 (talk)

B. Toury, F. Babonneau
Periodic mesoporous SiCO glasses from Sol-Gel templating approach
ICG XX, Kyoto (Japon) 26 September 26 -October 1 2004 (talk)

A. Turkovic and M. Gabercek
Characterization of TiO_2 films as nanostructured electrodes
7th ISSFIT International Symposium on Systems with Fast Ionic Transport, 5-9 May 2004 Bled, Slovenia (poster)

A. Turkovic, M. Gabercek and Z. Crnjak Orel
Electrical Conductivity of Nanostructured TiO2 Films on Glass Substrate Measured by Impedance Spectroscopy
IVC-16, ICSS-12, NANO-8, AIV-17, Venice, Italy, 2004 (poster)

A. Valenta, P. Roschger, B.M. Misof, O. Paris, W. Tesch, S. Bernstorff, H. Amenitsch, K. Klaushofer, P. Fratzl
Growth of the Mineral Particles in Bone - Combined Study of Small Angle X-ray Scattering (SAXS) and Electron Backscattering (qBEI)
Fruehjahrstagung des Arbeitskreises Festkoerperphysik (AKF) der DPG, Regensburg, Germany, Maerz 2004 (poster)

H. Wilhelm, A. Paris, E. Schafler, S. Bernstorff, J. Bonarski, T. Ungar, and M. J. Zehetbauer
Evidence For Dislocations In Melt-Crystallised And Plastically Deformed Polypropylene From Synchrotron X-Ray Diffraction Experiments
Symposium on the "Use of Synchrotron Radiation in Austria", Theatersaal Austrian Academy of Sciences, Vienna, Austria, 15.3.2004 (poster)

M. Zehetbauer
Parameters from X-Ray Line Shape Analysis Governing the Strength and Ductility of Nanomaterials
Annual Meeting of the Hungarian Physical Society, Szombathely, Hungary, Aug. 2004

M. Zehetbauer, E. Schafler, T. Ungár
Quantification of Nanocrystallization by Means of X-Ray Line Profile Analysis
Symposium on Texture and Microstructure Analysis of Functionally Graded Materials (SOTAMA-FGM), Krakow, Poland, Oct.2004 (Invited lecture)

ELETTRA Highlights 2003-2004

K. Flodström, V. Alfredsson, C. V. Teixeira, H. Amenitsch and M. Lindén
In-situ synchrotron SAXS/XRD study of the formation of SBA-15
Elettra Research Highlight, pp. 60-62 (2004)

Th. Schmidt, G. Alexe, D. Hommel, T. Clausen, J. Falta, S. Bernstorff
Small angle X-ray scattering reveals CdSe/ZnSSe quantum dot ordering
Elettra Research Highlight, pp. 63-67 (2004)

SAXS training courses

In March 2004, H. Amenitsch, S. Bernstorff, M. Rappolt and B. Sartori participated at the international school "Hercules", organized by the University "Joseph Fourier" (Grenoble, France) and the National Polytechniche Institute of Grenoble with the help of ERSF, ILL, ELETTRA, LLB, CEA and CNRS. They gave 8 tutorials a' 5 hours, including hands-on experience for the students during the measurements performed in the SAXS-lab and at the Austrian SAXS-beamline.

In May 2004, H. Amenitsch, S. Bernstorff and M. Rappolt participated at the "International ICTP School for Synchrotron Radiation", organized by the International Center for Theoretical Physics in Trieste, Italy. They gave 3 lectures, and 3 tutorials a' 4 hours, including hands-on experience during the measurements performed at the Austrian SAXS-beamline.

Habilitation Theses 2004

Dr. Wolfgang Binder
Synthesis and Self Assembly of Telechelic Macromolecules into Supramolecular Aggregates
Habilitationsschrift, Technical University of Vienna, 2004

PhD Thesis 2004

Gianluca Croce
Structural Study of Hybrid Organic/Inorganic Systems: Siliceous Spicules from Marine Sponges
University of Piemonte Orientale "A. Avogadro", Italy, 2004

Francesco Federiconi
Proprieta' strutturali ed origine delle interazioni tra quadrieliche di guanosina
Università di Ancona, Italy, 2004

D. Kalnin
Contribution à l?étude des structures développées par les lipides dans les émulsions congelées (Study of lipidic structures in frozen emulsions)
University of Paris-Sud-ENSIA, France, 15.12.2004

Michael Kunz
Synthese und strukturelle Untersuchungen an supramolekularen POly(etherketon)-Poly(isobutylen) pseudo block Copolymeren
Technical University of Vienna, Austria, 2004

Doris Machl
Synthese von Block-Copolymeren mit Polyisobutylen/Polyetherketon Segmenten
Technical University of Vienna, Austria, 2004

A. Orthen
Bildgebende Röntgendetektion mit Gasverstärkung durch Mikrostrukturen für Hochgeschwindigkeitsmessungen
University of Siegen, Germany, 2004

Maria Grazia Ortore
Proprietà strutturali e stabilità di proteine in solventi non-acquosi
Università di Perugia, Italy, 2004
C. Raffournier
Objets bicompartimentaux huile-eau, ...
that can be tentatively translated into:
Characterisation of hand bags: colloidal mixed aggregates associating liposome and emulsion properties
University of Paris-Sud, France, July 11, 2004

H. Wagner
Vielzellenwiderstandsauslese für zweidimensionale Röntgenabbildungen – Optimierung der Abbildungseigenschaften bei Anwendungen mit schneller Bildfolge
University of Siegen, Germany (2004)

Leonhard Zeipper
Defect Based Micromechanics of NanoSPD Titanium – Experiments, Simulations and Applications
University of Vienna, Wien, Austria (2001-2004)

Master Theses (Tesi di Laurea) 2004

Stefano Costacurta
Film mesostrutturati ibridi organico-inorganici ottenuti mediante tecniche di autoassemblaggio sopramolecolare
Università di Padova, Dipartimento di Ing. Meccanica, Settore Materiali, Italy, June 2004

Dominique Farnik
Synthese telecheler Polyetherketone mit multiplen Wasserstoffbrückenbindungen
Technical University of Vienna, Austria, 2004

Luca Malfatti
Film di titania mesostrutturata per applicazioni fotovoltaiche
Università di Padova, Dipartimento di Ing. Meccanica, Settore Materiali, Italy, March 2004

Sorin Martoiu
Intelligent local trigger technique for a multi-cell 2D interpolating resistive readout
University of Siegen, Germany, 2004

Modibo Ouattara
Encapsulation et caracterisation de produits pharmaceutiques dans des nanocapsules lipidiques
DEA Pharmacotechnie Biopharmacie, Chatenay Malabry, France, 2004

Francesco Voltolina
Progetto di un detector a camera di ionizzazione per esperimenti SAXS
University of Trieste, Italy, Anno Accademico 2003-2004

Author Index

ALBOUY P.A.	107
ALEKSANDROVIC V.	45
ALEXE G.	45
ALFREDSSON V.	114
AMENITSCH H.	64, 66, 68, 71, 74, 76, 78, 79, 80, 82, 83, 87, 93, 98, 105, 107, 114, 116, 118
ASHLEY C.C.	64
ASWAL V.K.	40
BAGNI M.A.	64
BALDRIAN J.	93
BERGAMINI C. M.	68
BERNSTORFF S.	40, 42, 45, 50, 53, 56, 59, 61, 64, 68, 78, 80, 83, 93, 95, 102, 111
BINDER W. H.	95
BOISSIÈRE C.	107
BOURGAUX C.	79
BRANDHUBER D.	102
BRETCANU O.	74
BREZESINSKI T.	107
BULJAN M.	42
BUSO D.	98
BYRON O.	89
CAMINITI R.	71
CARACCIOLO G.	71
CECCHI G.	64
CLAUSEN T.	45
COLOMBINI B.	64
COPLEY M. P.	105
COSTACURTA S.	98
CROCE G.	74
D'ANTONA P.	47
DEL PIERO G.	47
DESNICA U.V.	42
DESNICA FRANKOVIC I.D.	42
DEUTSCH G.	86
DINUNZIO S.	74
DUBČEK P.	42, 50, 53, 56, 59
FALCARO P.	98
FALTA J	45
FARNIK D.	95

FLEGE J. I.	45
FRITSCHER C.	102
GAJOVIC A.	50
GHISLETTI D.	47
GOYAL P.S.	40
GRACIN D.	50
GRIFFITHS P.J.	64
GROSSO D.	107
GUGLIELMI M.	98
HANRAHAN J. P.	105
HICKEL A.	76, 82
HODZIC A.	77
HOLMES J. D.	105
HOLZAPFEL G.A.	87
HÜSING N.	102, 111
INNOCENZI P.	98
JURAIC K.	50
KALNIN D.	79
KATSARAS J.	82
KELLER G.	79
KERBER M.	61
KLUGER C.	95
KOCH T.	102
KOHLBRECHER J.	40
KORNOWSKI A.	45
KOVAČEVIĆ I.	53, 56
KRIECHBAUM M.	78
KUEMMEL M.	107
LAGGNER P.	66, 77, 78, 87
LICHTENEGGER H. C.	102
LINDÉN M.	114
LINDSAY J.G.	89
LOHNER K.	76, 86
MALFATTI L.	98
MARIANI P.	68, 80, 83
MARTUCCI A.	98
MATTEI G.	98
MILANESIO M.	74
O'CALLAGHAN J. M.	105
OLLIVON M.	79
ONIDA B.	74
ONORI G.	80

ORTORE M.G.	80
PABST G.	66, 76, 77, 82, 86
PACCAMICCIO L.	83
PETRARU L.	95
PISANI M.	83
PIVAC B.	53, 56
POZO NAVAS B.	86
POZZI D.	71
RADIĆ N.	53, 56, 59
RANDJELOVIC I.	45
RAPPOLT M.	66, 76, 77, 78, 82, 87
REGITNIG P.	87
SADA C.	98
SALAMON K.	42, 59
SANCHEZ C.	107
SAPRA S.	118
SARMA D.D.	116, 118
SARTORI B.	66, 78
SCHAFLER E.	61
SCHMID F.	87
SCHMIDT TH.	45
SCHULZE BAUER C.A.J.	87
SEIDLER S.	102
SERINCAN U.	42
SEVCSIK E.	86
SIKORA A.	93
SINKO K.	109
SLAOUI A.	56
SMARSLY B.	107
SMOLLE M.	89
SOMMER G.	87
SPINOZZI F.	68, 80, 83
STANEVA M.	93
STEINER G.	61
STEINHART M.	78, 93, 105
ŠTRANCAR J.	77
SUPPLIT R.	111
TEIXEIRA C.V.	114
TORMA V.	109
TURAN R.	42
UNGÀR T.	61
VERNÉ E.	74

WELLER H.	45
VISWANATHA R.	116, 118
VITERBO D.	74
ZEHETBAUER M. J.	61